New constraints on the tectono-metamorphic evolution of the Fisher Terrane, central Prince Charles Mountains, eastern Antarctica

Thesis submitted in accordance with the requirements of the University of Adelaide for an Honours Degree in Geology/Geophysics

Alexander Thomas De Vries Van Leeuwen

November 2017

THE UNIVERSITY of ADELAIDE

NEW CONSTRAINTS ON THE TECTONO-METAMORPHIC EVOLUTION OF THE FISHER TERRANE, CENTRAL PRINCE CHARLES MOUNTAINS, EASTERN ANTARCTICA

TECTONO-METAMORPHIC EVOLUTION OF THE FISHER TERRANE

ABSTRACT

The Fisher Terrane, located in the central region of the Prince Charles Mountains, east Antarctica, evolved during the Mesoproterozoic as a magmatic arc system. Metapelitic schists from the Fisher Massif were deposited after 1206 ± 49 Ma and yield metamorphic monazite ages of c. 538–505 Ma relating to the regionally recognised Neoproterozoic to early Cambrian Prydz Event. Calculated phase equilibria modelling constrains the metamorphic conditions during this event to 2.6–4.0 kbar and 553–576 °C, relating to apparent thermal gradients of 144 °C/kbar to 212 °C/kbar. Conditions such as these are plausibly related to metamorphism taking place in an extensional back-arc setting which was then subsequently inverted and thickened via continental collision. A migmatitic felsic gneiss from Nilsson Rocks yields metamorphic monazite $^{206}Pb/^{238}U$ ages between 1115–1050 Ma with a weighted average age of 1085.0 ± 7.1 Ma. This metamorphic event may relate to a similarly aged episode of subduction related magmatism identified elsewhere in the central Prince Charles Mountains. This study therefore presents evidence of previously unidentified Prydz-aged high-thermal gradient metamorphism in the Fisher Terrane as well as identifying an older c. 1085 Ma metamorphic event not documented elsewhere in the Prince Charles Mountains.

KEYWORDS

East Antarctica, Prince Charles Mountains, THERMOCALC, Metamorphism, U–Pb Geochronology, Tectonics, Gondwana

TABLE OF CONTENTS

LIST OF FIGURES AND TABLES

INTRODUCTION

The Prince Charles Mountains region (PCMs) in eastern Antarctica, Figure 1, represents one of the largest exposed outcrops of basement rock on the continent, therefore the area is crucial for understanding the geological history and assembly of eastern Antarctica. From north to south the PCMs are comprised of several terranes with contrasting protolith ages: The Rayner Complex, Fisher Terrane, Lambert Terrane and Ruker Terrane (Mikhalsky, Sheraton, Laiba & Beliatsky, 1996; Mikhalsky, Laiba, & Beliatsky, 2006b). Numerous tectonic models have been proposed to explain the amalgamation of the various terranes making up the PCMs, with most models suggesting that it occurred during the Meso–Neoproterozoic (Grenvillian-aged) Rayner Event (c. 1000–900 Ma), and/or the late Neoproterozoic–Cambrian (Pan-African-aged) Prydz Event (c. 570–480 Ma) (Boger, Wilson, & Fanning, 2001; Boger, 2011; Fitzsimons, 2000; Kelly, Clarke, & Fanning, 2002).

The Fisher Terrane is located between the Meso–Neoproterozoic-aged Rayner Complex and Archean–Paleoproterozoic Lambert Terrane and therefore may hold key information to understand the evolution and amalgamation of the PCMs. However, the Fisher Terrane has been the subject of very few geological studies (Beliatsky, Laiba, & Mikhalsky, 1994; Crowe, 1994; Mikhalsky, Laiba, Beliatsky, & Stüwe, 1999; Mikhalsky et al., 1996). In particular, there is no clear framework of the age and thermal conditions of metamorphism in the Fisher Terrane, nor are there any constraints on depositional ages of the metasedimentary rocks. This paucity in our understanding of the terrane impacts on the validity and credibility of the tectonic models proposed for the evolution and amalgamation of this region of east Antarctica.

With this clear gap in knowledge, this study aims to provide constraints on the age and pressure–temperature (*P*–*T*) conditions of metamorphism from the Fisher Terrane. This is achieved by the application of *in situ* monazite U–Pb geochronology coupled with calculated phase equilibria modelling of metapelitic rocks of the Fisher Terrane. To accompany this data, U–Pb geochronology from detrital zircon grains from within the same metasedimentary succession is presented to provide constraints on the age and provenance of these sedimentary rocks. This study provides the first modern metamorphic analysis of the Fisher Terrane and aims to not only provide a more cohesive understanding of the temporal and genetic relationship of the Fisher Terrane in the context of other terranes in the PCMs, but also be the basis for more robust tectonic model interpretations of the evolution and amalgamation of the PCMs.

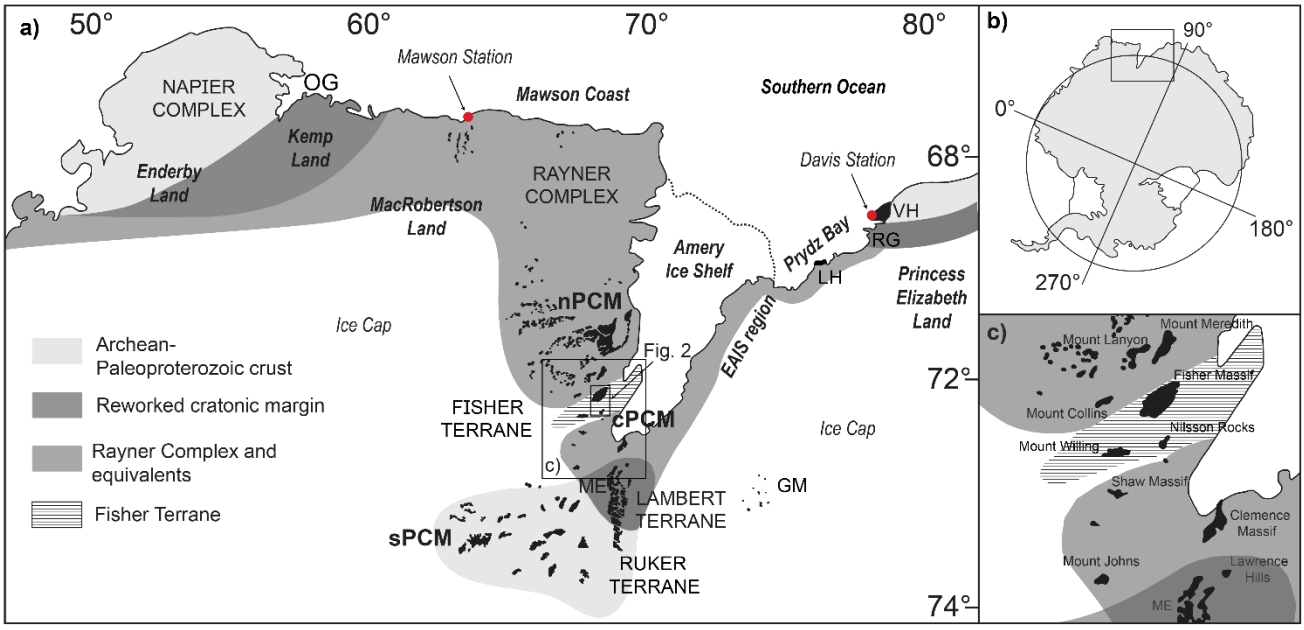

Figure 1: a) Outcrop map of the PCMs and surrounding areas showing the spatial relationships of terranes; b) Broader setting of the PCMs in Antarctica; c) Enlarged view of the cPCM region. Black regions indicate areas of rock exposure. Abbreviations as seen on map: OG = Oygarden Group, ME = Mawson Escarpment, LH = Larsemann Hills, RG = Rauer Group, VH = Vestfold Hills, GM = Grove Mountains. Modified from Morrissey, Hand, and Kelsey (2015)

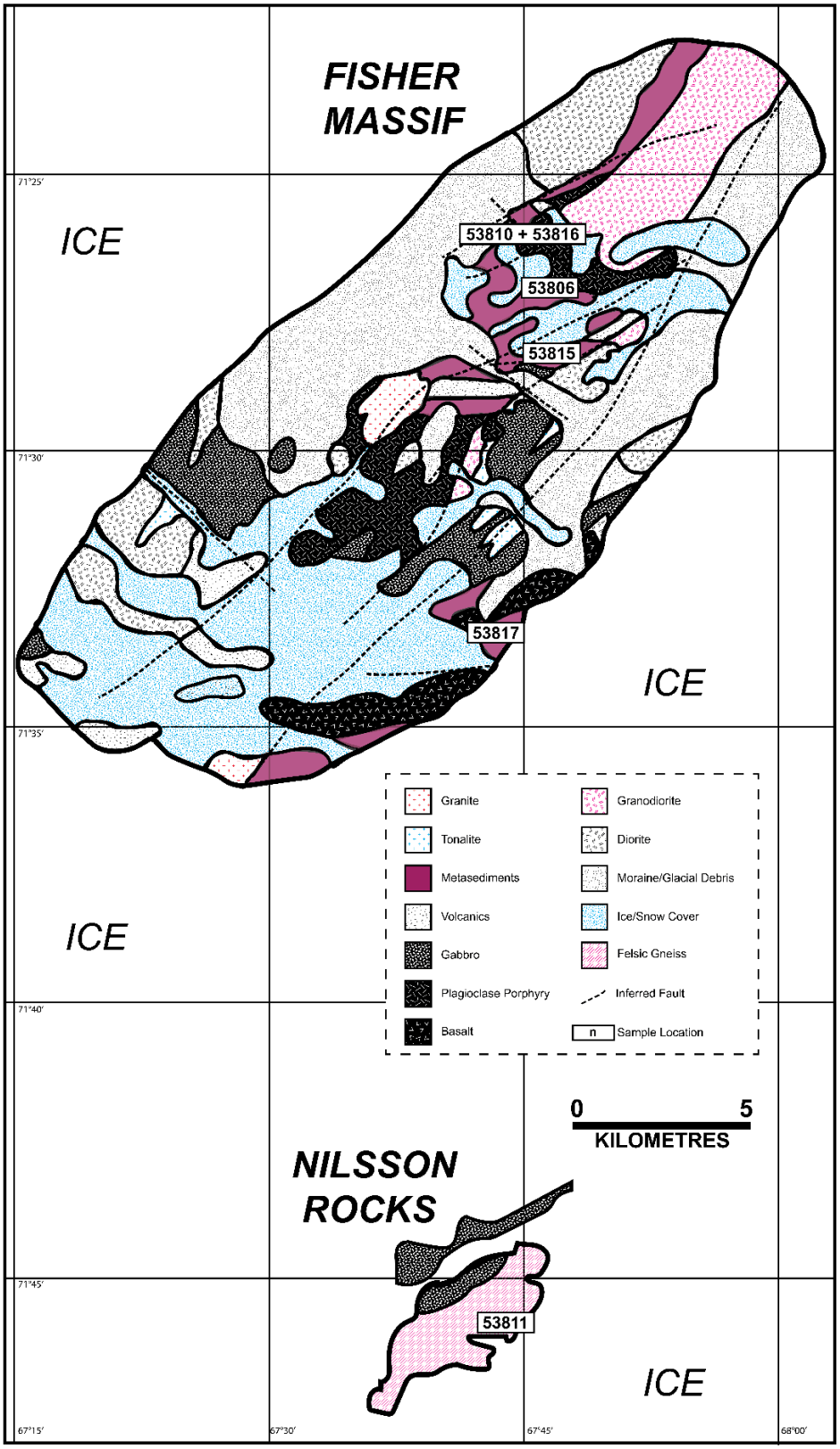

Figure 2: Geological map of Fisher Massif and Nilsson Rocks. Sampling locations are displayed and relate to samples defined in Table 1. Modified from Crowe (1994) and Mikhalsky et al., 1996.

GEOLOGICAL BACKGROUND

The PCMs, located in the southern portion of MacRobertson Land and bordering the Amery Ice Shelf (Fig. 1a), cover an area of ~180,000 km^2, representing one of the largest ice–free exposures of basement rock in eastern Antarctica. The PCMs are subdivided into northern, central and southern sections (nPCMs, cPCMs and sPCMs, see Fig. 1a), based upon geographical, geochronological, and geophysical data (e.g. Golynsky, Masolov, Volnukhin, & Golynsky, 2006; Mikhalsky et al., 2006b). Rocks in the PCMs range from Archean to Palaeozoic in age, with different portions of the PCMs having been variably created or reworked by tectonism of the Grenvillian-aged Rayner Event (c. 1000–900 Ma) and/or Pan-African-aged Prydz Event (c. 570–480 Ma) (Fig. 3). In the summary of existing data below, emphasis is placed on whether the terranes comprising the PCMs record the Grenvillian-aged Rayner Event or the Pan-African-aged Prydz Event, as this information is most critical for constraining the existing tectonic models.

Northern Prince Charles Mountains (nPCM)

The Rayner Complex (or Rayner–Eastern Ghats) (Fig. 1a), is dominantly composed of orthogneisses with subordinate interlayered paragneisses and scattered outcrops of felsic and charnockitic intrusives (Halpin, Daczko, Milan, & Clarke, 2012; Manton, Grew, Hofmann, & Sheraton, 1992; Thost & Hensen, 1992). Granulite facies, high-thermal gradient (~120–150 °C/kbar) metamorphism took place during the Rayner Event at c. 1020–900 Ma, attaining peak conditions of 6–7 kbar and 800–850 °C followed by near isobaric cooling, resulting in an anticlockwise *P–T* path (Boger & White, 2003; Morrissey et al., 2015). Metamorphism was accompanied by deformation and voluminous magmatism (Boger, Carson, Wilson, & Fanning, 2000; Carson, Boger,

Fanning, Wilson, & Thost, 2000; Halpin et al., 2012; Kelly et al., 2002). Subsequent reworking of the Rayner Complex took place during the Prydz Event at c. 550–475 Ma manifesting as localised granulite facies metamorphism, discrete greenschist facies shear zones and intrusion of pegmatite and granite. (Boger et al., 2002; Carson et al., 2000; Manton et al., 1992; Morrissey, Hand, Kelsey, & Wade, 2016). Peak metamorphic conditions during the Prydz Event reached 5.5–6.5 kbar and 800–850 °C, corresponding to thermal gradients of ~130–150 °C/kbar (Morrissey et al., 2016).

Central Prince Charles Mountains (cPCM)

The Fisher Terrane, comprised of Fisher Massif, Mount Willing and Nilsson Rocks (Fig. 1c & 2), is composed of metamorphosed intrusive igneous rocks of varying composition along with subordinate metavolcanics and metasediments (Crowe, 1994; Mikhalsky et al., 1996, 1999). Bimodal calc-alkaline magmatism began at c. 1300 Ma and ceased by c. 1190 Ma (Alexeev, Zinger, Glebovitsky, & Kapitonov, 2010; Beliatsky et al., 1994; Mikhalsky et al., 1996, 1999). Basaltic and rhyolitic lavas form an interlayered supracrustal succession with metasediments (volcaniclastics and metapelites) (Crowe, 1994; Mikhalsky et al., 1996). The relationship between the supracrustal succession and the underlying intrusive rocks is poorly constrained; however, the two units appear to be fault bound, with an indecipherable sense of movement or displacement (Crowe, 1994; Mikhalsky et al., 1996). Later emplacement of granites at Fisher Massif and pegmatites at Mount Willing occurred at c. 1020 Ma and c. 925 Ma, respectively (Kinny, Black, & Sheraton, 1997; Mikhalsky et al., 1999). The age of amphibolite facies metamorphism was tentatively constrained by discordant zircon U–Pb analyses that yielded an upper intercept age of c. 1110 Ma (Mikhalsky et al., 1999). Existing constraints on the metamorphic conditions were determined using

conventional thermobarometry: 3–4 kbar and 550–675 °C at Fisher Massif (Crowe, 1994) and 6–9 kbar and 480–670 °C at Mount Willing (Mikhalsky et al., 1999). The overall metamorphic grade of the Fisher Terrane is lower than the nPCMs and is therefore suggested to represent a shallower level of the crust with respect to the other terranes (Mikhalsky et al., 1996). To date, there is no record of the Prydz Event in the Fisher Terrane.

The Central Nunataks occur are located to the south of the Fisher Terrane. At Shaw Massif (Fig. 1c), magmatism occurred at 1081 ± 18 Ma, with subsequent overprinting during the Prydz Event in the form of new zircon growth and the emplacement of aplite dykes at c. 550–450 Ma (Maslov, Vorobiev, & Belyatsky, 2007). Further south, at Clemence Massif (Fig. 1c), magmatic zircons yield an age of 1062 ± 9 Ma with metamorphic rims of c. 535–464 Ma, metamorphic zircons also yield c. 910 Ma ages (Corvino, Boger, Wilson, & Fitzsimons, 2005). The southernmost Lawrence Hills (Fig. 1c), records evidence of magmatism at c. 2500 Ma, resembling ages found in the sPCMs, and c. 1080 Ma rocks with a calc-alkaline geochemical affinity (Corvino & Henjes-Kunst, 2007).

Southern Prince Charles Mountains (sPCM)

The Archean–Paleoproterozoic Lambert Terrane is comprised of various orthogneisses, metasedimentary packages and minor granitic dykes (Corvino, Boger, Henjes-Kunst, Wilson, & Fitzsimons, 2008; Mikhalsky, Beliatsky, Sheraton, & Roland, 2006a; Phillips, Kelsey, Corvino, & Dutch, 2009; Phillips, Wilson, Campbell, & Allen, 2006). The northern portion records pervasive Rayner-aged deformation, magmatism and metamorphism occurring at c. 950–900 Ma (Corvino et al., 2008; Phillips et al., 2009).

The southern Lambert Terrane records Prydz-aged reworking in the form of c. 530–490 granitoid emplacement and metamorphic zircon growth in orthogneisses (Boger, Maas, & Fanning, 2008). Peak metamorphic conditions in the Lambert Terrane during the Rayner Event were 6.5–7.1 kbar and 790–810 °C (Phillips et al., 2009). The subsequent Prydz-Event reached peak metamorphic conditions of 5.8–7 kbar and 620–670 °C (Boger & Wilson, 2005; Phillips et al., 2009) and records a clockwise *P–T* path to conditions of 3.7–4.2 kbar and 580–610 °C (Phillips et al., 2009).

The Archean Ruker Terrane comprises various orthogneisses intercalated with a metasedimentary unit; these units are overlain by various quartzitic to metapelitic units and intruded by pegmatite dykes (Boger et al., 2001; Boger, Wilson, & Fanning, 2006; Mikhalsky, Beliatsky, et al., 2006a; Phillips et al., 2009; Phillips, White, & Wilson, 2007a; Phillips et al., 2006). The Ruker Terrane does not record the Rayner Event. The Ruker Terrane records the Prydz Event in the form of high strain zones (Phillips, White, et al., 2007). Limited constraints on the event provide ages of c. 550 to 480 Ma and *P–T* conditions of 4.0–5.2 kbar and 565–640 °C (Boger et al., 2001; Phillips et al., 2007a; Phillips, Wilson, Phillips, & Szczepanski, 2007b).

Tectonic Models

Tectonic models explain the Rayner Event as a collision between India (India + Rayner–Eastern Ghats) and the Lambert Terrane at c. 1000–900 Ma (Fitzsimons, 2000; Liu, Jahn, Zhao, Liu, & Ren, 2014). Many of these models consider the Rayner–Eastern Ghats Terrane to exhibit a protracted (possibly spanning from c. 1500–880 Ma) and punctuated thermal history of arc magmatism, subduction–related accretion and extension, culminating in high temperature metamorphism during the Rayner Event

(Halpin et al., 2012; Liu et al., 2014; Liu et al., 2016; Morrissey et al., 2015). The models differ in the relative timing and the positioning of these continental fragments and island–arcs. In all models the Fisher Terrane is considered as an oceanic island-arc (Mikhalsky et al., 1996) which subsequently collided with the margin of either the Lambert Terrane (e.g. Liu et al., 2014) or Rayner Complex, and final suturing and amalgamation of these terranes into a continental block occurring by c. 900 Ma.

The subsequent Prydz Event is typically considered to be either a result of collision and suturing of Indo-Antarctica (India + Rayner–Eastern Ghats + Fisher and Lambert Terranes) and Australo-Antarctica (Ruker Terrane) or the inversion of extensional basins as a response to far field stresses produced during this collision and Gondwana amalgamation (Boger et al., 2001; Boger, 2011; Kelsey et al., 2008; Phillips et al., 2007b). The regional record of this event in some parts of the PCMs is spatially discrete (or 'patchy'), possibly due to the refractory and anhydrous nature of many of the rocks of the PCMs (Morrissey et al., 2016; Phillips et al., 2009), making deciphering the exact nature, extent and significance of this event difficult.

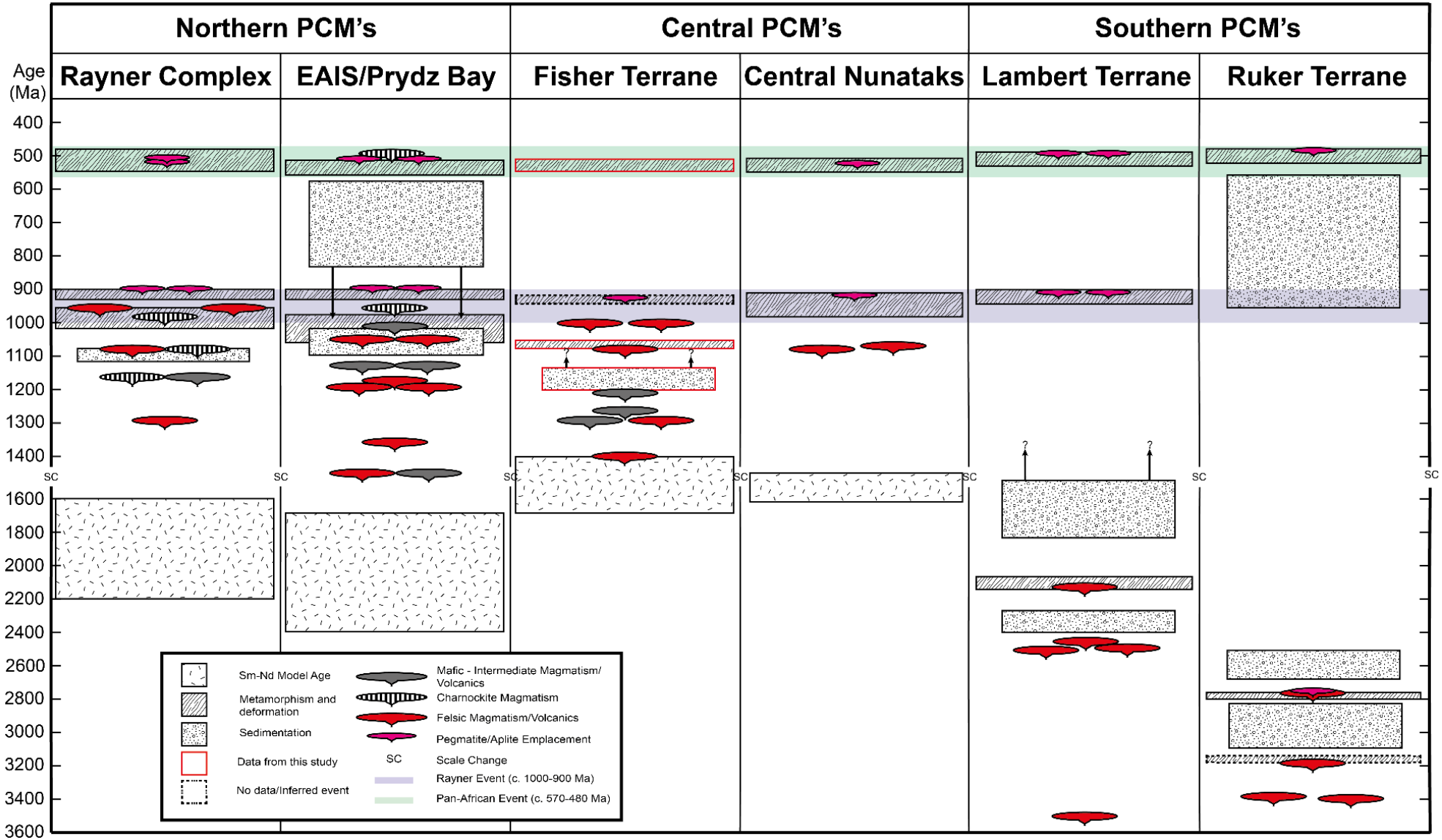
Northern PCM's
Central PCM's
Southern PCM's
Rayner Complex
EAIS/Prydz Bay
Fisher Terrane
Central Nunataks
Lambert Terrane
Ruker Terrane
Age (Ma)
400
500
600
700
800
900
1000
1100
1200
1300
1400
1600
1800
2000
2200
2400
2600
2800
3000
3200
3400
3600
SC
Sm-Nd Model Age
Metamorphism and deformation
Sedimentation
Data from this study
No data/Inferred event
Mafic - Intermediate Magmatism/ Volcanics
Charnockite Magmatism
Felsic Magmatism/Volcanics
Pegmatite/Aplite Emplacement
SC
Scale Change
Rayner Event (c. 1000-900 Ma)
Pan-African Event (c. 570-480 Ma)

Figure 3: Time–space plot outlining major terranes in the Prince Charles Mountains. EAIS and Prydz Bay regions are presented for comparison. Rayner Complex data from: Boger et al. (2000), Carson et al. (2000), Halpin, Clarke, White, and Kelsey (2007), Halpin et al. (2012), Halpin, Daczko, Clarke, and Murray (2013), Kinny et al. (1997), Manton et al. (1992), Mikhalsky et al. (2006b), Mikhalsky et al. (2013), Morrissey et al. (2015, 2016), Zhao, Ellis, Kilpatrick, and McCulloch (1997); EAIS/Prydz Bay data from: Grew et al. (2012), Kelsey, Hand, Clark, and Wilson (2007), Kelsey et al. (2008), Kinny, Black, and Sheraton (1993), Liu, Zhao, Zhao, Jian, and Xu (2007), Liu et al. (2009a, 2016), Liu, Zhao, Song, Liu, and Cui (2009b), Liu et al. (2014), Morrissey et al. (2015), Wang, Liu, Chung, Tong, and Ren (2008); Fisher Terrane data from: Alexeev et al. (2010), Beliatsky et al. (1994), Kinny et al. (1997), Mikhalsky et al. (1999, 2001, 2006b); Central Nunataks data from: Corvino et al. (2005), Corvino and Henjes-Kunst (2007), Maslov et al. (2007), Lambert Terrane Data from: Boger and Wilson (2005), Boger et al. (2008), Corvino et al. (2008), Mikhalsky et al. (2006a), Phillips et al. (2006); Ruker Terrane data from: Boger et al. (2006), Mikhalsky et al. (2006a), Phillips et al. (2006), Phillips et al. (2007b).

SAMPLE COLLECTION AND PETROGRAPHY

Samples used in this were collected by Warwick Crowe of the Australian National University during the 1990/91 and 1991/92 Australian Antarctic Research Expeditions (see Crowe, 1994). Table 1 summarises the samples and their locations (see Fig. 2). Metapelitic rocks were sampled for *P–T–time* work and other rocks for detrital zircon analysis.

Table 1: List of samples used in this study. Sample locations are shown in Figure 2.

Sample	Rock Type	Location	Approx. Coordinates (WGS84, Zone 42S)	Use
53806	Meta–volcanic breccia	Fisher Massif	456800 N 2072200 E	U–Pb zircon
53810	Meta–volcanic sandstone	Fisher Massif	455800 N 2073400 E	U–Pb zircon
53811	Garnet–bearing felsic gneiss	Nilsson Rocks	456400 N 2038300 E	U–Pb monazite
53815	Cordierite–andalusite–staurolite schist	Fisher Massif	457000 N 2069800 E	*P–T–t* (U–Pb monazite)
53816	Garnet–staurolite schist	Fisher Massif	455800 N 2073400 E	*P–T–t* (U–Pb monazite)
53817	Gedrite bearing garnet–staurolite schist	Fisher Massif	453600 N 2058100 E	U–Pb monazite

Petrographic Descriptions

Interpretation of the sample petrography is based on the logic that minerals forming part of the 'peak' mineral assemblage are either coarse grained and/or define (in part) the main tectonic fabric. Retrograde minerals are interpreted based on overprinting the main fabric. Descriptions for samples 53806, 53810, 53811 and 53817 are presented in Appendix A as these samples were not used for metamorphic analysis.

53815 CORDIERITE–ANDALUSITE–STAUROLITE SCHIST

The matrix mineralogy is defined by biotite (100–1000 μm), quartz (<100 μm), plagioclase (<100 μm) and ilmenite (<50 μm). An S_1 fabric is defined predominantly by biotite (<600 μm); other more tabular biotite grains (<1000 μm) overprint the S_1 fabric. Poikiloblastic andalusite (up to 2 cm), cordierite (up to 2 cm) and staurolite (up to 1 cm) are aligned with S_1. Andalusite contains inclusions of quartz, plagioclase, ilmenite and biotite that are aligned with S_1 and occurs in contact with, but does not include, staurolite (Fig. 4a). There is no clear timing relationship between andalusite and cordierite as they are separated by large (up to 5 cm) distances. Cordierite poikiloblasts contain inclusions of quartz, ilmenite, biotite and staurolite that are aligned with S_1 (Fig. 4b). Staurolite poikiloblasts occur throughout the sample, rarely observed as being partially included or overprinting biotite and cordierite (Fig. 4b-c). In addition, staurolite commonly occurs concentrated near or at the margins of cordierite and andalusite (Fig. 4a-b). Staurolite contains inclusions of quartz, plagioclase and ilmenite that are not aligned with S_1. Poikiloblastic garnet (<1000 μm) is very rare and contains inclusions of quartz, plagioclase and ilmenite aligned with S_1. Garnet occurs in a cordierite–rich region but is not in contact with cordierite. Chlorite occurs mantling biotite grains and as rare (<50 μm) matrix grains aligned with S_1 (Fig. 4a). Based on the

grain sizes and fabrics, the interpreted peak assemblage is andalusite + cordierite + staurolite + biotite + garnet + ilmenite + plagioclase + quartz. However, this assemblage, particularly coexisting andalusite + cordierite + staurolite has an extremely restricted stability (e.g. Pattison, Spear, & Cheney, 1999; Pattison & Tinkham, 2009). As petrographic relationships are ambiguous, the actual peak assemblage may involve cordierite + andalusite (staurolite absent), cordierite + staurolite (andalusite absent) or andalusite + staurolite (cordierite absent). Post-peak chlorite and biotite can also be interpreted from these observations.

53816 GARNET–STAUROLITE SCHIST

The matrix mineralogy is defined by biotite (<100–300 μm), quartz (<150 μm), plagioclase (<150 μm) and ilmenite (<50 μm). A pervasive S_1 fabric is defined by biotite and quartz-rich layers. Lensoidal aggregates of granoblastic quartz are common, the long axis of which are aligned with S_1 (Fig. 4d). Planar, quartz-rich layers typically 200–500 μm in width occur at an angle of ~40° to S_1 and are interpreted to represent relict bedding (S_0). Porphyroblastic garnet (200–700 μm) and poikiloblastic staurolite (800–1400 μm) occur sparsely throughout the matrix. Garnet is commonly euhedral, (Fig. 4d) and contains minor inclusions of quartz and rare ilmenite. Staurolite is commonly euhedral and contains abundant inclusions of quartz (Fig. 4e). Inclusions within garnet and staurolite are not oriented. Matrix biotite grains defining S_1 are rarely observed deflecting around garnet. Chlorite that is aligned with S_1 is 100–1000 μm and does not contain biotite inclusions (Fig. 4f). Chlorite that overprints S_1 contains inclusions of biotite. Less common tabular biotite occurs at a high angle to S_1. The interpreted peak assemblage is garnet + staurolite + biotite + chlorite + ilmenite + plagioclase + quartz, with chlorite and biotite also occurring as post-peak minerals.

Table 2: Modal proportions or 'mode' of minerals present in samples selected for *P–T* modelling. Modes were visually estimated from thin section and hand sample observations. Mineral abbreviations: and (andalusite), bi (biotite), cd (cordierite), chl (chlorite), g (garnet), ilm (ilmenite), pl (plagioclase), st (staurolite), q (quartz), st (staurolite).

Sample	**Modal proportion (%)**									
	and	bi	cd	chl	g	ilm	pl	st	q	Total
53815	3	25	6	<1	<1	<1	30	4	30	~99
53816	–	35	–	2	2	<1	28	2	30	~99

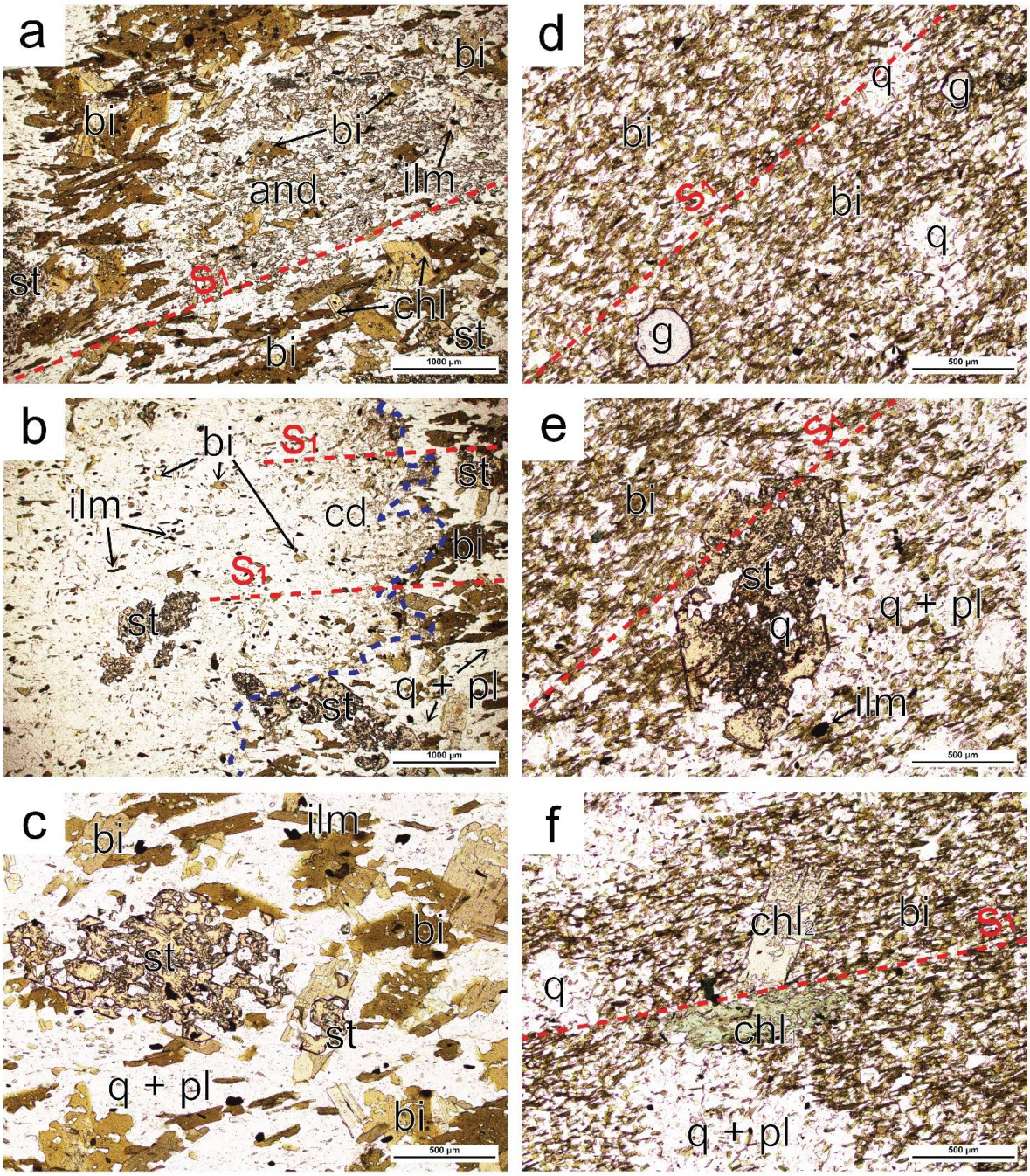

Figure 4: Petrographic photomicrographs a, b and c are from sample 53815 and d, e and f are from sample 53816. a) Andalusite grain aligned with S_1 with inclusions of matrix minerals, staurolite grains proximal to the andalusite grain boundary; b) Cordierite grain (boundary defined by blue dashed line) with inclusions of matrix minerals aligned with S_1, staurolite is observed being included in or overprinting cordierite and in the matrix proximal to cordierite; c) Staurolite present amongst matrix minerals with a smaller staurolite grain partially included or overprinting biotite; d) Matrix minerals and quartz-rich aggregates aligned with the S_1 fabric defined by biotite, minor euhedral garnet porphyroblasts; e) Staurolite grain with inclusions of quartz; f) Chlorite (chl_1) occurring aligned with the biotite defined S_1 fabric, second chlorite grain (chl_2) of different morphology at an angle to S_1.

METHODS

Geochronology

Zircon and monazite geochronology was employed determine the timing of sedimentation and metamorphism. Zircon geochronology was done on epoxy resin-mounted zircon grains from samples 53806 and 53810. Monazite geochronology was conducted *in situ*, i.e. in thin section for samples 53811, 53815, 53816 and 53817. Zircon and monazite U–Pb data were collected at Adelaide Microscopy. For detailed operational procedures and data reduction techniques, see Appendix F.

Phase Equilibria Forward Modelling

Whole-rock chemical compositions for phase equilibria modelling were done by Bureau Veritas, Perth. Phase equilibria models were calculated for samples 53815 and 53816 using THERMOCALC v3.40, the latest internally-consistent thermodynamic dataset 'ds6' (Holland & Powell, 1998; Holland & Powell, 2011) and activity–composition models re-parameterised for metapelitic rocks in the MnNCKFMASHTO system (Powell, White, Green, Holland, & Diener, 2014; White, Powell, Holland, Johnson, & Green, 2014a; White, Powell, & Johnson, 2014b). The model chemical system MnO–Na_2O–CaO–K_2O–FeO–MgO–Al_2O_3–SiO_2–H2O–TiO_2–O (MnNCKFMASHTO) was used due to it most accurately representing the major chemical composition of the selected samples and because MnO may significantly affect the stability of minerals such as garnet at amphibolite facies conditions (Mahar, Baker, Powell, Holland, & Howell, 1997; Tinkham & Ghent, 2005). Temperature–molar oxygen (T–M_o) models were used to constrain the oxidation state of the system, i.e. the amount of Fe_2O_3 versus FeO. The pressure used for the calculation of T–M_o models was determined by

considering the peak metamorphic assemblage recorded in each sample coupled with previously published petrogenetic grids and *P–T* models from White et al. (2014b). Subsolidus metamorphism is typically interpreted to involve an aqueous fluid and therefore models were calculated with H_2O set in excess. Phase equilibria models were contoured for the normalised abundances (mode) of phases using the automated software TCInvestigator (TCI) v2.0 (Pearce, White, & Gazley, 2015).

RESULTS

Detrital Zircon U–Pb Geochronology

53806

The total zircon yield from sample 53806 was very low. Grains range from ~70–250 μm, are mostly cloudy with a slight brown colouration and have aspect ratios between 2:1 and 3:1. Twenty-Eight U–Pb analyses were done on 20 zircon grains, twelve of these analyses are more than 5% discordant and were excluded from age considerations. The remaining 16 analyses yield $^{207}Pb/^{206}Pb$ ages between c. 1150 and 2330 Ma (Fig. 5a). Due to the low yield, distinct age peaks are less readily distinguished (Fig. 5b). However, single analysis ages occur at 1149 ± 97 Ma, 1693 ± 29 Ma and 2330 ±23 Ma and groupings of ages occur at c. 1300 Ma (n = 5), c. 1500 Ma (n = 2) and c. 2100 Ma (n = 6). Grains from the c. 1300 Ma and c. 1500 Ma sub-population display oscillatory zoning, and have respectively poor-to-high and moderately luminescent CL responses (Fig. 7c-d). Grains from the c. 2100 Ma population display oscillatory zoning or are unzoned, and have poor-to-highly luminescent CL responses (Fig. 7a-b). One grain from the c. 2100 Ma sub-population has a bright core with an age of 2330 ± 30 Ma and

a dark rim with an age of 2114 ± 22 Ma (Fig. 7a). The remaining grains range from sub-rounded to angular, display oscillatory zoning and have variable CL responses.

53810

The zircon yield for sample 53810 was high. Grains range from ~70–300 μm, are mostly cloudy with a slight brown colouration and have aspect ratios between 2:1 and 3:1. One-hundred-and-ninety-three U–Pb analyses were collected from 165 grains, 92 of these analyses are more than 5% discordant and were rejected from further interpretation. The remaining 101 analyses yield $^{207}Pb/^{206}Pb$ ages between c. 1250 and 2400 Ma (Fig. 6a). Age clusters occur at c. 1250–1400 Ma (n = 42), c. 1450–1550 Ma (n = 24), c. 1730 Ma (n = 2), c. 1880–1940 Ma (n = 4), c. 2000 –2150 Ma (n = 20), c. 2260 Ma (n = 5) and c. 2400 Ma (n = 4) (Fig. 6b). The major groupings occur at c. 1250–1400 Ma, c. 1450–1550 Ma and c. 2000–2150 Ma comprise 41.6, 23.8 and 19.8 percent of the dataset, respectively. Grain morphologies from the c. 1250–1350 Ma sub-population are typically heavily fractured euhedral grains, displaying oscillatory and sector zoning and have moderate-to-highly-luminescent CL responses (Fig. 7k-l). Within this sub-population is the youngest concordant grain, with a $^{207}Pb/^{206}Pb$ age of 1173 ± 85 Ma (104% concordance) (Fig. 7l). Grains from the c. 1450–1550 Ma sub-population typically display oscillatory zoning with some grains having two truncating generations of oscillatory zoning and have a moderately luminescent CL response (Fig. 7i-j). Grains from the c. 2000–2150 Ma sub-population are typically sub-rounded to sub-angular, display oscillatory and sector zoning and have a moderate-to-highly-luminescent CL response (Fig. 7f-g). Some grains display dark, unzoned rims

surrounding brighter cores (Fig. 7e). Grains from the subordinate sub-populations display oscillatory zoning, and variable CL responses.

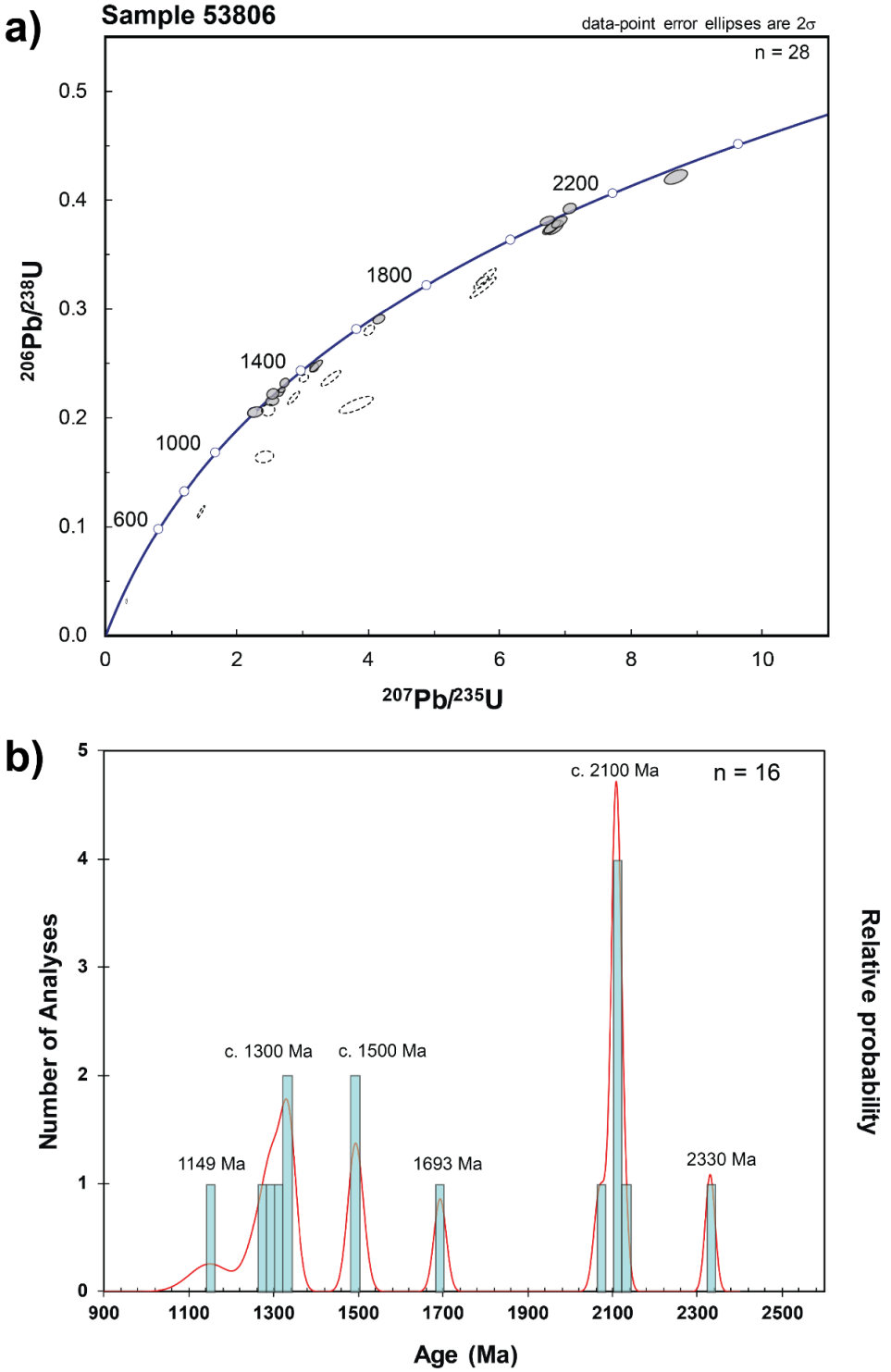

Figure 5: a) Wetherill concordia plot of detrital zircons from sample 53806. Grey filled error ellipses represent analyses ≤5 % discordant, dashed error ellipses are analyses with ≥5 % discordance which were excluded from age calculations; b) Probability density plot of analyses ≤5 % discordant. All data is presented as $^{207}Pb/^{206}Pb$ ages across both plots.

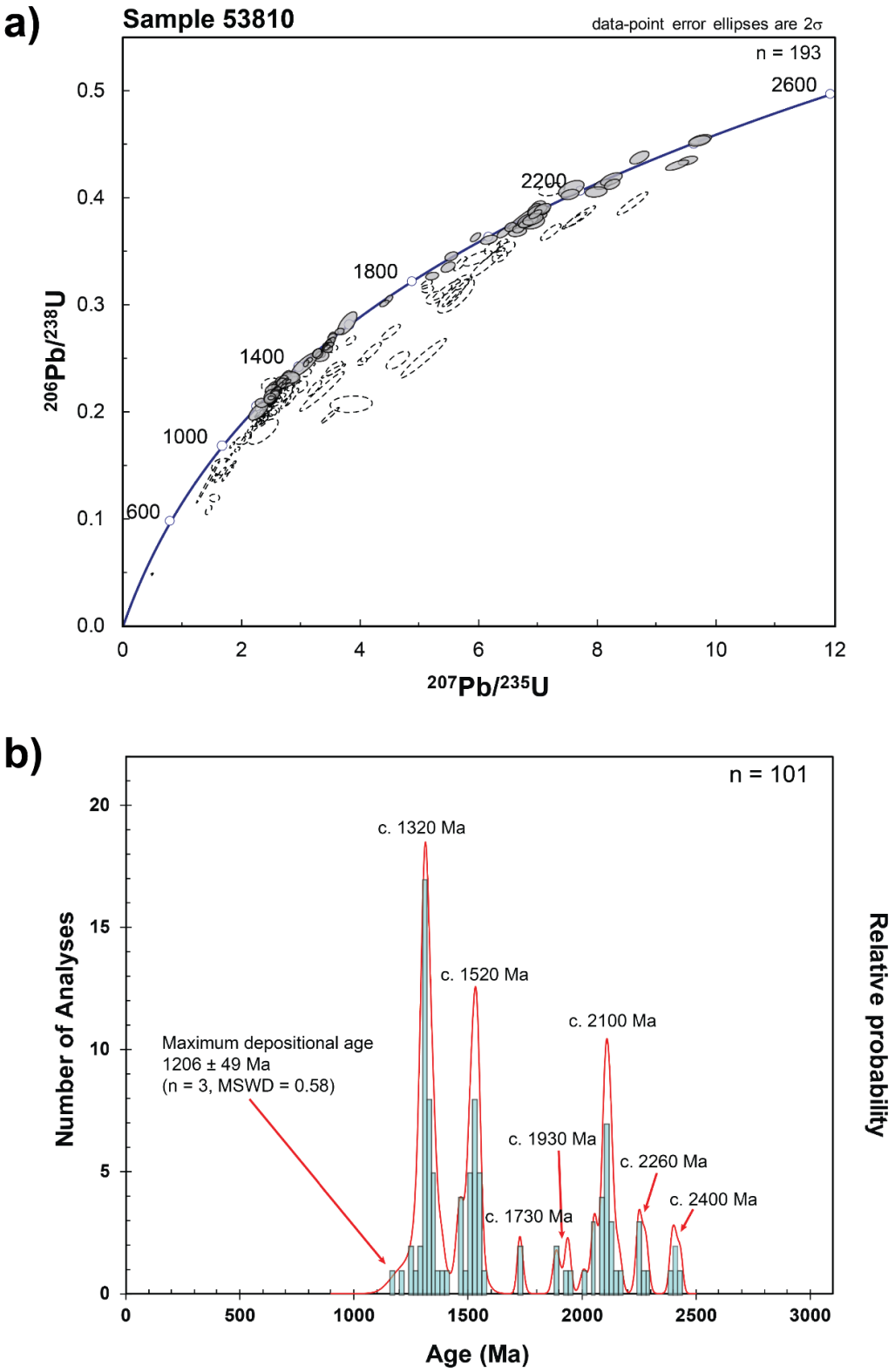

Figure 6: a) Wetherill concordia plot of detrital zircons from sample 53810. Grey filled error ellipses represent analyses ≤5 % discordant, dashed error ellipses are analyses with ≥5 % discordance which were excluded from age calculations; b) Probability density plot of analyses ≤5 % discordant. All data is presented as $^{207}Pb/^{206}Pb$ ages across both plots.

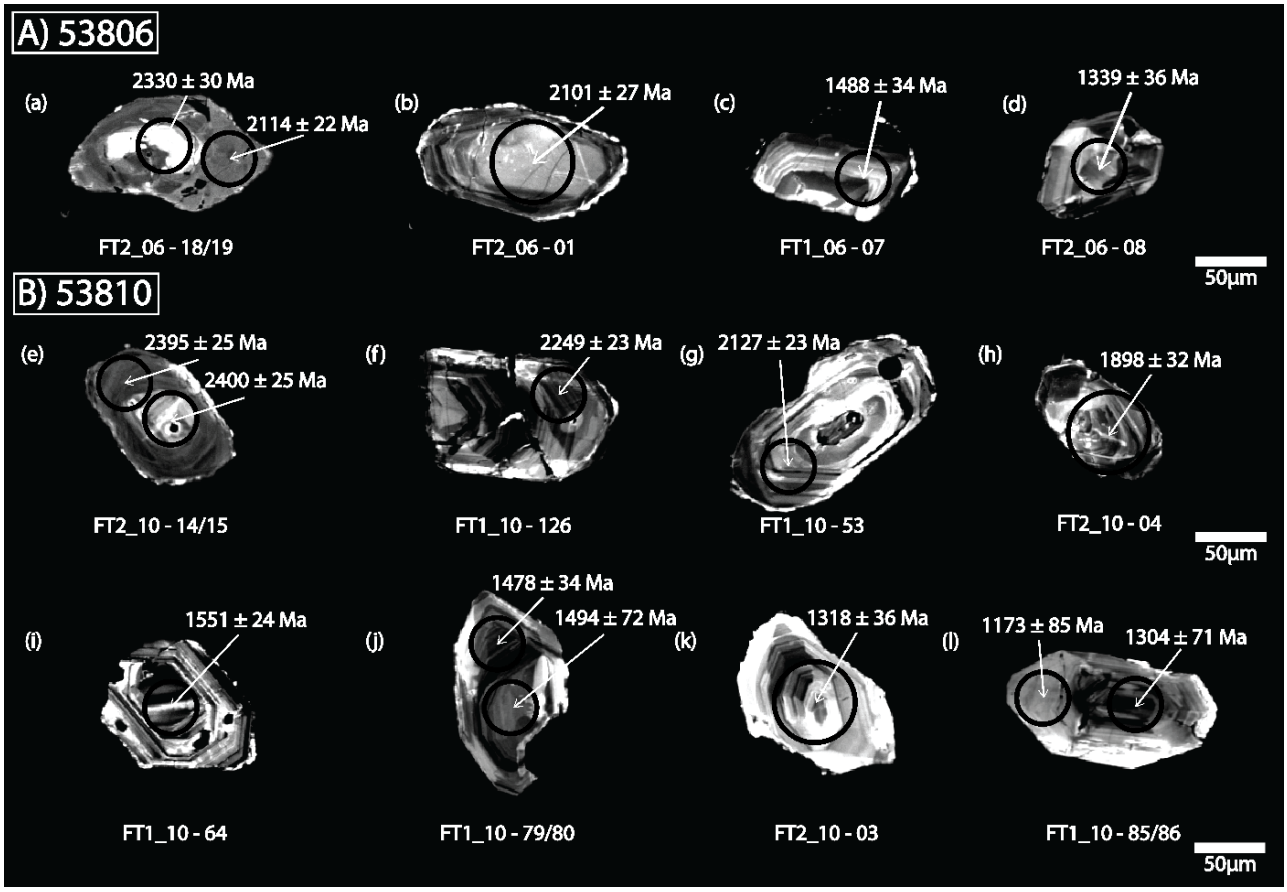

Figure 7: Representative CL images of zircons from samples 53806 (A) and 53810 (B). Spot sizes and locations for individual analyses are denoted by black circles, larger circles relate to a 29 µm spot and smaller circles relate to a 19 µm spot; a) Bright core with dark rim of contrasting ages; b) Oscillatory zoned sub-rounded grain with poor-to-moderate luminescence; c) Fragmented, oscillatory zoned grain with variable luminescence; d) Sub-angular, sector zoned grain with variable luminescence; e) Bright core with dark rim of similar age; f) Fragmented, oscillatory zoned grain with poor-to-high luminescence; g) Rare euhedral grain displaying oscillatory zoning around a xenocrystic core; h) Sub-rounded oscillatory zoned grain; i) Angular grain with two generations of oscillatory zoning; j) Angular, oscillatory zoned grain with moderate luminescence; k) Angular, oscillatory zoned grain with high luminescence; l) Oscillatory zoned grain with moderate luminescence, this grain is also the youngest concordant grain and one of three used to calculate the maximum depositional age. Spot analysis numbers are presented below each grain, data can be found in Appendix G. All data is presented as $^{207}Pb/^{206}Pb$ ages.

Monazite U–Pb Geochronology

53811

Twenty-Nine U–Pb analyses were done on 27 monazite grains. Five analyses were excluded from further age calculations based on discordance (i.e. no overlap of the analyses 2σ covaried error ellipse with the concordia curve) (Fig. 8a). An additional

anomalously young analysis with a $^{206}Pb/^{238}U$ age of 1015 ± 24 Ma (Fig. 8a) was also excluded from age calculations. The remaining 23 analyses range in age from c. 1052 to c. 1116 Ma and yield a $^{206}Pb/^{238}U$ weighted mean age of 1085.0 ± 7.1 Ma (n = 23, MSWD = 6.8). Rare grains display minor patchy zoning in backscattered electron (BSE) images, however most are unzoned (Fig. 8b).

53815

Nineteen U–Pb analyses were done on 18 monazite grains. Three of these analyses were rejected from further age calculations based on discordance (Fig. 9a). The remaining sixteen analyses yield a $^{206}Pb/^{238}U$ weighted mean age of 508.6 ± 3.7 Ma (n = 16, MSWD = 1.19) and a concordia age of 508.2 ± 3.3 Ma (n = 16, MSWD = 1.5, probability of concordia = 0.59). All the grains analysed are unzoned in BSE images (Fig. 9b).

53816

Forty U–Pb analyses were done on 38 monazite grains. Six of these analyses were excluded based on discordance (Fig. 10a). The remaining thirty-four analyses yield a $^{206}Pb/^{238}U$ weighted mean age of 512.3 ± 2.5 Ma (n = 34, MSWD = 2.00). The analysed grains are unzoned in BSE images (Fig. 10b).

53817

Fourteen U–Pb analyses were done on 13 monazite grains. Two of these analyses were excluded based on discordance (Fig. 11a). Three analyses yield older $^{206}Pb/^{238}U$ ages of 864 ± 26 Ma, 877 ± 60 Ma and 1037 ± 22 Ma and were also excluded. The remaining

nine analyses yield a $^{206}Pb/^{238}U$ weighted mean age of 528.9 ± 9.3 Ma (n = 9, MSWD = 3.50). The analysed grains appear unzoned in BSE images (Fig. 11b).

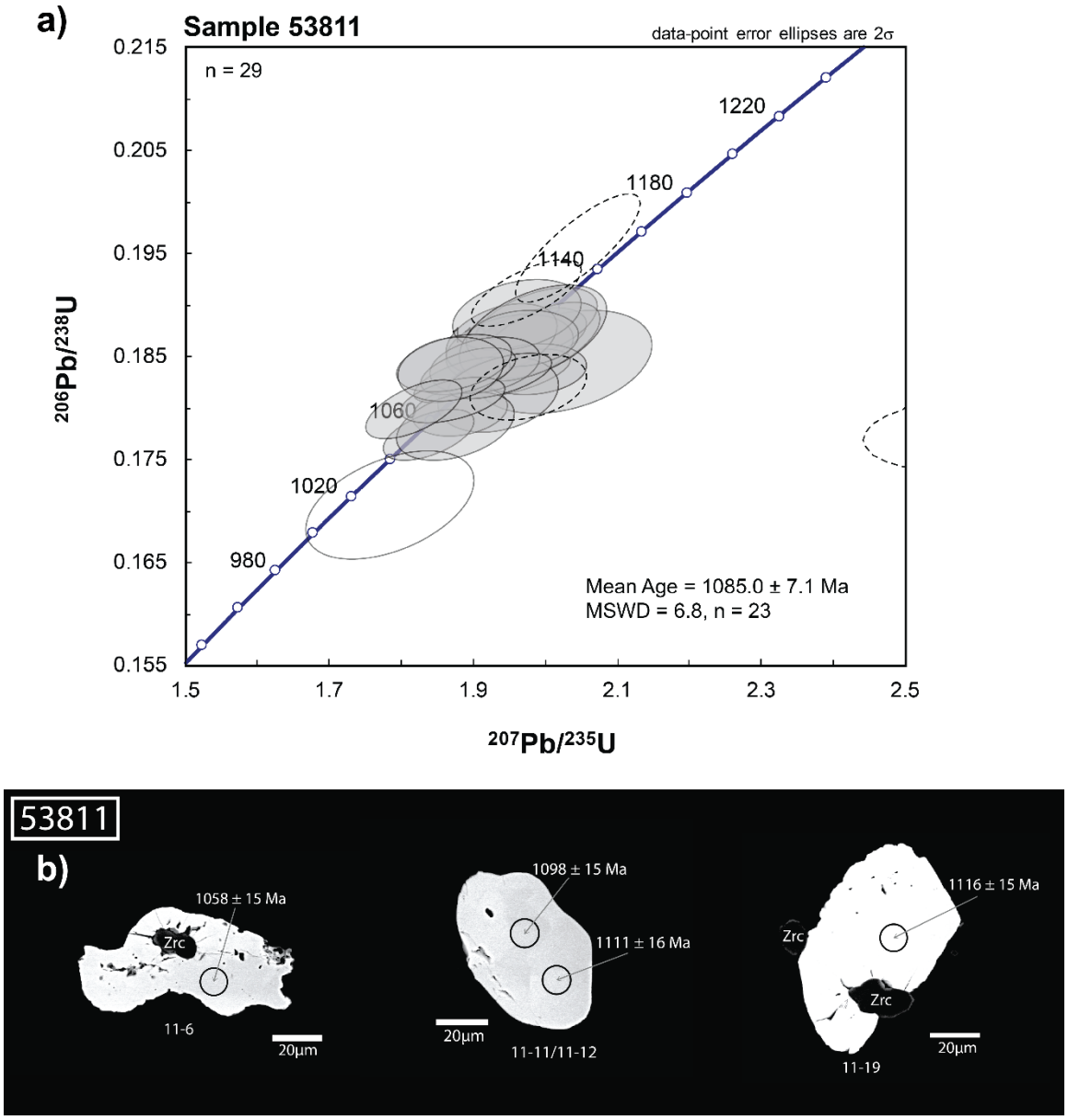

Figure 8: a) Wetherill concordia plot of all monazite U–Pb analyses from sample 53811. Grey filled ellipses are concordant analyses. These analyses were used to define the quoted weighted mean age. Ellipses with dashed outlines and no fill are discordant and rejected from U–Pb age calculations. Ellipses with no fill were excluded from age calculations due to not statistically constituting part of the main population; b) BSE images of representative monazite grains from sample 53811. Spot analysis numbers are presented below each grain, data can be found in Appendix H. All data is presented as $^{206}Pb/^{238}U$ ages.

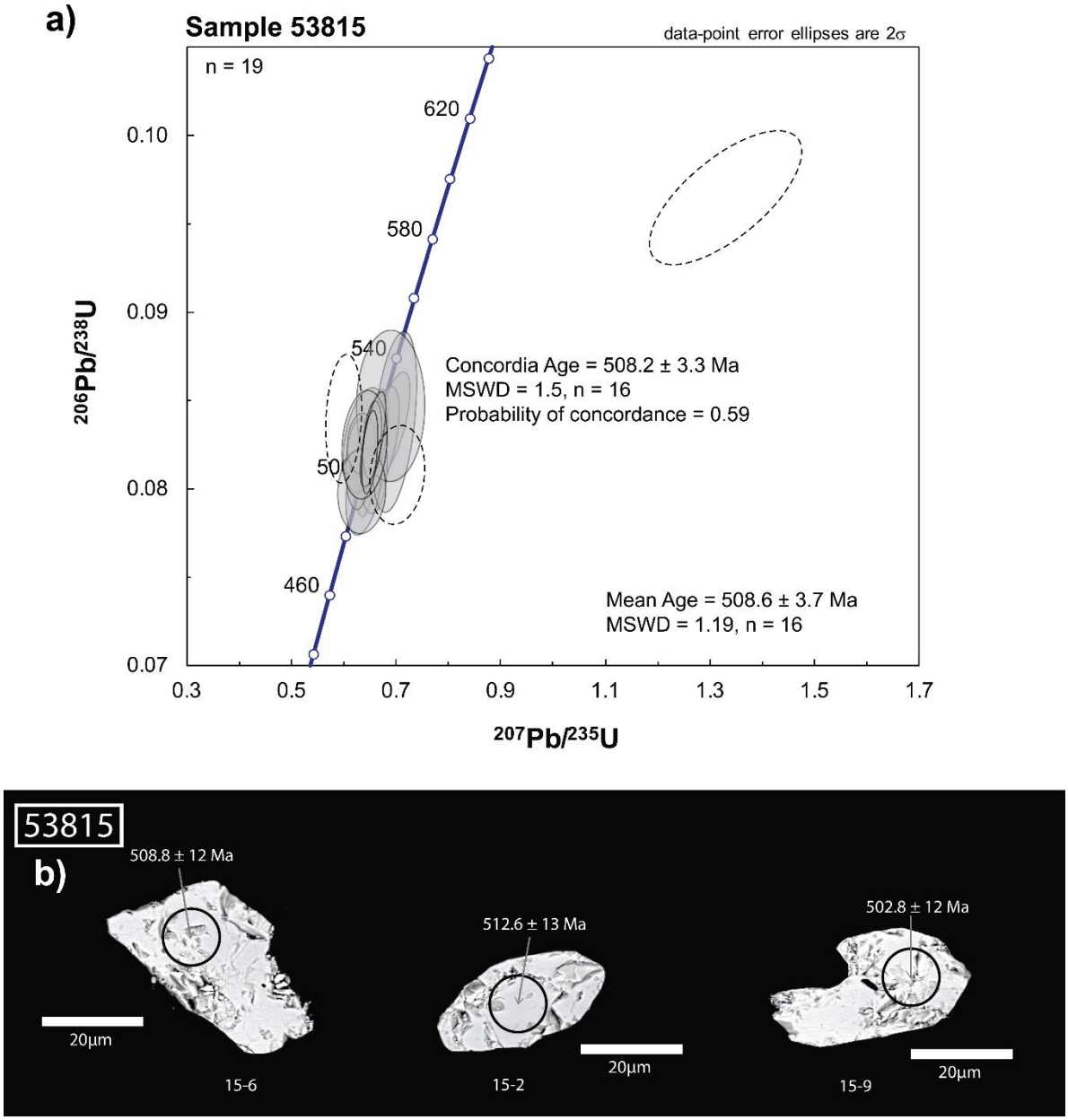

Figure 9: a) Wetherill concordia plot of all monazite U–Pb analyses from sample 53815. Grey filled ellipses are concordant analyses. These analyses were used to define the quoted weighted mean age and concordia age. Ellipses with dashed outlines and no fill are discordant and rejected from U–Pb age calculations; b) BSE images of representative monazite grains from sample 53815. Spot analysis numbers are presented below each grain, data can be found in Appendix H. All data is presented as $^{206}Pb/^{238}U$ ages.

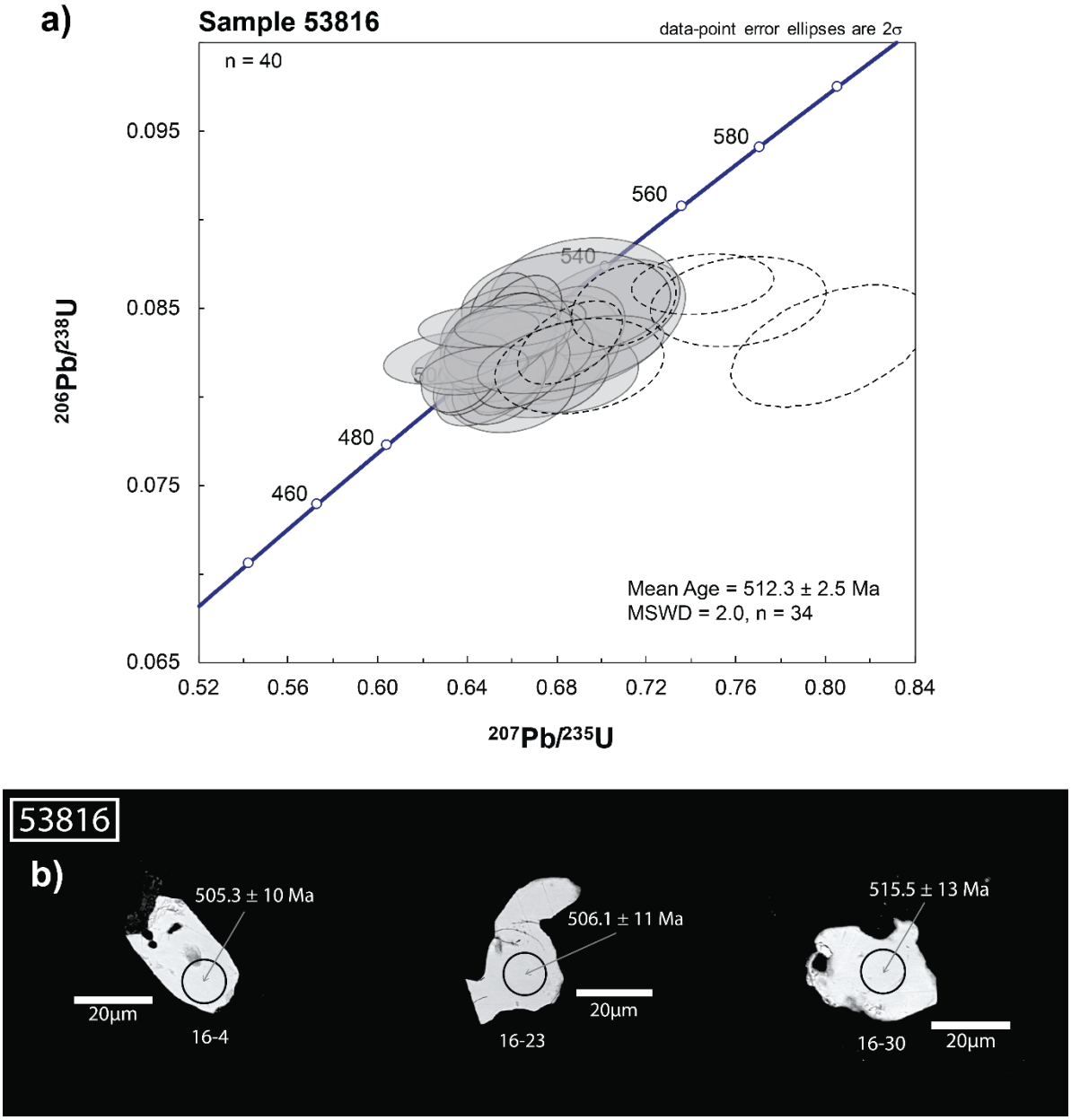

Figure 10: a) Wetherill concordia plot of all monazite U–Pb analyses from sample 53816. Grey filled ellipses are concordant analyses. These analyses were used to define the quoted weighted mean age. Ellipses with dashed outlines and no fill are discordant and rejected from U–Pb age calculations; b) BSE images of representative monazite grains from sample 53816. Spot analysis numbers are presented below each grain, data can be found in Appendix H. All data is presented as $^{206}Pb/^{238}U$ ages.

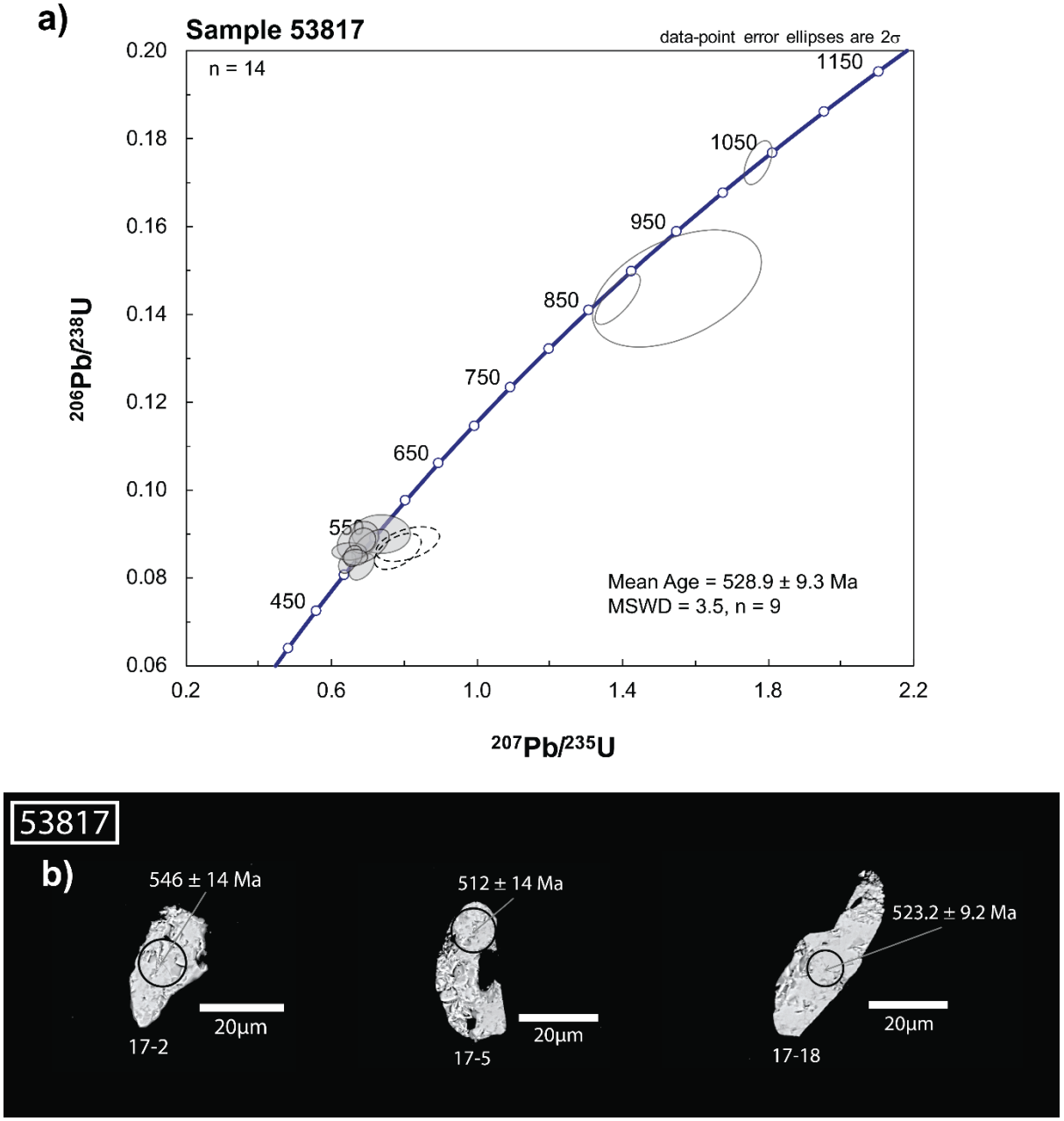

Figure 11: a) Wetherill concordia plot of all monazite U–Pb analyses from sample 53817. Grey filled ellipses are concordant analyses. These analyses were used to define the quoted weighted mean age. Ellipses with dashed outlines and no fill are discordant and rejected from U–Pb age calculations. Ellipses with black outline are rejected from age calculations due to not statistically constituting part of the main population; b) BSE images of representative monazite grains from sample 53817. Spot analysis numbers are presented below each grain, data can be found in Appendix H. All data is presented as $^{206}Pb/^{238}U$ ages.

Phase Equilibria Forward Modelling

Samples 53815 and 53816 were selected for phase equilibria forward modelling as their metapelitic compositions make them sensitive to changes in *P–T* conditions. The $T–M_o$ models for both samples were calculated at a pressure of 3.5 kbar, based on the presence of andalusite within the metasedimentary sequence (Crowe, 1994). *P–T* models were calculated using an oxidation state determined by the corresponding $T–M_o$ model.

SAMPLE 53815

The calculated $T–M_o$ model for sample 53815 is presented in Figure 12. As previously stated, there is ambiguity surrounding the peak assemblage. However, for the purposes of determining the oxidation state this is not a major issue, as the sample does not contain magnetite; therefore, M_o must be <0.11. The possible peak assemblage fields are outlined by bold coloured lines in Figure 12: black for the andalusite + cordierite + staurolite + biotite + garnet + ilmenite + plagioclase + quartz field, red for the equivalent but andalusite-absent field and blue for the equivalent but staurolite-absent field. These fields occur at M_o ~ 0–0.11 and T ~ 580–605 °C. An oxidation state of M_o = 0.07 was selected to avoid the stabilisation of magnetite at higher temperatures than the inferred peak assemblage fields at 3.5 kbar.

The calculated *P–T* model for sample 53815 is presented in Figure 13. The possible peak assemblage fields are outlined by bold coloured lines in Figure 13: black for the cordierite + staurolite + biotite + garnet + ilmenite + plagioclase + quartz field and blue for the andalusite + cordierite + biotite + garnet + ilmenite + plagioclase + quartz field. Together these span the *P–T* range of ~2.45–4.70 kbar and ~550–635 °C. A narrow

field with the full assemblage of andalusite + cordierite + staurolite + biotite + garnet + ilmenite + plagioclase + quartz occurs between the blue and black outlined fields. The absence of peak chlorite provides a lower temperature constraint of ~550–590 °C whereas the presence of garnet provides a lower pressure constraint of ~2.5–3 kbar. The presence of andalusite-bearing rather than kyanite or sillimanite-bearing lithologies in the Fisher Terrane suggests that pressures did not exceed 3.7 kbar.

SAMPLE 53816

The calculated T–M_o model for sample 53816 is presented in Figure 14. The interpreted peak assemblage of garnet + staurolite + biotite + chlorite + ilmenite + plagioclase + quartz occurs at M_o ~ 0–0.15 and T ~ 560–580 °C. Toward higher M_o values (more oxidised), magnetite–bearing assemblages occur. The oxidation state of M_o = 0.08 was selected to avoid the stabilisation of magnetite at temperatures higher than the inferred peak field.

The calculated P–T model for sample 53816 is presented in Figure 15a. The interpreted peak assemblage field of garnet + staurolite + biotite + chlorite + ilmenite + plagioclase + quartz occurs between 3.1–6.2 kbar and 564–596 °C (Fig. 15a-b). The upper and lower temperature bounds for the field are defined by the disappearance of chlorite and garnet, respectively. The peak assemblage field spans the kyanite–sillimanite and andalusite–sillimanite reaction boundaries. However, the presence of andalusite-bearing lithologies within the same metasedimentary package suggests that the most likely peak conditions are 3–4 kbar and 565–575 °C.

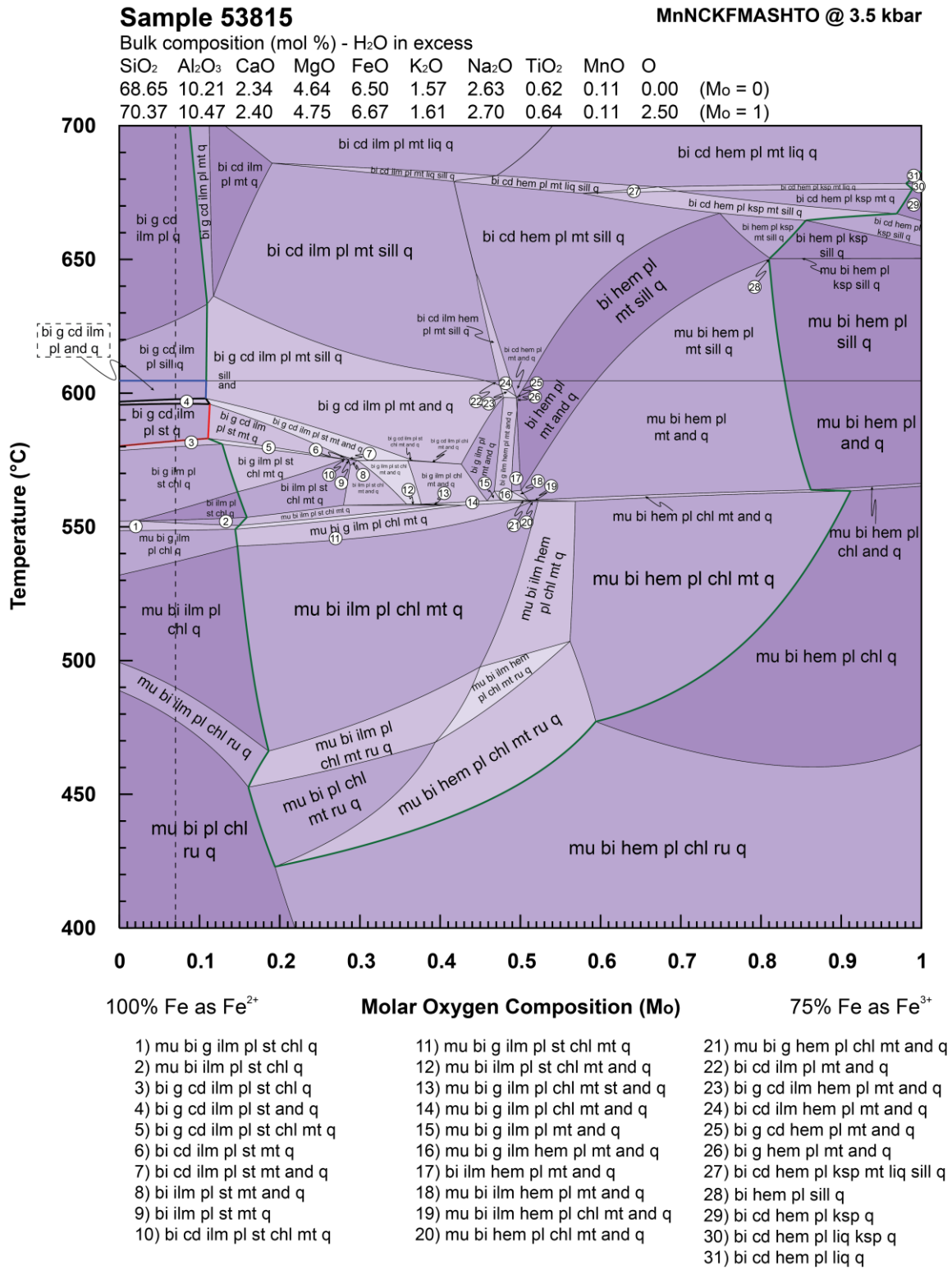

1) mu bi g ilm pl st chl q
2) mu bi ilm pl st chl q
3) bi g cd ilm pl st chl q
4) bi g cd ilm pl st and q
5) bi g cd ilm pl st chl mt q
6) bi cd ilm pl st mt q
7) bi cd ilm pl st mt and q
8) bi ilm pl st mt and q
9) bi ilm pl st mt q
10) bi cd ilm pl st chl mt q
11) mu bi g ilm pl st chl mt q
12) mu bi ilm pl st chl mt and q
13) mu bi g ilm pl chl mt st and q
14) mu bi g ilm pl chl mt and q
15) mu bi g ilm pl mt and q
16) mu bi g ilm hem pl mt and q
17) bi ilm hem pl mt and q
18) mu bi ilm hem pl mt and q
19) mu bi ilm hem pl chl mt and q
20) mu bi hem pl chl mt and q
21) mu bi g hem pl chl mt and q
22) bi cd ilm pl mt and q
23) bi g cd ilm hem pl mt and q
24) bi cd ilm hem pl mt and q
25) bi g cd hem pl mt and q
26) bi g hem pl mt and q
27) bi cd hem pl ksp mt liq sill q
28) bi hem pl sill q
29) bi cd hem pl ksp q
30) bi cd hem pl liq ksp q
31) bi cd hem pl liq q

Figure 12: Calculated *T–Mo* model for sample 53815. The possible peak assemblage fields are outlined in bold coloured lines: red outline = bi + g + cd + ilm + pl + st + q; black outline = bi + g + cd + ilm + pl + st + and + q; blue outline = bi + g + cd + ilm + pl + and + q. *Mo* value used for calculation of *P–T* model for the same sample is indicated by the vertical dashed black line (*Mo* = 0.07). Magnetite zero–mode boundary is coloured green throughout the diagram. Field colour shading is related to the variance of the assemblage, where darker fields represent higher variance assemblages. Variance (V) = C-P+2, where C = the number of components (MnNCKFMASHTO = 11) and P = the number of phases.

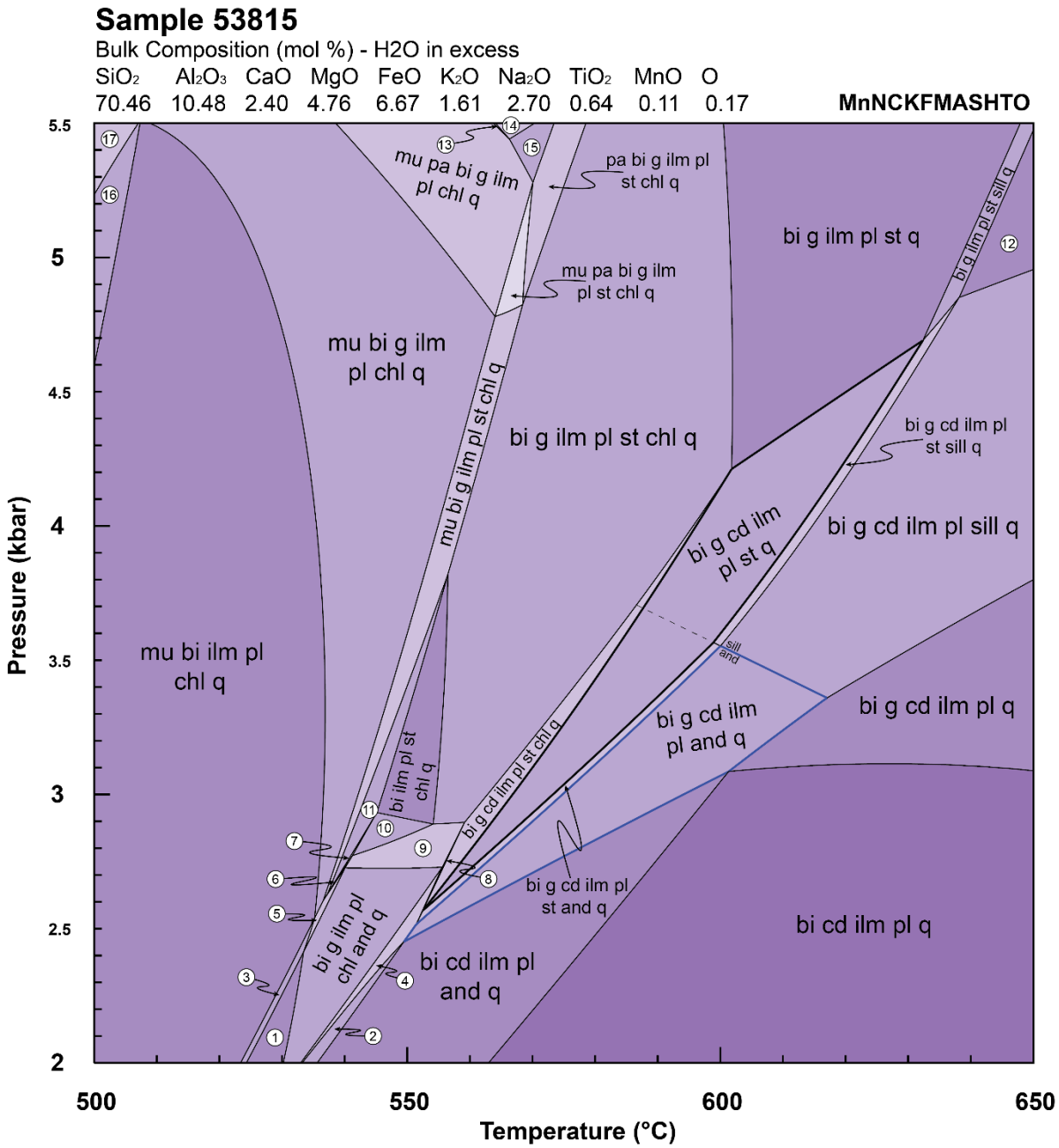

1. bi ilm pl chl and q
2. bi cd ilm pl chl and q
3. mu bi ilm pl chl and q
4. bi g cd ilm pl chl and q
5. mu bi g ilm pl chl and q
6. mu bi g ilm pl st chl and q
7. mu bi ilm pl st chl and q
8. bi g cd ilm pl st chl and q
9. bi g ilm pl st chl and q
10. mu bi ilm pl chl and q
11. mu bi ilm pl st chl q
12. bi g ilm pl sill q
13. mu pa ma bi g ilm pl chl q
14. pa ma bi g ilm pl chl q
15. pa bi g ilm pl st q
16. mu bi ilm pl chl ru q
17. mu bi g ilm pl chl ru q

Figure 13: Calculated *P–T* model for sample 53815. The possible peak assemblage fields are outlined in bold coloured lines: black outline = bi + g + cd + ilm + pl + st + q; blue outline = bi + g + cd + ilm + pl + and + q. Field colour shading is related to the variance of the assemblage, where darker fields represent higher variance assemblages. Variance (V) = C-P+2, where C = the number of components (MnNCKFMASHTO = 11) and P = the number of phases.

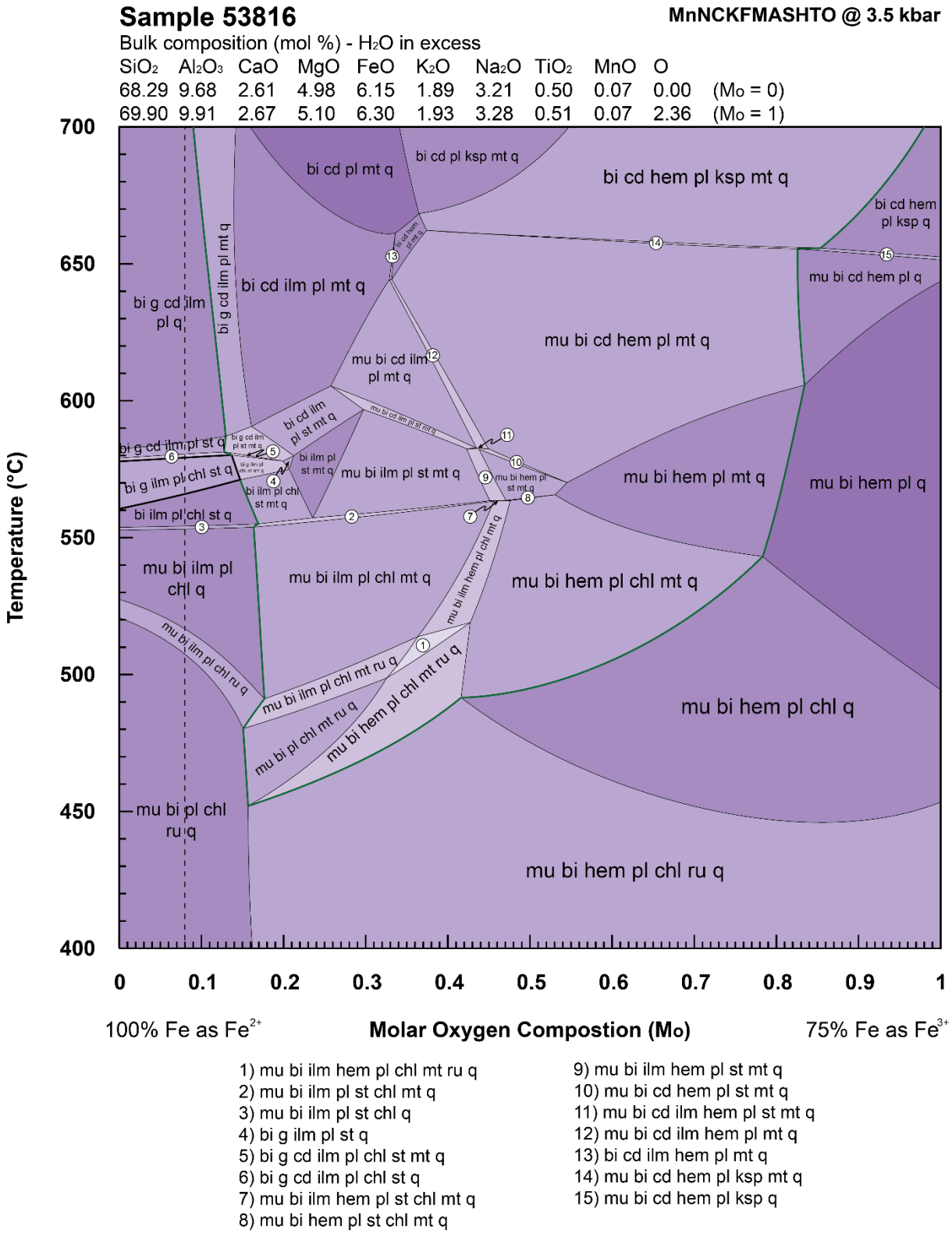

Figure 14: Calculated *T*–*M*o model for sample 53816. The interpreted peak assemblage field of bi + g + ilm + pl + chl + st + q is outlined in bold black lines. *M*o value used for calculation of *P*–*T* model for the same sample is indicated by the vertical dashed black line (*M*o = 0.08). Magnetite zero–mode boundary is coloured green throughout the diagram. Field colour shading is related to the variance of the assemblage, where darker fields represent higher variance assemblages. Variance (V) = C-P+2, where C = the number of components (MnNCKFMASHTO = 11) and P = the number of phases.

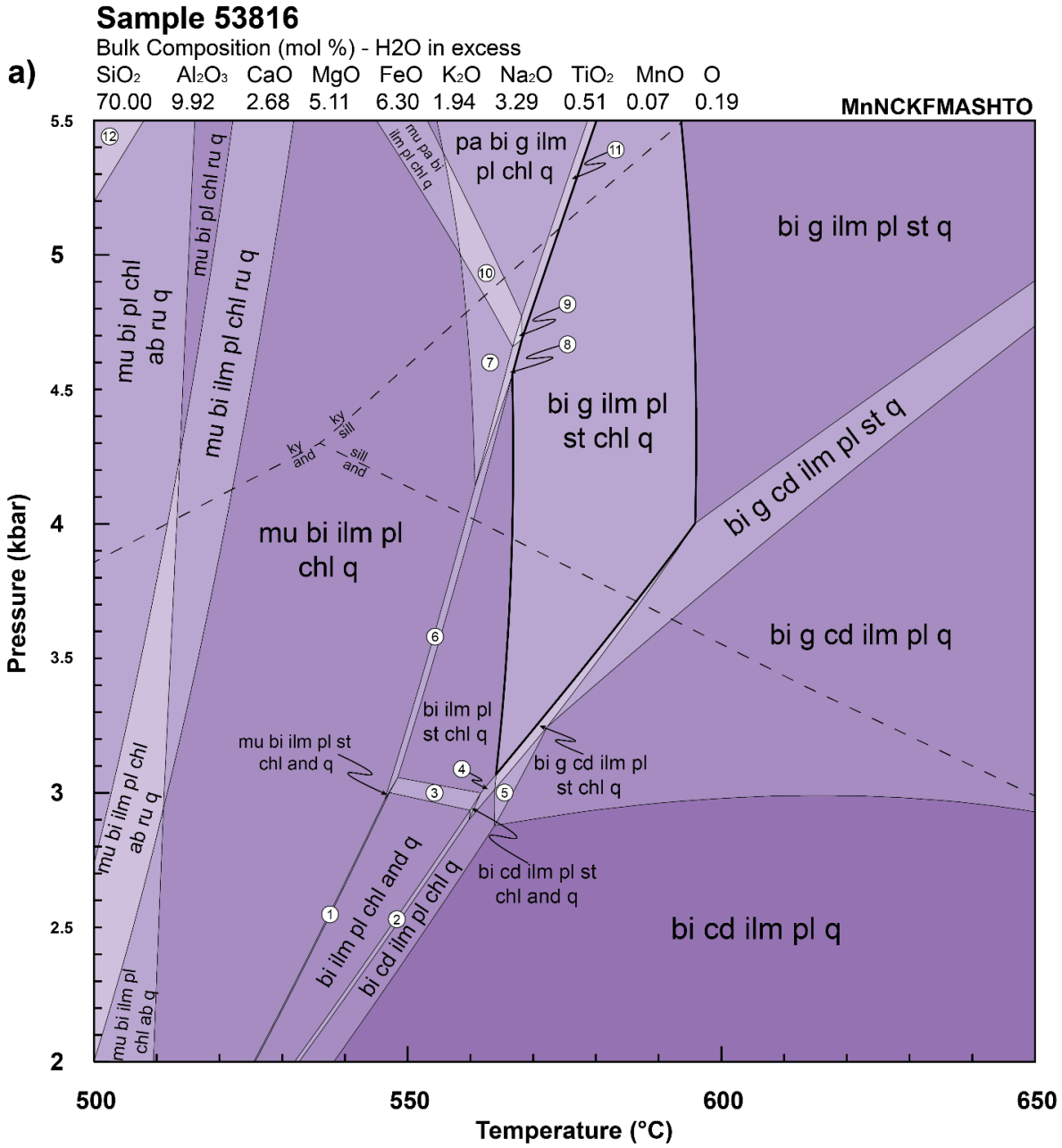

1. mu bi ilm pl chl and q
2. bi cd ilm pl chl and q
3. bi ilm pl st chl and q
4. bi cd ilm pl st chl q
5. bi g ilm pl st chl q
6. mu bi ilm pl st chl q
7. mu bi g ilm pl chl q
8. mu bi g ilm pl st chl q
9. mu pa bi g ilm pl st chl q
10. mu pa bi g ilm pl chl q
11. pa bi g ilm pl st chl q
12. mu bi pl ep chl ab ru q

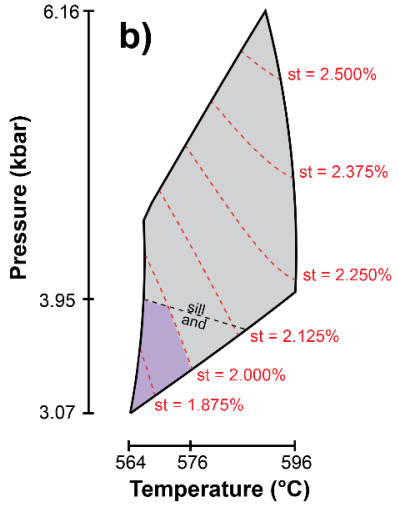

Figure 15: a) Calculated *P–T* model for sample 53816. The interpreted peak assemblage field of bi + g + ilm + pl + st + chl + q is outlined in bold black lines. Field colour shading is related to the variance of the assemblage, where darker fields represent higher variance assemblages. Variance (V) = C-P+2, where C = the number of components (MnNCKFMASHTO = 11) and P = the number of phases; b) Interpreted peak assemblage field with contoured modal abundance isopleths of staurolite calculated using TCI.

DISCUSSION

Geochronology

The rocks of the Fisher Terrane analysed during this study record high-temperature, amphibolite to granulite facies metamorphism (Crowe, 1994; Mikhalsky et al., 1996). Zircon and monazite geochronometers were used to assess the depositional age and source of metasediments and the timing of metamorphism. The ability of zircon and monazite to grow and be preserved during high-temperature magmatic and metamorphic processes, coupled with their refractory nature, makes these minerals well-suited for studies such as this (e.g. Spear & Pyle, 2002; Taylor, Kirkland, & Clark, 2016). The resistivity of zircon to mechanical weathering and its relative unresponsiveness to subsolidus metamorphism and resetting makes it an ideal mineral for characterising the depositional history of metasediments (e.g. Fedo, Sircombe, & Rainbird, 2003). Monazite is useful for constraining the timing of prograde and peak metamorphism, as metamorphic monazite growth at amphibolite facies in metapelites is well known (e.g. Janots et al., 2008; Smith & Barreiro, 1990; Wing, Ferry, & Harrison, 2003).

U–PB DETRITAL ZIRCON GEOCHRONOLOGY

To interpret the zircon geochronology in this study, it is necessary to determine the origin of the zircon grains. The morphology and internal structure, observed via CL imaging, is the most common way to deduce the origin of individual zircon grains

(Corfu, Hanchar, Hoskin, & Kinny, 2003; Rubatto & Gebauer, 2000; Taylor et al., 2016). Zircon grains exhibiting oscillatory or sector zoning are interpreted to represent grains of igneous origin (Corfu et al., 2003). Inherited grains generally display xenocrystic cores mantled by a second generation of oscillatory zoning (Corfu et al., 2003). Metamorphic zircon generally occurs as sub-rounded grains or overgrowths on pre-existing grains, they are also typified by their homogeneous CL responses (Corfu et al., 2003; Taylor et al., 2016). Although zircon is typically considered to grow at high-temperatures in melt bearing assemblages (e.g. Rubatto, Williams, & Buick, 2001), there are instances where zircon grows at subsolidus conditions (Dempster, Hay, Gordon, & Kelly, 2008; Rasmussen, 2005).

Zircon grains from samples 53806 (n = 16) and 53810 (n = 101) both display very similar internal structures. The CL response of individual grains vary dramatically, however there is similarity between grains in the same sub-populations. Most of the grains from these two samples are characterised by oscillatory zoning with less common sector zoning. Few grains display xenocrystic cores (e.g. Fig. 7g), of which none were analysed due to their very small (<20 μm) diameters. Also present are grains displaying cores with oscillatory zoning mantled by what are interpreted to be metamorphic rims due to their characteristic lack of structure and homogeneous CL response (Fig. 7a) (Corfu et al., 2003; Taylor et al., 2016). However, based on the age disparity between these metamorphic overgrowths and the timing of metamorphism determined in the Fisher Terrane in this study (discussed below), the inference is made that these grains were metamorphosed prior to their transportation and subsequent deposition. Therefore, it can be concluded that all zircons present in these samples are detrital in nature.

SEDIMENT DEPOSITIONAL AGE AND PROVENANCE

The age data collected from detrital zircons in samples 53806 and 53810 effectively record the same age spectrum (Fig. 5b, 6b). Despite the small zircon yield from 53806, the spatial proximity (< 1 km; Fig. 2) and the lack of any know major structural discontinuities between sample locations (Crowe, 1994), it is assumed that the age spectra for both samples are effectively the same. The maximum depositional age for the metasedimentary succession at Fisher Massif is constrained to 1206 ± 49 Ma (n = 3, MSWD = 0.58) based on the $^{207}Pb/^{206}Pb$ weighted mean age of the three youngest concordant grains which overlap at 2σ (Fig. 6b; Dickinson & Gehrels, 2009).

Many potential sources for the metasediments of the Fisher Terrane exist, of which the most plausible are outlined in summary Table 3. The youngest c. 1250–1400 Ma sub-population is most likely sourced from the Fisher Terrane itself. Magmatism at c. 1450–1550 Ma has not been identified in the Fisher Terrane, but this grouping approximately corresponds to magmatic ages from parts of the Rayner–Eastern Ghats Complex. The older Paleoproterozoic aged sub-populations could have been sourced from either the Rayner–Eastern Ghats Complex or the Lambert Terrane (Table 3). However, the key identification of c. 2400 Ma zircons with metamorphic rims of c. 2100 Ma (e.g. Fig. 7a) suggests some input from the Lambert Terrane, as this age population is not identified elsewhere in the region (Corvino et al., 2008). Furthermore, the absence of any Rayner-(c. 1000–900 Ma) aged detrital grains suggests that metasediments of Fisher Massif were deposited prior to the onset of the Rayner Event at c. 1000 Ma. The interpretation that deposition of the metasedimentary rocks predates the Rayner event is consistent with the inferred maximum depositional age of >1200 Ma for both samples. The

absence of any Rayner-aged metamorphic zircon (and monazite, see below) growth in these metasedimentary rocks requires them to either have remained at a very shallow level in the crust throughout the Rayner Event, or that the Fisher Terrane was an exotic terrane that did not amalgamate with the Rayner Complex until after the main phase of Rayner-aged metamorphism.

Table 3: Compiled table of geochronological data used for comparison with the detrital age data from this study to assess provenance of the metasediments present in the Fisher Terrane. All ages are zircon U–Pb ages unless otherwise stated.

Detrital zircon age range (this study)	Study with approximate age	Age range in study	Terrane of study	Location	Event Dated	Rock type
c. 1250–1400 Ma	Beliatsky et al. (1994)	c. 1300 Ma 1224 ± 1.1 Ma (youngest) 1310 ± 9.0 Ma (oldest)	Fisher Terrane	Fisher Massif	Volcanism	Various metavolcanics (rhyodacite, andesite)
	Alexeev et al. (2010)	c. 1420–1240 Ma 1244 ± 11 Ma (andesitic basalt) 1399 ± 11 Ma (plagiogranite)	Fisher Terrane	Fisher Massif	Volcanism	Andesitic basalt, plagiogranite
	Mikhalsky et al. (1999)	1289 ± 10 Ma	Fisher Terrane	Mount Willing	Volcanism	Biotite–amphibole plagiogneiss
	Kinny et al. (1997)	1293 ± 28 Ma	Fisher Terrane	Fisher Massif	Magmatism	Granodiorite
c. 1450–1550 Ma	Black, Harley, Sun, and McCulloch (1987)	c. 1500 Ma	Rayner Complex	Amphitheatre Lakes	Magmatism (protolith emplacement)	Felsic orthogneiss
	Upadhyay, Gerdes, and Raith (2009)	c. 1380–1640	Eastern Ghats Province (India)	Vijayawada	Magmatism	Metapelite
	Liu et al. (2016)	c. 1490–1400 Ma	Eastern Princess Elizabeth Land	Mount Brown	Magmatism (protolith emplacement)	Mafic granulite and felsic orthogneiss
	Alexeev et al. (2010)	1440 ± 21 Ma	Fisher Terrane	Fisher Massif	Magmatic inheritance	Andesitic basalt

	Halpin et al. (2013)	c. 1450 Ma c. 1530 Ma	Reworked Napier Complex (Kemp Land)	Oygarden Group	Metamorphism	Metapelitic gneiss
c. 1730 Ma	Mikhalsky, Henjes-Kunst, Belyatsky, Roland, and Sergeev (2010)	c. 1740 Ma	Lambert Terrane	Rofe Glacier	Vein emplacement	Felsic vein (microtonalite)
	Alexeev et al. (2010)	1793 ± 41 Ma	Fisher Terrane	Fisher Massif	Magmatic inheritance	Andesitic Basalt
	Young and Black (1991)	c. 1700–2000 Ma	Rayner Complex	Mawson Coast	Zircons from a felsic gneiss xenolith within charnockite	Felsic gneiss xenolith within charnockite
c. 1880–1940 Ma	Kinny et al. (1997)	c. 1900 Ma	Fisher Terrane	Fisher Massif	Magmatic inheritance	Metadacite
	Phillips et al. (2006)	1862 ± 12 Ma	Lambert Terrane	Komsomolsky Peak	Detrital zircon age population	Quartzite
c. 2000–2150 Ma	Corvino et al. (2008)	c. 1990–1960 Ma (amphibolite) 2104 ± 6 Ma (pegmatite) 2152 ± 10 Ma (augen gneiss) 2155 ± 77 Ma (felsic leucosome) c. 2160–2060 Ma (amphibolite)	Lambert Terrane	Rofe Glacier, Waller hills, Harbour Bluff	Metamorphism, pegmatite emplacement, leucosome crystallisation	Amphibolite, augen gneiss, felsic leucosome
	Mikhalsky et al. (2006a)	2065 ± 23 Ma	Lambert Terrane	Harbour Bluff	Metamorphism	Augen gneiss
	Phillips et al. (2006)	c. 2200–2000	Lambert Terrane	Cumpton Massif, Mount Maguire, Komsomolsky Peak	Detrital zircon age populations	Various Quartzites
	Boger et al. (2008)	2123 ± 12 Ma	Lambert Terrane	Harbour Bluff	Granitic protolith emplacement	Felsic orthogneiss

	Halpin, Gerakiteys, Clarke, Belousova, and Griffin (2005)	c. 1790–1870 Ma ($^{176}Hf/^{177}Hf$) c. 2150–2550 Ma ($^{176}Hf/^{177}Hf$)	Rayner Complex	Stillwell Hills	Protolith ages for charnockite magmas	Charnockite (protolith ages inferred)
c. 2260 Ma	Mikhalsky, Henjes-Kunst, and Roland (2007)	c. 2200 Ma	Lambert Terrane	Rofe Glacier	Metamorphism	Felsic vein
c. 2400 Ma	Corvino et al. (2008)	c. 2450–2380 Ma	Lambert Terrane	Waller Hills, Rofe Glacier, Sulzberger Bluff	Magmatism (protolith emplacement)	Felsic Orthogneiss
	Mikhalsky et al. (2006a)	2423 ± 18 Ma	Lambert Terrane	Lines Ridge	Granitoid emplacement	Leucocratic granodiorite
	Halpin et al. (2013)	c. 2430–2440 Ma	Kemp Land	Oygarden Group	Metamorphism	Metapelitic gneiss
	Carson, Ague, and Coath (2002)	c. 2450–2480 Ma	Enderby Land	Tonagh Island	Metamorphism	Orthogneiss

INTERPRETATION OF U–PB MONAZITE GEOCHRONOLOGY

The significance of monazite U–Pb age constraints are based upon the ability to discern whether monazite grew during metamorphism, is inherited (detrital) or has been subsequently reset by low-temperature fluid activity or metasomatism (e.g. Seydoux-Guillaume et al., 2012; Seydoux-Guillaume, Paquette, Wiedenbeck, Montel, & Heinrich, 2002; Williams, Jercinovic, Harlov, Budzyń, & Hetherington, 2011). Detrital monazite present in metapelitic rocks is typically not considered to persist above ~ 400 °C (Rasmussen & Muhling, 2007; Wing et al., 2003). The metapelitic rocks in the Fisher Terrane experienced temperatures of >550 °C, suggesting that the monazite U–Pb age data collected is not likely to reflect detrital ages. Furthermore, garnet grains in sample 53816 display prograde zoning (Appendix E). This suggests that the silicate mineral assemblage only records one major metamorphic event, and therefore the monazite ages are likely to reflect the timing of metamorphism.

The age data obtained from monazite U–Pb analyses from metapelitic samples 53815, 53816 and 53817 yield weighted mean monazite ages of 508.6 ± 3.7 Ma (MSWD = 1.19), 512.3 ± 2.5 Ma (MSWD = 2.0) and 528.9 ± 9.3 Ma (MSWD = 3.5) respectively. The weighted mean ages for samples 53815 and 53816 are within error of each other, suggesting that these two samples record the same metamorphic event. Sample 53817 records a slightly older weighted mean age, which may reflect that this sample has a slightly different whole-rock composition. Where monazite growth occurs along a single *P–T* path is a function of the whole-rock composition, including that which comprises accessory minerals, and major silicate mineral reactions (e.g. Corrie & Kohn, 2008; Gibson, Carr, Brown, & Hamilton, 2004; Pyle & Spear, 2003). Monazite age data

from all three samples spans from c. 538–505 Ma and corresponds to the c. 570–480 Ma ages for the Prydz Event amphibolite to granulite facies metamorphism observed throughout the PCMs and EAIS/Prydz Bay regions (e.g. Kelsey et al., 2007; Kelsey, Powell, Wilson, & Steele, 2003a; Liu et al., 2009a; Liu et al., 2009b; Morrissey et al., 2016; Phillips et al., 2009; Phillips et al., 2007a; Phillips et al., 2007b). These results coupled with the findings from the detrital zircon study suggest that the metasediments of the Fisher Terrane resided at a shallow level in the crust throughout the Rayner event (<4–6 km), so as to hold no record of its occurrence.

Sample 53811, a migmatitic felsic gneiss from Nilsson Rocks (Fig. 2), records a weighted mean monazite $^{206}Pb/^{238}U$ age of 1085.0 ± 7.1 Ma (MSWD = 6.8). The 'population' is defined by a spread of ages along concordia between c. 1050–1115 Ma and has a very high MSWD. Therefore, it is possible that the weighted mean age does not represent a short–lived pulse of tectonism and monazite growth and could instead reflect protracted monazite growth. Protracted growth of monazite was documented in high-temperature partially melted rocks from high thermal gradient terrranes by Hermann and Rubatto (2003), Korhonen, Clark, Brown, Bhattacharya and Taylor, (2013) and Morrissey et al. (2015) and in most cases, records the late prograde through to retrograde portion of the metamorphic history, where rocks begin to cool and melt crystallises. There is a lack of correlation between the monazite age data and microstructural location, thus inhibiting the ability to determine whether this range reflects a partial resetting of an older population or protracted monazite growth. However, it is possible that it records either the prograde–to–retrograde segment of the rocks history, or protracted cooling by analogy with other terranes.

Significant evidence for metamorphism occurring at c. 1085 Ma is not documented elsewhere in the PCMs. However, similarly aged magmatic events and slightly younger metamorphism considered to be related to the Rayner Event do occur. Along the Mawson Coast (Fig. 1a), the northmost extent of the Rayner Complex, Halpin et al. (2012) identified a phase of charnockitic magmatism occurring at c. 1080–1050 Ma. In the southern Rayner Complex at Mount Lanyon (Fig. 1c), metamorphic monazite ages are c. 1040–1010 Ma (Morrissey et al., 2015). Granitoid emplacement in the Fisher Terrane at Mount Willing and Fisher Massif occurred at c. 1110 and c. 1020 Ma respectively (Kinny et al., 1997; Mikhalsky et al., 2001). Further south in the Central Nunataks region of the cPCMs, Corvino et al. (2005), Corvino and Henjes-Kunst (2007) and Maslov et al. (2007) all identified the occurrence of c. 1080 Ma magmatism. Due to the spatial proximity of the Central Nunataks and similar magmatic ages, it is likely that the c. 1085 Ma metamorphism at Nilsson Rocks is related.

Pressure–Temperature Conditions

LIMITATIONS OF PHASE EQUILIBRIA FORWARD MODELLING

One limitation associated with phase equilibria forward modelling lies in the inability of the most current model chemical system, MnNCKFMASHTO, to totally account for the chemistry of the rocks being modelled. To quantitatively model the stability of phases throughout *P*–*T* space in a 'real' system, additional components such as Cr_2O_3, P_2O_5 and ZnO would need be accounted for. For example, staurolite can incorporate Zn into its structure. However, the current activity–composition (*a*–*x*) relationships in this model chemical system cannot account for the effect Zn has on staurolite stability (e.g. Ashworth, 1975). Another uncertainty arises from the inherent heterogeneity of the

rocks being modelled. The XRF-derived whole rock compositions are obtained from a three-dimensional volume of a sample. However, the mineralogy, petrographic relationships and modal abundance of minerals are obtained from a two-dimensional thin section of a sample. This can sometimes lead to a large degree of discrepancy between what is observed in thin section and the results from calculated phase equilibria models (Palin, Weller, Waters, & Dyck, 2016). The presence of numerous porphyroblastic minerals (e.g. cordierite, garnet, staurolite and andalusite) which progressively fractionate the effective bulk composition during their growth, coupled with the inherited compositional variability of a metamorphosed sediment, may explain the apparent disparities between some of the observed versus modelled outcomes.

PRESSURE–TEMPERATURE CONSTRAINTS

As previously stated, sample 53815 could at face value be interpreted to have a peak assemblage of andalusite + cordierite + staurolite + biotite + garnet + ilmenite + plagioclase + quartz. However, as can be seen in Figure 13 and as previously noted by Pattison et al. (1999) and Pattison and Tinkham (2009), the coexistence of andalusite + cordierite + staurolite has an extremely restricted stability. Therefore, the peak assemblage in the rock is more likely to involve either cordierite + andalusite (staurolite absent) or cordierite + staurolite (andalusite absent) (black and blue bold outlined fields in Fig. 13). The possibility of cordierite + andalusite (staurolite absent) as the peak assemblage is less favourable as staurolite is aligned with the main fabric and does not contain inclusions of cordierite, suggesting that it is not likely to be a retrograde mineral. This scenario would also lead to the interpretation of an anticlockwise *P–T* path, which is contradictory what is recorded by sample 53816. The other possible peak assemblage, cordierite + staurolite (andalusite absent), is more favourable. This scenario

places andalusite as a relict prograde mineral, which is plausible as Pattison and Tinkham (2009) characterise andalusite as being a sluggish reactor. Due to the ambiguity surrounding the peak assemblage along with the heterogenous nature of the porphyroblastic minerals, mineral modes were not used to aid in constraining the peak metamorphic conditions. The peak *P*–*T* conditions can be constrained to ~2.6–3.6 kbar and ~553–598 °C using the andalusite–sillimanite transition as the upper pressure–temperature bound as there is no sillimanite observed. These conditions correspond to an apparent thermal gradient between 166 °C/kbar and 212 °C/kbar.

The prograde trajectory for the *P*–*T* path of sample 53815 cannot be tightly constrained, However, adopting the interpretation of cordierite + staurolite as the peak assemblage with relict prograde andalusite would necessitate the prograde path to have passed through andalusite stability. This would suggest a gradual increase in pressure and temperature from andalusite stability with the progressive growth of staurolite followed by cordierite up to peak conditions. The presence of retrograde chlorite and absence of observable secondary andalusite growth or staurolite breakdown suggests cooling occurred with an unknown amount of decompression. A retrograde path exhibiting a sharp ‘hairpin’ type geometry following a similar path to the inferred prograde evolution is favourable to explain the presence of retrograde chlorite growth. However, there is no significant record of the post-peak evolution.

Sample 53816 has a peak assemblage of garnet + staurolite + biotite + chlorite + ilmenite + plagioclase + quartz, with chlorite and biotite also present as retrograde minerals. Due to the spatial proximity of samples (<1 km) 53815 and 53816, the

inference is made that the *P–T* conditions recorded by sample 53816 must exist within the region below the andalusite–sillimanite reaction (Fig. 15a-b). The extent of development of retrograde chlorite and biotite is minor. Therefore, modal abundances of the peak minerals as calculated in TCI remain valid for refining peak *P–T* conditions within the peak assemblage field. Calculated contours of the modal abundance of staurolite and the constraint that the rock was metamorphosed below the andalusite–sillimanite transition. constrains the peak *P–T* conditions during metamorphism to ~3.1–4.0 kbar and ~564–576 °C (Fig. 15b), resulting in an apparent thermal gradient between 144 °C/kbar and 182 °C/kbar.

The trajectory of the prograde *P–T* path enigmatic, but there are tentative constraints. An absence of andalusite in the rock likely precludes the prograde path from having passed through the andalusite stability field, as andalusite is a sluggish reactor (Pattison & Tinkham, 2009) and therefore relict andalusite would likely survive. A prograde *P–T* path with a gradual increase of pressure and temperature, analogous to what is inferred for sample 53815 is likely, as this is a typical burial-type trajectory. The absence of any significant retrograde mineral growth, besides chlorite and biotite, hinders the interpretation of the retrograde path trajectory. Notably, cordierite is absent from the rock, precluding the *P–T* path from having appreciable pressure–decrease from peak conditions.

Regional Implications

MESOPROTEROZOIC TO NEOPROTEROZOIC EVOLUTION

Metaigneous rocks of the Fisher Terrane were proposed to have evolved in an ocean island-arc setting, evidenced by comparatively young Sm–Nd model ages (T_{DM2} = 1700–1400 Ma) relative to the adjacent terranes and significant evidence of bimodal, calc-alkaline magmatism occurring at c. 1300 Ma (Beliatsky et al., 1994; Mikhalsky et al., 2006b; Mikhalsky et al., 1996, 1999). The metasedimentary rocks analysed in this study form an interlayered succession with metavolcanic rocks erupted at c. 1300 Ma (Beliatsky et al., 1994; Crowe, 1994). Together with the new constraint on the maximum depositional age of 1206 ± 49 Ma the data suggests these metasediments were present during the c. 1085 Ma metamorphic event identified in this study as well as later high-temperature Rayner-aged metamorphism. However, garnet grains in sample 53816 display prograde zoning and the monazite ages in these samples do not record significant evidence for earlier metamorphism, suggesting that the metasedimentary rocks of the Fisher Terrane escaped the earlier metamorphic events. This suggests they remained at shallow levels in the crust for the duration of the Rayner Event, likely at thermal conditions <400 °C, as to inhibit metamorphic monazite growth (Rasmussen & Muhling, 2007; Wing et al., 2003). Significant burial to result in metamorphism only occurred during the Prydz Event.

The Meso–Neoproterozoic evolution of the Fisher Terrane cannot be tightly constrained from the data of this study. However, a previously undocumented c. 1085 Ma metamorphic event has been identified in a migmatitic felsic gneiss (sample 53811) at

Nilsson Rocks that is the same age as magmatism in the Fisher Terrane, Shaw Massif, Clemence Massif and Lawrence Hills (Corvino et al., 2005; Corvino & Henjes-Kunst, 2007; Kinny et al., 1997; Maslov et al., 2007; Mikhalsky et al., 2001). A plausible scenario would link the c. 1085 Ma metamorphism at Nilsson Rocks to these similarly-aged magmatic events. Corvino and Henjes-Kunst (2007) characterise the c. 1080 Ma rocks of the Lawrence Hills as exhibiting calc-alkaline affinities and infer they had formed in a magmatic arc. The next outcrop to the south is c. 2500 Ma aged crust, inferred to represent a portion of the Lambert Terrane. No evidence has been found for a metamorphic event at c. 1080 Ma in the Lambert Terrane, hindering the possible interpretation of a c. 1085 Ma collision between the Fisher Terrane (and arc system) with the Lambert Terrane. A scenario where the Fisher Terrane formed as a volcanic arc at the margin of the Lambert Terrane could also be possible, but the comparatively old Sm–Nd model ages of the Lambert Terrane (T_{DM2} = 3400–3000 Ma; Mikhalsky et al. 2006) versus the young ages of the Fisher Terrane (T_{DM2} = 1700–1400 Ma; Mikhalsky et al. 2006) are not consistent with this interpretation, as older Sm–Nd model ages for the Fisher Terrane would be expected. However, an interpretation where the Fisher Terrane evolves spatially proximal to the Lambert Terrane during the Mesoproterozoic and before the regionally recognised Rayner Event is favourable to explain the observed detrital zircon age spectrum recorded in the metasediments of the Fisher Terrane. However, it remains uncertain why the Fisher Terrane seemingly escaped metamorphic reworking during the c. 1000–900 Ma Rayner Event, when the terranes to the north and south both hold a pervasive record of this event.

LATE NEOPROTEROZOIC TO CAMBRIAN EVOLUTION

Metapelites from the Fisher Massif record mid to upper amphibolite facies metamorphism during the period c. 538–505 Ma, attaining peak metamorphic conditions of ~2.6–4.0 kbar and ~553–576 °C. Conditions such as these relate to apparent thermal gradients of 144 to 212 °C/kbar, substantially hotter than normal crustal geotherms of ~60 °C/kbar (Brown, 2006, 2014). Thermal regimes such as this fall into the category of high-temperature–low-pressure (HT–LP) and ultrahigh-temperature (UHT) metamorphism, characterised by thermal gradients of ~75–150 °C/kbar and >150 °C/kbar respectively (Brown, 2006, 2014; Kelsey & Hand, 2015). These thermal regimes are synonymous with orogenic back-arc extensional settings, where greatly perturbed thermal regimes exist due to increased convective and advective heating from the asthenosphere (e.g. Hyndman, Currie, & Mazzotti, 2005; Sizova, Gerya, & Brown, 2014). Advective heat from magmatism, the consequence of thinned crust, can result in high-thermal gradient metamorphism within a regionally elevated thermal gradient regime. If the thermal gradients for the studied metapelites are reflective of a regional thermal regime (Fig. 16), the approximate crustal thickness would correspond to ~7 kbar (≤ 21 km, assuming a crustal density of 3.0 g/cm^3 and a 1000 °C Moho). Such thin crust supports the notion of an extensional tectonic regime during this time.

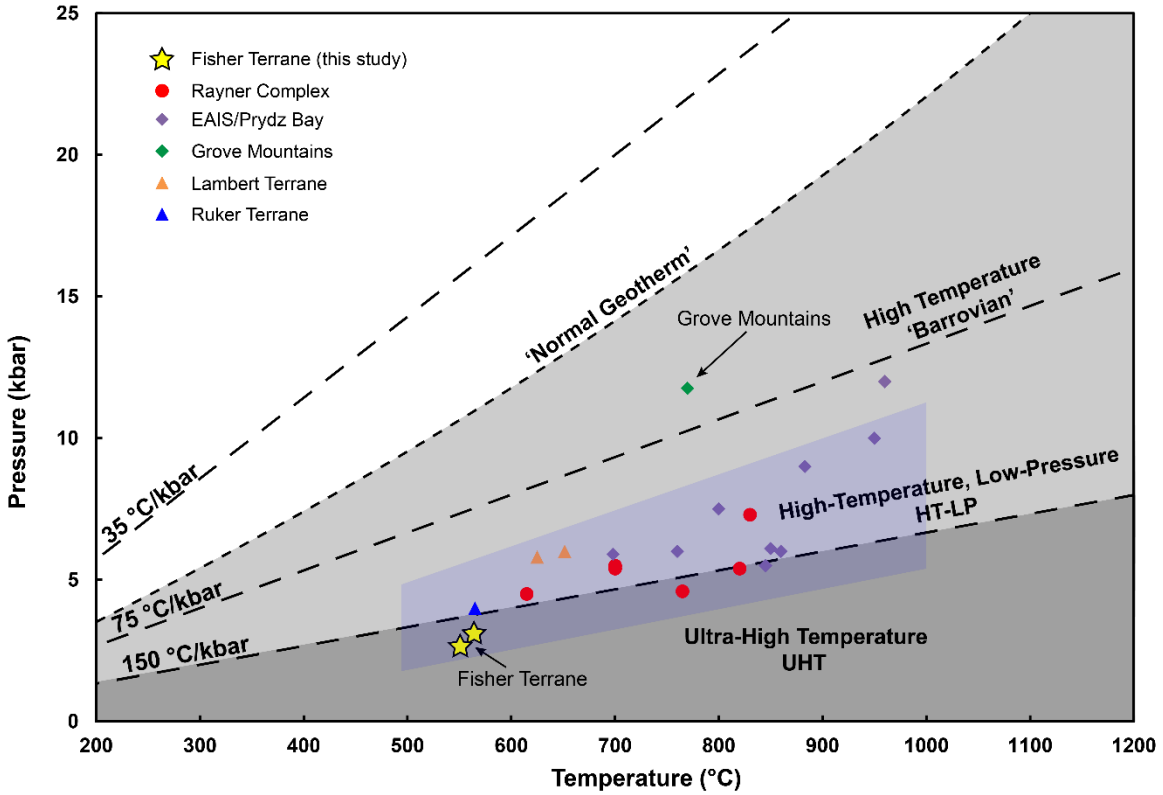

Figure 16: Diagram adapted from Brown et al. (2006, 2014) used to depict the thermal regimes present during the Prydz Event which was observed throughout the PCMs and surrounding regions. Data from the Rayner Complex from: Hand, Scrimgeour, Powell, Stüwe, and Wilson (1994), Scrimgeour and Hand (1997), Morrissey et al. (2016); EAIS/Prydz Bay Region: Carson, Wilson, and Dirks (1997), Fitzsimons (1996), Kelsey, White, Powell, Wilson, and Quinn (2003b), Morrissey et al. (2016), Liu et al. (2007), Motoyoshi, Thost, and Hensen (1991); Fisher Terrane (this study); Lambert Terrane: Boger and Wilson (2005), Phillips et al. (2009); Ruker Terrane Phillips et al. (2007a); Grove Mountains: Liu et al. (2009a). The blue shaded region represents the thermal gradient envelope of most other published data from the region.

Prydz-aged tectonism is said to be the result of collision between the Indian and Antarctic continental blocks during the amalgamation of Gondwana (e.g. Boger et al., 2002; Boger et al., 2001), rather than extension. This event marks the final amalgamation of the PCMs into their approximately current configuration, with suturing of the Rayner Complex, Fisher Terrane and Lambert Terrane (as part of India) to the Ruker Terrane (as part of Antarctica) (Boger et al., 2002; Fitzsimons, 2003; Kelsey et al., 2008). Initial collision between these two blocks was proposed to have occurred at c. 570 Ma, with metamorphic monazite and zircon growth occurring in the Prydz Bay

and EAIS regions (Kelsey et al., 2007; Liu et al., 2009b). The thermal record of this study, supportive of thin crust, is apparently at odds with collisional tectonics of the Prydz Event. However, the closure, inversion and thickening of back-arc basins is a critical part of tectonic switching from extension to convergence during supercontinent assembly (e.g. Brown, 2007; Clark, Fitzsimons, Healy, and Harley, 2011). Rocks within such tectonic regimes often record—but are not limited to—tight clockwise P–T paths (Brown, 2007). The regional foliation throughout the Fisher Terrane is steeply dipping to near vertical (Crowe 1994), supportive of a convergent tectonic setting. Therefore, a plausible scenario for the rocks of the Fisher Terrane would be prograde to peak metamorphism occurring in an extensional back-arc setting, followed by its closure and thickening in a collisional regime, resulting in the development of steeply dipping tectonic fabrics. *P–T* results from the Grove Mountains (Fig. 1a, 18; Liu et al., 2009b), show a lower apparent thermal gradient, synonymous with a more 'Barrovian' style of collision/convergence-related metamorphism (Stüwe, 2007). This could mean that the locus of crustal thickening during Gondwana amalgamation occurred proximal to the Grove Mountains, with the more northerly exposures in the PCMs (including the Fisher Terrane) representing the formerly extended back-arc region.

CONCLUSIONS

During the Meso–Neoproterozoic the Fisher Terrane evolved as an oceanic island–arc (Mikhalsky et al., 1996) with the deposition of metasediments occurring to 1206 ± 49 Ma, with detritus being sourced locally and from the Lambert Terrane. Evidence for a metamorphic event occurring at c. 1085 Ma is found in a migmatitic felsic gneiss from

Nilsson Rocks. This age pre-dates the regional Rayner Event and is coeval with a period of calc-alkaline magmatism identified in the southern portion of the cPCMs towards the Lambert Terrane. This leads to the tentative proposal for the Fisher Terrane at this time evolving in proximity to the Lambert Terrane with metamorphism likely being related to a period of c. 1080 Ma subduction related magmatism. Metapelites from the Fisher Terrane record evidence of metamorphism occurring within a highly perturbed thermal regime (apparent thermal gradients of 144 °C/kbar to 212 °C/kbar) at c. 538–505 Ma. The timing of this event is contemporaneous with the regionally recognised c. 570–480 Ma Prydz Event, relating to the collision of the Indian and Antarctic continents during the amalgamation of Gondwana. Conditions such as these were most plausibly related to metamorphism taking place in an extensional back-arc setting which was subsequently inverted and thickened via collision.

ACKNOWLEDGMENTS

My supervisor's Dr David Kelsey and Dr Laura Morrissey are thanked for their invaluable guidance, input and support throughout the duration of this project. Further thanks are extended to Dr Alec Walsh for sample preparation and training. The staff of Adelaide Microscopy including Ben Wade, Ken Neubauer and Sarah Gilbert are thanked for their training and assistance during data collection and processing.

REFERENCES

Alexeev, N., Zinger, T., Glebovitsky, V., & Kapitonov, I. (2010). *U-Pb age of igneous and metamorphic events on the Fisher Massif (East Antarctica) and its significance for geodynamic reconstruction.* Paper presented at the Doklady Earth Sciences.

Ashworth, J. (1975). Staurolite at anomalously high grade. *Contributions to Mineralogy and Petrology*, *53*(4), 281-291.

Beliatsky, B. V., Laiba, A. A., & Mikhalsky, E. V. (1994). U-PB ZIRCON AGE OF THE METAVOLCANIC ROCKS OF FISHER MASSIF (PRINCE CHARLES MOUNTAINS, EAST ANTARCTICA). *Antarctic Science*, *6*(3), 355-358.

Black, L. P., Harley, S. L., Sun, S. S., & McCulloch, M. T. (1987). The Rayner Complex of East Antarctica: complex isotopic systematics within a Proterozoic

mobile belt. *Journal of Metamorphic Geology, 5*(1), 1-26. doi:10.1111/j.1525-1314.1987.tb00366.x

Boger, S. D., Carson, C. J., Wilson, C. J. L., & Fanning, C. M. (2000). Neoproterozoic deformation in the Radok Lake region of the northern Prince Charles Mountains, east Antarctica; evidence for a single protracted orogenic event. *Precambrian Research, 104*(1-2), 1-24. doi:10.1016/s0301-9268(00)00079-6

Boger, S. D., Wilson, C. J. L., & Fanning, C. M. (2001). Early Paleozoic tectonism within the East Antarctic craton: The final suture between east and west Gondwana? *Geology, 29*(5), 463-466. doi:10.1130/0091-7613(2001)029<0463:EPTWTE>2.0.CO;2

Boger, S. D., Carson, C. J., Fanning, C. M., Hergt, J. M., Wilson, C. J. L., & Woodhead, J. D. (2002). Pan-African intraplate deformation in the Northern Prince Charles Mountains, East Antarctica. *Earth and Planetary Science Letters, 195*(3-4), 195-210. doi:10.1016/S0012-821X(01)00587-8

Boger, S. D., & White, R. W. (2003). The metamorphic evolution of metapelitic granulites from Radok Lake, northern Prince Charles Mountains, east Antarctica; evidence for an anticlockwise P-T path. *Journal of Metamorphic Geology, 21*(3), 285-298.

Boger, S. D., & Wilson, C. J. L. (2005). Early Cambrian crustal shortening and a clockwise P-T-t path from the southern Prince Charles Mountains, East Antartica: Implications for the formation of Gondwana. *Journal of Metamorphic Geology, 23*(7), 603-623. doi:10.1111/j.1525-1314.2005.00598.x

Boger, S. D., Wilson, C. J. L., & Mark Fanning, C. (2006). An Archaean province in the southern Prince Charles Mountains, East Antarctica: U-Pb zircon evidence for c. 3170 Ma granite plutonism and c. 2780 Ma partial melting and orogenesis. *Precambrian Research, 145*(3-4), 207-228. doi:10.1016/j.precamres.2005.12.003

Boger, S. D., Maas, R., & Fanning, C. M. (2008). Isotopic and geochemical constraints on the age and origin of granitoids from the central Mawson Escarpment, southern Prince Charles Mountains, East Antarctica. *Contributions to Mineralogy and Petrology, 155*(3), 379-400. doi:10.1007/s00410-007-0249-x

Boger, S. D. (2011). Antarctica—before and after Gondwana. *Gondwana Research, 19*(2), 335-371.

Brown, M. (2006). Duality of thermal regimes is the distinctive characteristic of plate tectonics since the Neoarchean. *Geology, 34*(11), 961-964.

Brown, M. (2007). Metamorphic conditions in orogenic belts: a record of secular change. *International Geology Review, 49*(3), 193-234.

Brown, M. (2014). The contribution of metamorphic petrology to understanding lithosphere evolution and geodynamics. *Geoscience Frontiers, 5*(4), 553-569.

Carson, C. J., Wilson, C., & Dirks, P. (1997). Partial melting during tectonic exhumation of a granulite terrane: an example from the Larsemann Hills, East Antarctica. *Journal of Metamorphic Geology, 15*(1), 105-126.

Carson, C. J., Boger, S. D., Fanning, C. M., Wilson, C. J. L., & Thost, D. E. (2000). SHRIMP U-Pb geochronology from Mount Kirkby, northern Prince Charles Mountains, East Antarctica. *Antarctic Science, 12*(4), 429-442.

Carson, C. J., Ague, J. J., & Coath, C. D. (2002). U–Pb geochronology from Tonagh Island, East Antarctica: implications for the timing of ultra-high temperature

metamorphism of the Napier Complex. *Precambrian Research, 116*(3), 237-263. doi:https://doi.org/10.1016/S0301-9268(02)00023-2

Clark, C., Fitzsimons, I. C., Healy, D., & Harley, S. L. (2011). How does the continental crust get really hot? *Elements, 7*(4), 235-240.

Corfu, F., Hanchar, J. M., Hoskin, P. W., & Kinny, P. (2003). Atlas of zircon textures. *Reviews in Mineralogy and Geochemistry, 53*(1), 469-500.

Corrie, S. L., & Kohn, M. J. (2008). Trace-element distributions in silicates during prograde metamorphic reactions: Implications for monazite formation. *Journal of Metamorphic Geology, 26*(4), 451-464.

Corvino, A. F., Boger, S., Wilson, C., & Fitzsimons, I. (2005). Geology and SHRIMP U-Pb zircon chronology of the Clemence Massif, central Prince Charles Mountains, East Antarctica. *Terra Antartica, 12*(1/2), 55.

Corvino, A. F., & Henjes-Kunst, F. (2007). A record of 2.5 and 1.1 billion year old crust in the Lawrence Hills, Antarctic Southern Prince Charles Mountains. *Terra Antartica, 14*(1-2), 13-30.

Corvino, A. F., Boger, S. D., Henjes-Kunst, F., Wilson, C. J. L., & Fitzsimons, I. C. W. (2008). Superimposed tectonic events at 2450 Ma, 2100 Ma, 900 Ma and 500 Ma in the North Mawson Escarpment, Antarctic Prince Charles Mountains. *Precambrian Research, 167*(3-4), 281-302. doi:10.1016/j.precamres.2008.09.001

Crowe, W. (1994). *Geology, metamorphism and petrogenesis of the Fisher Terrane, Prince Charles Mountains, East Antarctica*. Australian National University. Canberra.

Dempster, T., Hay, D., Gordon, S., & Kelly, N. (2008). Micro-zircon: origin and evolution during metamorphism. *Journal of Metamorphic Geology, 26*(5), 499-507.

Dickinson, W. R., & Gehrels, G. E. (2009). Use of U–Pb ages of detrital zircons to infer maximum depositional ages of strata: a test against a Colorado Plateau Mesozoic database. *Earth and Planetary Science Letters, 288*(1), 115-125.

Fedo, C. M., Sircombe, K. N., & Rainbird, R. H. (2003). Detrital zircon analysis of the sedimentary record. *Reviews in Mineralogy and Geochemistry, 53*(1), 277-303.

Fitzsimons, I. (1996). Metapelitic migmatites from Brattstrand Bluffs, East Antarctica—metamorphism, melting and exhumation of the mid crust. *Journal of Petrology, 37*(2), 395-414.

Fitzsimons, I. (2000). Grenville-age basement provinces in East Antarctica: Evidence for three separate collisional orogens. *Geology, 28*(10), 879-882. doi:10.1130/0091-7613(2000)28<879:GBPIEA>2.0.CO;2

Fitzsimons, I. (2003). Proterozoic basement provinces of southern and southwestern Australia, and their correlation with Antarctica. *Geological Society, London, Special Publications, 206*(1), 93-130.

Gibson, H. D., Carr, S. D., Brown, R. L., & Hamilton, M. A. (2004). Correlations between chemical and age domains in monazite, and metamorphic reactions involving major pelitic phases: an integration of ID-TIMS and SHRIMP geochronology with Y–Th–U X-ray mapping. *Chemical Geology, 211*(3), 237-260.

Golynsky, A. V., Masolov, V. N., Volnukhin, V. S., & Golynsky, D. A. (2006). Crustal provinces of the Prince Charles Mountains region and surrounding areas in the light of aeromagnetic data *Antarctica* (pp. 83-94): Springer.

Grew, E. S., Carson, C. J., Christy, A. G., Maas, R., Yaxley, G. M., Boger, S. D., & Fanning, C. M. (2012). New constraints from U–Pb, Lu–Hf and Sm–Nd isotopic data on the timing of sedimentation and felsic magmatism in the Larsemann Hills, Prydz Bay, East Antarctica. *Precambrian Research, 206*, 87-108.

Halpin, J. A., Gerakiteys, C., Clarke, G., Belousova, E., & Griffin, W. (2005). In-situ U–Pb geochronology and Hf isotope analyses of the Rayner Complex, east Antarctica. *Contributions to Mineralogy and Petrology, 148*(6), 689-706.

Halpin, J. A., Clarke, G. L., White, R. W., & Kelsey, D. E. (2007). Contrasting P-T-t paths for Neoproterozoic metamorphism in MacRobertson and Kemp Lands, east Antarctica. *Journal of Metamorphic Geology, 25*(6), 683-701. doi:10.1111/j.1525-1314.2007.00723.x

Halpin, J. A., Daczko, N. R., Milan, L. A., & Clarke, G. L. (2012). Decoding near-concordant U-Pb zircon ages spanning several hundred million years: Recrystallisation, metamictisation or diffusion? *Contributions to Mineralogy and Petrology, 163*(1), 67-85. doi:10.1007/s00410-011-0659-7

Halpin, J. A., Daczko, N. R., Clarke, G. L., & Murray, K. R. (2013). Basin analysis in polymetamorphic terranes: An example from east Antarctica. *Precambrian Research, 231*, 78-97. doi:10.1016/j.precamres.2013.03.015

Hand, M., Scrimgeour, I., Powell, R., Stüwe, K., & Wilson, C. J. L. (1994). Metapelitic granulites from Jetty Peninsula, east Antarctica: formation during a single event or by polymetamorphism? *Journal of Metamorphic Geology, 12*(4), 557-573. doi:10.1111/j.1525-1314.1994.tb00042.x

Hermann, J., & Rubatto, D. (2003). *Relating zircon and monazite domains to garnet growth zones: Age and duration of granulite facies metamorphism in the Val Malenco lower crust* (Vol. 21).

Holland, T., & Powell, R. (1998). An internally consistent thermodynamic data set for phases of petrological interest. *Journal of Metamorphic Geology, 16*(3), 309-343.

Holland, T., & Powell, R. (2011). An improved and extended internally consistent thermodynamic dataset for phases of petrological interest, involving a new equation of state for solids. *Journal of Metamorphic Geology, 29*(3), 333-383.

Hyndman, R. D., Currie, C. A., & Mazzotti, S. P. (2005). Subduction zone backarcs, mobile belts, and orogenic heat. *GSA Today, 15*(2), 4-10.

Jackson, S. E., Pearson, N. J., Griffin, W. L., & Belousova, E. A. (2004). The application of laser ablation-inductively coupled plasma-mass spectrometry to in situ U–Pb zircon geochronology. *Chemical Geology, 211*(1), 47-69.

Janots, E., Engi, M., Berger, A., Allaz, J., Schwarz, J. O., & Spandler, C. (2008). Prograde metamorphic sequence of REE minerals in pelitic rocks of the Central Alps: implications for allanite–monazite–xenotime phase relations from 250 to 610 C. *Journal of Metamorphic Geology, 26*(5), 509-526.

Kelly, N. M., Clarke, G. L., & Fanning, C. M. (2002). A two-stage evolution of the Neoproterozoic Rayner Structural Episode: New U-Pb sensitive high resolution ion microprobe constraints from the Oygarden Group, Kemp Land, East Antarctica. *Precambrian Research, 116*(3-4), 307-330. doi:10.1016/S0301-9268(02)00028-1

Kelsey, D. E., Powell, R., Wilson, C., & Steele, D. (2003a). (Th+ U)-Pb monazite ages from Al-Mg-rich metapelites, Rauer Group, East Antarctica. *Contributions to Mineralogy and Petrology, 146*(3), 326-340.

Kelsey, D. E., White, R. W., Powell, R., Wilson, C. J. L., & Quinn, C. D. (2003b). New constraints on metamorphism in the Rauer Group, Prydz Bay, east Antarctica. *Journal of Metamorphic Geology, 21*(8), 739-759. doi:10.1046/j.1525-1314.2003.00476.x

Kelsey, D. E., Hand, M., Clark, C., & Wilson, C. (2007). On the application of in situ monazite chemical geochronology to constraining P–T–t histories in high-temperature (> 850° C) polymetamorphic granulites from Prydz Bay, East Antarctica. *Journal of the Geological Society, 164*(3), 667-683.

Kelsey, D. E., Wade, B. P., Collins, A. S., Hand, M., Sealing, C. R., & Netting, A. (2008). Discovery of a Neoproterozoic basin in the Prydz belt in East Antarctica and its implications for Gondwana assembly and ultrahigh temperature metamorphism. *Precambrian Research, 161*(3-4), 355-388. doi:10.1016/j.precamres.2007.09.003

Kelsey, D. E., & Hand, M. (2015). On ultrahigh temperature crustal metamorphism: phase equilibria, trace element thermometry, bulk composition, heat sources, timescales and tectonic settings. *Geoscience Frontiers, 6*(3), 311-356.

Kinny, P. D., Black, L., & Sheraton, J. (1993). Zircon ages and the distribution of Archaean and Proterozoic rocks in the Rauer Islands. *Antarctic Science, 5*(2), 193-206.

Kinny, P. D., Black, L. P., & Sheraton, J. W. (1997). Zircon U-Pb ages and geochemistry of igneous and metamorphic rocks in the northern Prince Charles Mountains, Antarctica. *AGSO Journal of Australian Geology and Geophysics, 16*(5), 637-654.

Korhonen, F., Clark, C., Brown, M., Bhattacharya, S., & Taylor, R. (2013). *How long-lived is ultrahigh temperature (UHT) metamorphism? Constraints from zircon and monazite geochronology in the Eastern Ghats orogenic belt, India* (Vol. 234).

Liu, X., Zhao, Y., Zhao, G., Jian, P., & Xu, G. (2007). Petrology and geochronology of granulites from the McKaskle Hills, Eastern Amery Ice Shelf, Antarctica, and implications for the evolution of the Prydz Belt. *Journal of Petrology, 48*(8), 1443-1470. doi:10.1093/petrology/egm024

Liu, X., Hu, J., Zhao, Y., Lou, Y., Wei, C., & Liu, X. (2009a). Late Neoproterozoic/Cambrian high-pressure mafic granulites from the Grove Mountains, East Antarctica: P–T–t path, collisional orogeny and implications for assembly of East Gondwana. *Precambrian Research, 174*(1), 181-199.

Liu, X., Zhao, Y., Song, B., Liu, J., & Cui, J. (2009b). SHRIMP U–Pb zircon geochronology of high-grade rocks and charnockites from the eastern Amery Ice Shelf and southwestern Prydz Bay, East Antarctica: constraints on Late Mesoproterozoic to Cambrian tectonothermal events related to supercontinent assembly. *Gondwana Research, 16*(2), 342-361.

Liu, X., Jahn, B. M., Zhao, Y., Liu, J., & Ren, L. (2014). Geochemistry and geochronology of mesoproterozoic basement rocks from the eastern amery ice shelf and southwestern prydz bay, EAST ANTARCTICA: Implications for a long-lived magmatic accretion in a continental arc. *American Journal of Science, 314*(2), 508-547. doi:10.2475/02.2014.03

Liu, X., Zhao, Y., Liu, J., Chen, H., Cui, Y., & Song, B. (2016). Early Mesoproterozoic arc magmatism followed by early Neoproterozoic granulite facies

metamorphism with a near-isobaric cooling path at Mount Brown, Princess Elizabeth Land, East Antarctica. *Precambrian Research, 284*, 30-48.

Mahar, E. M., Baker, J., Powell, R., Holland, T., & Howell, N. (1997). The effect of Mn on mineral stability in metapelites. *Journal of Metamorphic Geology, 15*(2), 223-238.

Manton, W. I., Grew, E. S., Hofmann, J., & Sheraton, J. W. (1992). Granitic Rocks of the Jetty Peninsula, Amery Ice Shelf Area, East Antarctica. In Y. Yoshida (Ed.), *Recent Progress in Antarctic Earth Science* (pp. 179-189). Tokyo: Terra Scientific Publishing (TERRAPUB) Company.

Maslov, V., Vorobiev, D., & Belyatsky, B. (2007). Geological structure and evolution of Shaw Massif, central part of the Prince Charles Mountains (East Antarctica). *Antarctica: A Keystone in a Changing World. Online Proceedings of the ISEAS X. USGS Open-File Report, 1047*.

Mikhalsky, E. V., Sheraton, J. W., Laiba, A. A., & Beliatsky, B. V. (1996). Geochemistry and origin of Mesoproterozoic metavolcanic rocks from Fisher Massif, Prince Charles Mountains, East Antarctica. *Antarctic Science, 8*(1), 85-104.

Mikhalsky, E. V., Laiba, A. A., Beliatsky, B. V., & Stüwe, K. (1999). Geology, age and origin of the Mount Willing area (Prince Charles Mountains, East Antarctica). *Antarctic Science, 11*(3), 338-352.

Mikhalsky, E. V., Sheraton, J. W., Laiba, A. A., Tingey, R. J., Thost, D. E., Kamenov, E. N., & Fedorov, L. V. (2001). *Geology of the Prince Charles Mountains, Antarctica*. Canberra: AGSO-Geoscience Australia Bulletin.

Mikhalsky, E. V., Beliatsky, B. V., Sheraton, J. W., & Roland, N. W. (2006a). Two distinct Precambrian terranes in the Southern Prince Charles Mountains, East Antarctica: SHRIMP dating and geochemical constraints. *Gondwana Research, 9*(3), 291-309. doi:10.1016/j.gr.2005.10.002

Mikhalsky, E. V., Laiba, A. A., & Beliatsky, B. V. (2006b). Tectonic subdivision of the Prince Charles Mountains: A review of geologic and isotopic data. *Antarctica: Contributions to Global Earth Sciences*, 69-+. doi:10.1007/3-540-32934-x_9

Mikhalsky, E. V., Henjes-Kunst, F., & Roland, N. (2007). Early Precambrian mantle derived rocks in the southern Prince Charles Mountains, East Antarctica: age and isotopic constraints. *Antarctica: A Keystone in a Changing World. Online Proceedings of the 10th ISAES. USGS Open-File Report, 1047*.

Mikhalsky, E. V., Henjes-Kunst, F., Belyatsky, B. V., Roland, N. W., & Sergeev, S. A. (2010). New Sm-Nd, Rb-Sr, U-Pb and Hf isotope systematics for the southern Prince Charles Mountains (East Antarctica) and its tectonic implications. *Precambrian Research, 182*(1-2), 101-123. doi:10.1016/j.precamres.2010.07.004

Mikhalsky, E. V., Sheraton, J. W., Kudriavtsev, I. V., Sergeev, S. A., Kovach, V. P., Kamenev, I. A., & Laiba, A. A. (2013). The mesoproterozoic Rayner Province in the Lambert Glacier area: Its age, origin, isotopic structure and implications for Australia-Antarctica correlations *Geological Society Special Publication* (Vol. 383, pp. 35-57).

Morrissey, L. J., Hand, M., & Kelsey, D. E. (2015). Multi-stage metamorphism in the Rayner-Eastern Ghats Terrane: P-T-t constraints from the northern Prince Charles Mountains, east Antarctica. *Precambrian Research, 267*, 137-163. doi:10.1016/j.precamres.2015.06.003

Morrissey, L. J., Hand, M., Kelsey, D. E., & Wade, B. P. (2016). Cambrian high-temperature reworking of the Rayner-Eastern ghats terrane: Constraints from the Northern Prince Charles Mountains region, East Antarctica. *Journal of Petrology, 57*(1), 53-91. doi:10.1093/petrology/egv082

Motoyoshi, Y., Thost, D., & Hensen, B. (1991). Reaction textures in calc-silicate granulites from the Bolingen Islands, Prydz Bay, East Antarctica: implications for the retrograde P–T path. *Journal of Metamorphic Geology, 9*(3), 293-300.

Palin, R. M., Weller, O. M., Waters, D. J., & Dyck, B. (2016). Quantifying geological uncertainty in metamorphic phase equilibria modelling; a Monte Carlo assessment and implications for tectonic interpretations. *Geoscience Frontiers, 7*(4), 591-607.

Paton, C., Hellstrom, J., Paul, B., Woodhead, J., & Hergt, J. (2011). Iolite: Freeware for the visualisation and processing of mass spectrometric data. *Journal of Analytical Atomic Spectrometry, 26*(12), 2508-2518. doi:10.1039/c1ja10172b

Pattison, D. R., Spear, F., & Cheney, J. (1999). Polymetamorphic origin of muscovite+ cordierite+ staurolite+ biotite assemblages: implications for the metapelitic petrogenetic grid and for PT paths. *Journal of Metamorphic Geology, 17*, 685-704.

Pattison, D. R., & Tinkham, D. (2009). Interplay between equilibrium and kinetics in prograde metamorphism of pelites: an example from the Nelson aureole, British Columbia. *Journal of Metamorphic Geology, 27*(4), 249-279.

Payne, J. L., Hand, M., Barovich, K. M., & Wade, B. P. (2008). Temporal constraints on the timing of high-grade metamorphism in the northern Gawler Craton: Implications for assembly of the Australian Proterozoic. *Australian Journal of Earth Sciences, 55*(5), 623-640. doi:10.1080/08120090801982595

Pearce, M. A., White, A. J. R., & Gazley, M. F. (2015). TCInvestigator: Automated calculation of mineral mode and composition contours for thermocalc pseudosections. *Journal of Metamorphic Geology, 33*(4), 413-425. doi:10.1111/jmg.12126

Phillips, G., Wilson, C. J. L., Campbell, I. H., & Allen, C. M. (2006). U-Th-Pb detrital zircon geochronology from the southern Prince Charles Mountains, East Antarctica-Defining the Archaean to Neoproterozoic Ruker Province. *Precambrian Research, 148*(3-4), 292-306. doi:10.1016/j.precamres.2006.05.001

Phillips, G., White, R. W., & Wilson, C. J. L. (2007a). On the roles of deformation and fluid during rejuvenation of a polymetamorphic terrane: Inferences on the geodynamic evolution of the Ruker Province, East Antarctica. *Journal of Metamorphic Geology, 25*(8), 855-871. doi:10.1111/j.1525-1314.2007.00732.x

Phillips, G., Wilson, C. J. L., Phillips, D., & Szczepanski, S. K. (2007b). Thermochronological (40Ar/39Ar) evidence of Early Palaeozoic basin inversion within the southern Prince Charles Mountains, East Antarctica: Implications for East Gondwana. *Journal of the Geological Society, 164*(4), 771-784. doi:10.1144/0016-76492006-073

Phillips, G., Kelsey, D. E., Corvino, A. F., & Dutch, R. A. (2009). Continental reworking during overprinting orogenic events, Southern Prince Charles Mountains, East Antarctica. *Journal of Petrology, 50*(11), 2017-2041. doi:10.1093/petrology/egp065

Powell, R., White, R., Green, E., Holland, T., & Diener, J. (2014). On parameterizing thermodynamic descriptions of minerals for petrological calculations. *Journal of Metamorphic Geology, 32*(3), 245-260.

Pyle, J. M., & Spear, F. S. (2003). Four generations of accessory-phase growth in low-pressure migmatites from SW New Hampshire. *American Mineralogist, 88*(2-3), 338-351.

Rasmussen, B. (2005). Zircon growth in very low grade metasedimentary rocks: evidence for zirconium mobility at~ 250 C. *Contributions to Mineralogy and Petrology, 150*(2), 146-155.

Rasmussen, B., & Muhling, J. R. (2007). Monazite begets monazite: evidence for dissolution of detrital monazite and reprecipitation of syntectonic monazite during low-grade regional metamorphism. *Contributions to Mineralogy and Petrology, 154*(6), 675-689.

Rubatto, D., & Gebauer, D. (2000). Use of cathodoluminescence for U-Pb zircon dating by ion microprobe: some examples from the Western Alps *Cathodoluminescence in geosciences* (pp. 373-400): Springer.

Rubatto, D., Williams, I. S., & Buick, I. S. (2001). Zircon and monazite response to prograde metamorphism in the Reynolds Range, central Australia. *Contributions to Mineralogy and Petrology, 140*(4), 458-468.

Scrimgeour, I., & Hand, M. (1997). A metamorphic perspective on the Pan African overprint in the Amery area of Mac. Robertson Land, East Antarctica. *Antarctic Science, 9*(3), 313-335.

Seydoux-Guillaume, A.-M., Paquette, J.-L., Wiedenbeck, M., Montel, J.-M., & Heinrich, W. (2002). Experimental resetting of the U–Th–Pb systems in monazite. *Chemical Geology, 191*(1), 165-181.

Seydoux-Guillaume, A.-M., Montel, J.-M., Bingen, B., Bosse, V., De Parseval, P., Paquette, J.-L., . . . Wirth, R. (2012). Low-temperature alteration of monazite: Fluid mediated coupled dissolution–precipitation, irradiation damage, and disturbance of the U–Pb and Th–Pb chronometers. *Chemical Geology, 330*, 140-158.

Sizova, E., Gerya, T., & Brown, M. (2014). Contrasting styles of Phanerozoic and Precambrian continental collision. *Gondwana Research, 25*(2), 522-545.

Sláma, J., Košler, J., Condon, D. J., Crowley, J. L., Gerdes, A., Hanchar, J. M., . . . Norberg, N. (2008). Plešovice zircon—a new natural reference material for U–Pb and Hf isotopic microanalysis. *Chemical Geology, 249*(1), 1-35.

Smith, H. A., & Barreiro, B. (1990). Monazite U-Pb dating of staurolite grade metamorphism in pelitic schists. *Contributions to Mineralogy and Petrology, 105*(5), 602-615.

Spear, F. S., & Pyle, J. M. (2002). Apatite, monazite, and xenotime in metamorphic rocks. *Reviews in Mineralogy and Geochemistry, 48*(1), 293-335.

Spencer, C. J., Kirkland, C. L., & Taylor, R. J. M. (2016). Strategies towards statistically robust interpretations of in situ U-Pb zircon geochronology. *Geoscience Frontiers, 7*(4), 581-589. doi:10.1016/j.gsf.2015.11.006

Stüwe, K. (2007). *Geodynamics of the lithosphere: an introduction*: Springer Science & Business Media.

Taylor, R. J., Kirkland, C. L., & Clark, C. (2016). Accessories after the facts: Constraining the timing, duration and conditions of high-temperature metamorphic processes. *Lithos, 264*, 239-257.

Thost, D., & Hensen, B. (1992). Gneisses of the Porthos and Athos Ranges, Northern Prince Charles Mountains, East Antarctica: constraints on the prograde and retrograde P–T path. *Recent Progress in Antarctic Earth Science*, 93-102.

Tinkham, D. K., & Ghent, E. D. (2005). Estimating PT conditions of garnet growth with isochemical phase-diagram sections and the problem of effective bulk-composition. *The Canadian Mineralogist, 43*(1), 35-50.

Upadhyay, D., Gerdes, A., & Raith, M. M. (2009). Unraveling sedimentary provenance and tectonothermal history of high-temperature metapelites, using zircon and monazite chemistry: a case study from the Eastern Ghats Belt, India. *The Journal of Geology, 117*(6), 665-683.

Wang, Y., Liu, D., Chung, S.-L., Tong, L., & Ren, L. (2008). SHRIMP zircon age constraints from the Larsemann Hills region, Prydz Bay, for a late Mesoproterozoic to early Neoproterozoic tectono-thermal event in East Antarctica. *American Journal of Science, 308*(4), 573-617.

White, R. W., Powell, R., Holland, T. J. B., Johnson, T. E., & Green, E. C. R. (2014a). New mineral activity-composition relations for thermodynamic calculations in metapelitic systems. *Journal of Metamorphic Geology, 32*(3), 261-286. doi:10.1111/jmg.12071

White, R. W., Powell, R., & Johnson, T. E. (2014b). The effect of Mn on mineral stability in metapelites revisited: New a-x relations for manganese-bearing minerals. *Journal of Metamorphic Geology, 32*(8), 809-828. doi:10.1111/jmg.12095

Wiedenbeck, M., Alle, P., Corfu, F., Griffin, W., Meier, M., Oberli, F. v., . . . Spiegel, W. (1995). Three natural zircon standards for U-Th-Pb, Lu-Hf, trace element and REE analyses. *Geostandards and Geoanalytical Research, 19*(1), 1-23.

Williams, M. L., Jercinovic, M. J., Harlov, D. E., Budzyń, B., & Hetherington, C. J. (2011). Resetting monazite ages during fluid-related alteration. *Chemical Geology, 283*(3), 218-225. doi:https://doi.org/10.1016/j.chemgeo.2011.01.019

Wing, B. A., Ferry, J. M., & Harrison, T. M. (2003). Prograde destruction and formation of monazite and allanite during contact and regional metamorphism of pelites: petrology and geochronology. *Contributions to Mineralogy and Petrology, 145*(2), 228-250.

Young, D. N., & Black, L. P. (1991). U-Pb zircon dating of Proterozoic igneous charnockites from the Mawson Coast, East Antarctica. *Antarctic Science, 3*(2), 205-216.

Zhao, J. X., Ellis, D. J., Kilpatrick, J. A., & McCulloch, M. T. (1997). Geochemical and Sr-Nd isotopic study of charnockites and related rocks in the northern Prince Charles Mountains, East Antarctica: Implications for charnockite petrogenesis and proterozoic crustal evolution. *Precambrian Research, 81*(1-2), 37-66.

APPENDIX A: ADDITIONAL SAMPLE PETROGRAPHY

53806 Meta–volcanic breccia

This sample comprises volcanogenic clasts of varying size and composition amongst a finer grained volcaniclastic matrix.

53810 Meta–volcanic sandstone

This sample is a bedded meta-volcanic sandstone comprised of coarser grained plagioclase and amphibole bearing layers and finer grained quartz rich layers.

53811 Garnet bearing felsic gneiss

The matrix mineralogy is defined by tabular biotite (200–1000 μm), plagioclase (200–800 μm), alkali feldspar (200–800 μm) and perthite (200–800 μm). Quartz was not observed, but is assumed to be present in low abundance. Garnet porphyroblasts (300–1 cm) occur in perthite dominated regions. Perthite forms large >5 mm grains. Garnet forms euhedral to subhedral grains and are commonly fractured with fractures being filled by fine grained biotite (< 200 μm). Garnet porphyroblasts are separated from the perthitic regions by a two–layered corona of fine grained (<200 μm) biotite, proximal to garnet and fine grained (<100 μm) plagioclase, proximal to perthite. The interpreted peak assemblage is interpreted to be garnet + alkali feldspar + plagioclase + perthite + biotite, with post–peak biotite.

53817 Gedrite bearing garnet–biotite schist

The matrix mineralogy is defined by biotite (<1 mm), quartz (<300 μm), plagioclase (<300 μm), ilmenite (<100 μm**)** and minor chlorite (<200 μm). Biotite defines an S_1 fabric throughout the sample. Euhedral porphyroblasts of magnetite (400–1000 μm) occur throughout the rock. Elongate prisms of gedrite (up to 3mm) occur aligned with S_1. Cordierite grains (>5 mm) are highly poikiloblastic and contain inclusions of matrix minerals aligned with S_1, magnetite and staurolite. Rare euhedral porphyroblasts of staurolite (<400 μm) occur throughout the sample, and as minor inclusions within cordierite. Large anhedral garnet porphyroblasts (up to 2mm) occur near the boundaries of cordierite and within the matrix and contain minor inclusions of quartz and plagioclase. Chlorite occurs throughout the matrix and occurs pseudomorphing gedrite. The interpreted peak assemblage is garnet + gedrite + biotite + plagioclase + ilmenite + staurolite + quartz ± cordierite with post–peak chlorite ± cordierite.

APPENDIX B: MONAZITE PETROGRAPHIC LOCATIONS

53811 Garnet bearing felsic gneiss

Microstructurally, monazite occurs as inclusions and along grain boundaries in matrix biotite, plagioclase and alkali feldspar; within a perthite–rich domain interpreted to represent a leucosome and within porphyroblastic garnet, not secluded from microfractures. There does not appear to be a link between microstructural location and age. Typically, monazite grains are rounded, 30–150 μm in size and occur in the presence of zircon grains.

53815 Cordierite–andalusite–staurolite schist
Microstructurally, monazite occurs in matrix biotite and plagioclase and along grain boundaries of other matrix minerals. Monazite is also observed as minor inclusions in poikiloblastic staurolite and cordierite, however there does not appear to be a link between microstructural location and age. Typically, monazite grains are rounded and sometimes occur oriented with the foliation and are 10–50 μm in size.

53816 Garnet–staurolite schist
Microstructurally, monazite grains occur as inclusions in matrix biotite or along the grain boundaries of other matrix minerals. There does not appear to be a link between microstructural location and age. Typically, monazite grains are rounded, sometimes aligned with the foliation and contain inclusions of silicate minerals with sizes in the range of 10–50 μm.

53817 Gedrite bearing garnet–biotite schist
Microstructurally, monazite occurs as inclusions in matrix biotite and plagioclase, while also being present independently in the matrix. Monazite is also observed as inclusions in garnet and cordierite. There does not appear to be a link between microstructural location and age. Monazite grains are elongate and appear aligned to the foliation and very small in size (< 40 μm).

APPENDIX C: WHOLE ROCK GEOCHEMISTRY

Bulk-rock chemical compositions for phase equilibria modelling were determined externally at Bureau Veritas, Perth. Samples were cast using a 66:34 flux with 4% Lithium Nitrate and were then analysed using X-Ray Fluorescence Spectrometry (XRF) and Laser Ablation–Inductively Coupled Plasma–Mass Spectrometry (LA–ICP–MS).

Appendix Table 4: Whole rock geochemistry (in wt %). Fe2O3T = total iron, represented as ferric iron.

Sample	53815	53816	538317
SiO_2	64.01	64.00	64.02
Al_2O_3	16.16	15.39	15.96
CaO	2.04	2.28	2.71
Fe_2O_3T	8.06	7.66	8.06
K_2O	2.30	2.77	1.21
MgO	2.90	3.13	3.17
Na_2O	2.53	3.10	3.36
P_2O_5	0.08	0.14	0.09
SO_3	0.02	0.01	0.03
TiO_2	0.77	0.62	0.58
MnO	0.12	0.08	0.15
BaO	0.08	0.05	0.04
LOI	0.76	0.74	0.48

APPENDIX D: EPMA METHODS

Mineral chemical analyses were obtained using a Cameca SXFive electron microprobe with five Wavelength Dispersive Spectrometers (WDS) at Adelaide Microscopy, using a beam current of 20 nA and an accelerating voltage of 15 kV. Calibration was performed on certified synthetic and natural mineral standards from Astimex Ltd and P&H Associates. Data calibration and reduction was carried out in Probe for EPMA, distributed by Probe Software Inc. Measurements were taken of SiO_2, TiO_2, Al_2O_3, Cr_2O_3, FeO, MnO, MgO, CaO, Na_2O, K_2O, Cl, F, H_2O during each analysis.

APPENDIX E: MINERAL CHEMISTRY FROM EPMA ANALYSIS

Appendix Table 5 & 3: Representative mineral chemistries for samples 53815 and 53816.

Sample:			**53815**			
Mineral:	**cd**	**bi**	**chl**	**ilm**	**st**	**pl**
SiO_2	47.79	34.76	23.17	0.08	27.13	61.50
TiO_2	0.03	1.28	0.08	50.74	0.31	0.01
Al_2O_3	33.86	21.25	23.88	0.15	55.53	25.60
Cr_2O_3	0.00	0.10	0.01	0.05	0.04	0.00
FeO	9.91	21.14	25.33	42.14	14.45	0.06
MnO	0.67	0.16	0.32	2.34	0.49	0.00
MgO	7.35	7.80	12.86	0.22	1.59	0.00
ZnO	0.00	0.00	0.00	0.00	0.26	0.00
CaO	0.00	0.00	0.00	0.12	0.03	5.45
Na_2O	0.19	0.28	0.02	0.04	0.00	8.82
K_2O	0.00	7.98	0.00	0.01	0.00	0.02
Cl	0.00	0.00	0.01	0.00	0.01	0.00
F	0.00	0.03	0.00	0.00	0.00	0.00
H_2O	0.00	3.91	11.08	0.00	2.19	0.00
Total	99.81	98.68	96.74	95.89	99.84	101.47
No. Oxygens	18.00	11.00	14.00	3.00	46.00	8
Si	4.87	2.66	2.51	0.00	7.41	2.69
Ti	0.00	0.07	0.01	1.00	0.06	0.00
Al	4.07	1.91	3.05	0.00	17.89	1.32
Cr	0.00	0.01	0.00	0.00	0.01	0.00
Fe^{3+}	0.22	-	-	0.00	0.14	-
Fe^{2+}	0.62	1.35	2.29	0.92	3.16	0.00
Mn^{2+}	0.06	0.01	0.03	0.05	0.11	0.00
Mg	1.12	0.89	2.08	0.01	0.65	0.00
Zn	0.00	0.00	0.00	0.00	0.05	0.00
Ca	0.00	0.00	0.00	0.00	0.01	0.26
Na	0.04	0.04	0.01	0.00	0.00	0.75
K	0.00	0.78	0.00	0.00	0.00	0.00
Cl	0.00	0.00	0.00	0.00	0.00	0.00
F	0.00	0.01	0.00	0.00	0.00	0.00
OH^-	0.00	1.99	8.00	0.00	4.00	-

Sample:				**53816**			
Mineral:	**st**	**bi**	**chl**	**ilm**	**pl**	**g rim**	**g core**
SiO_2	26.83	35.01	24.23	0.66	61.07	37.11	37.03
TiO_2	0.44	1.50	0.06	52.95	0.02	0.00	0.02
Al_2O_3	55.81	19.43	23.79	0.20	24.60	20.83	20.85
Cr_2O_3	0.00	0.03	0.00	0.01	0.00	0.00	0.01
FeO	13.47	19.47	24.81	34.97	0.03	32.12	31.17
MnO	0.32	0.09	0.17	0.99	0.00	5.72	5.55
MgO	1.74	9.98	14.79	0.39	0.01	2.76	2.69
ZnO	1.25	0.00	0.00	0.01	0.00	0.00	0.00
CaO	0.00	0.02	0.00	0.07	5.51	1.15	2.24
Na_2O	0.00	0.19	0.01	0.11	8.55	0.07	0.01
K_2O	0.00	8.97	0.00	0.06	0.00	0.00	0.00
Cl	0.00	0.04	0.02	0.04	0.00	0.01	0.00
F	0.00	0.15	0.00	0.00	0.00	0.00	0.00
H_2O	2.19	3.85	11.44	0.00	0.00	0.00	0.00
Total	99.86	98.66	99.31	90.46	99.78	99.76	99.57
No. Oxygens	46.00	11	14.00	3.00	8.00	12.00	12.00
Si	7.33	2.67	2.54	0.02	2.72	3.00	3.00
Ti	0.09	0.09	0.00	1.11	0.00	0.00	0.00
Al	17.97	1.75	2.94	0.01	1.29	1.99	1.99
Cr	0.00	0.00	0.00	0.00	0.00	0.00	0.00
Fe^{3+}	0.19	-	-	0.00	-	0.02	0.01
Fe^{2+}	2.88	1.24	2.17	0.81	0.00	2.16	2.10
Mn^{2+}	0.07	0.01	0.02	0.02	0.00	0.39	0.38
Mg	0.71	1.14	2.31	0.02	0.00	0.33	0.32
Zn	0.25	0.00	0.00	0.00	0.00	0.00	0.00
Ca	0.00	0.00	0.00	0.00	0.26	0.10	0.19
Na	0.00	0.03	0.00	0.01	0.74	0.01	0.00
K	0.00	0.87	0.00	0.00	0.00	0.00	0.00
Cl	0.00	0.01	0.00	0.00	0.00	0.00	0.00
F	0.00	0.04	0.00	0.00	0.00	0.00	0.00
OH^-	4.00	1.96	8.00	0.00	-	0.00	0.00

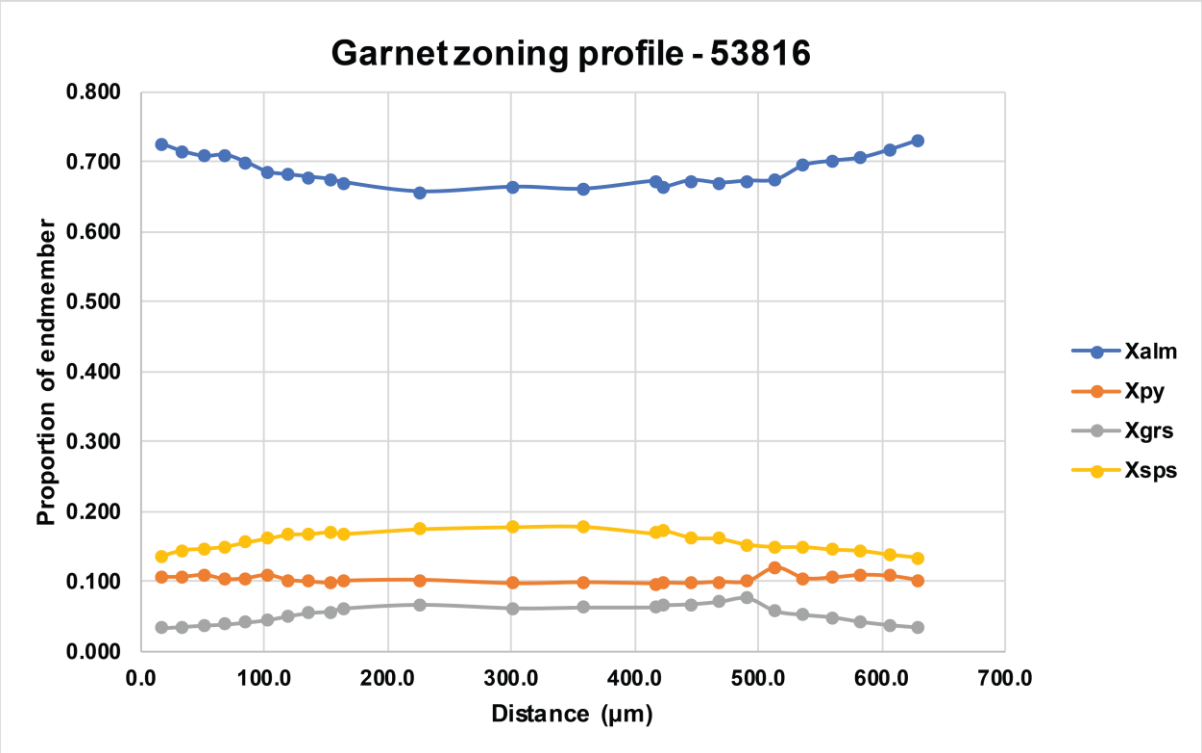

Appendix Figure 17: Garnet zoning profile from sample 53816 exhibiting prograde growth zoning. The garnet core is comparatively almandine poor in the core increasing towards the rim. Spessartine shows decrease from core to rim and pyrope and grossular have little variation.

Appendix Table 6: Range of mineral chemistries for samples 53811, 53815, 53816 and 53817.

Sample	53811	53815	53816	53817
Garnet core				
X_{alm}	0.726–0.752	–	0.656–0.672	0.714–0.721
X_{py}	0.070–0.135	–	0.097–0.102	0.152–0.157
X_{grs}	0.023–0.024	–	0.061–0.066	0.079–0.067
X_{sps}	0.115–0.157	–	0.169–0.179	0.055–0.055
X_{Fe}	0.843–0.914	–	0.866–0.874	0.825–0.821
Garnet rim				
X_{alm}	0.695–0.749	–	0.714–0.730	0.779–0.750
X_{py}	0.090–0.196	–	0.102–0.108	0.121–0.171
X_{grs}	0.028–0.040	–	0.033–0.038	0.042–0.039
X_{sps}	0.079–0.134	–	0.134–0.145	0.058–0.040
X_{Fe}	0.780–0.891	–	0.869–0.878	0.865–0.814
Biotite				
F (wt%)	0.545–0.651	0.027–0.076	0.059–0.151	0.114–0.160
TiO_2 (wt%)	0.362–0.461	1.279–1.361	1.325–1.823	1.191–1.434
X_{Fe}	0.540–0.566	0.590–0.603	0.522–0.536	0.435–0.451
Chlorite				
X_{Fe}	–	0.509–0.525	0.481–0.492	0.407–0.463
Cordierite				
X_{Fe}	–	0.355–0.369	–	0.213–0.227
MnO (wt%)		0.620–0.670		0.090–0.140
Staurolite				
X_{Fe}	–	0.823–0.840	0.798–0.815	0.716–0.735
ZnO (wt%)	–	0.160–0.290	0.120–0.131	0.630–0.740
Plagioclase				
X_{ab}	0.833–0.925	0.598–0.744	0.728–0.739	0.700–0.766
X_{an}	0.075–0.167	0.236–0.289	0.248–0.271	0.232–0.298
X_{or}	0.004–0.046	0.001–0.167	0.000–0.013	0.001–0.002
Alkali Feldspar				
X_{ab}	0.858–0.949	–	–	–
X_{an}	0.051–0.135	–	–	–
X_{or}	0.000–0.059	–	–	–
Magnetite				
x(mt)	–	–	–	0.999–0.999
Ilmenite				
MnO (wt%)	–	2.205–3.818	0.991–1.110	0.330–0.510
TiO_2 (wt%)	–	49.548–51.773	52.951–53.068	46.103–51.158

$X_{alm} = Fe^{2+} / (Fe^{2+} + Mg + Ca + Mn)$; $X_{py} = Mg / (Fe^{2+} + Mg + Ca + Mn)$; $X_{grs} = Ca / (Fe^{2+} + Mg + Ca + Mn)$; $X_{sps} = Mn / (Fe^{2+} + Mg + Ca + Mn)$; $X_{Fe} = Fe^{2+} / (Fe^{2+} + Mg)$; $X_{ab} = Na / (Na + Ca + K)$; $X_{an} = Ca / (Na + Ca + K)$; $X_{or} = K / (Na + Ca + K)$; $x(mt) = Fe^{2+} / (Fe^{2+} + Mg)$

APPENDIX F: EXTENDED GEOCHRONOLOGY METHODS

Zircon geochronology was done on epoxy resin-mounted zircon grains from samples 53806 and 53810. Zircons were extracted from the rock by crushing, sieving, panning, Frantz Isodynamic separation and heavy liquids. Mounted grains were imaged using a Gatan Cathodoluminescence (CL) detector attached to a FEI Quanta 600 SEM at Adelaide Microscopy. Zircons were not found in sample 53815.

Monazite geochronology was conducted *in situ*, i.e. in thin section for samples 53811, 53815, 53816 and 53817. Monazites were first located in each thin section using a back-scattered electron detector on a FEI Quanta 600 Scanning Electron Microscope (SEM) accompanied with Mineral Liberation Analysis (MLA) software. Selected grains were then imaged using a back-scattered electron (BSE) detector on a Phillips XL30 SEM to determine the microstructural location and compositional variability of each grain. BSE images and MLA maps were collected using an accelerating voltage of 15–25 kV, spot size of 4–6 and working distance of 10 mm.

Zircon U–Pb data was collected at Adelaide Microscopy using a RESOlution LR 193 nm Excimer laser in a He–ablation atmosphere, coupled to an Agilent 7700s ICP–MS for isotopic characterisation. Ablation was performed with a frequency of 5 Hz and spot sizes of both 19 and 29 μm for each sample, based on grain size. Data acquisition was undertaken with 30 seconds of background measurement and 30 seconds of sample ablation. Isotopes measured were ^{202}Hg, ^{204}Pb, ^{206}Pb, ^{207}Pb, ^{208}Pb, ^{232}Th and ^{238}U.

Monazite U–Pb and trace element data was collected at Adelaide Microscopy using a RESOlution LR 193 nm Excimer laser in a He–ablation atmosphere, coupled to an Agilent 7700s ICP–MS for isotopic characterisation. Ablation was performed with a frequency of 5 Hz. A spot size of 13 μm was used for samples 53811 and 53816, whereas samples 53815 and 53817 were analysed using both 9 μm and 13 μm spot sizes due to the variability in monazite size. Data acquisition included 30 seconds of background measurement and 30 seconds of sample ablation. Isotopes measured were ^{29}Si, ^{43}Ca, ^{89}Y, ^{90}Zr, ^{139}La, ^{140}Ce, ^{141}Pr, ^{146}Nd, ^{147}Sm, ^{153}Eu, ^{157}Gd, ^{159}Tb, ^{163}Dy, ^{165}Ho, ^{166}Er, ^{169}Tm, ^{172}Yb, ^{175}Lu, ^{202}Hg, ^{204}Pb, ^{206}Pb, ^{207}Pb, ^{208}Pb, ^{232}Th and ^{238}U. Trace element data was used to assist in the assessment and interpretation of U–Pb data.

Zircon and monazite isotopic data were reduced using Iolite software (Paton, Hellstrom, Paul, Woodhead, & Hergt, 2011). Elemental fractionation and mass bias for zircon geochronology was corrected by using the primary standard GJ (TIMS data: ^{207}Pb/^{206}Pb = 607.7 ± 4.3 Ma, ^{206}Pb/^{238}U = 600.7 ± 1.1 Ma and ^{207}Pb/^{235}U = 602.0 ± 1.0; Jackson, Pearson, Griffin, & Belousova, 2004) with standard bracketing every 10 unknown zircon analyses. Data accuracy was monitored using secondary zircon standards Plešovice (TIMS data: ^{206}Pb/^{238}U = 337.13 ± 0.37 Ma; Sláma et al., 2008) and 91500 (TIMS data: ^{206}Pb/^{238}U = 1065 Ma; Wiedenbeck et al., 1995). For monazite, the primary standard MAdel (TIMS data: ^{207}Pb/^{206}Pb = 492.01 ± 0.77 Ma, ^{206}Pb/^{238}U = 517.9 ± 2.6 Ma and ^{207}Pb/^{235}U = 513.13 ± 0.20 Ma (updated from Payne, Hand, Barovich, and Wade (2008) with additional TIMS analyses), was used, with standard bracketing every 10–15 unknown Monazite analyses. Data accuracy was monitored using in-house monazite standards 222 (SHRIMP data: ^{206}Pb/^{238}U = 450.2 ± 3.4 Ma) and Ambat (^{206}Pb/^{238}U = ~520–525 Ma).

The weighted mean ages of primary and in-house zircon standards analysed over the course of this study are as follows: GJ: $^{207}Pb/^{206}Pb$ = 580.5 ± 6.6 (n = 100, MSWD = 1.02), $^{206}Pb/^{238}U$ = 600.34 ± 0.78 (n = 100, MSWD = 0.94), $^{207}Pb/^{235}U$ = 600.5 ± 1.3 (n = 100, MSWD = 0.92); Plesovice: $^{207}Pb/^{206}Pb$ = 322 ± 15 (n = 50, MSWD = 2.3), $^{206}Pb/^{238}U$ = 336.61 ± 0.71 (n = 50, MSWD = 1.3), $^{207}Pb/^{235}U$ = 337.3 ± 1.6 (n = 50, MSWD = 1.8); 91500: $^{207}Pb/^{206}Pb$ = 1032 ± 15 (n = 50, MSWD = 1.8), $^{206}Pb/^{238}U$ = 1051.6 ± 2.4 (n = 50, MSWD = 1.07), $^{207}Pb/^{235}U$ = 1051.6 ± 4.5 (n = 50, MSWD = 1.7).

The weighted mean ages of primary and in-house monazite standards analysed over the course of this study are as follows: MAdel: $^{207}Pb/^{206}Pb$ = 477 ± 11 (n = 34, MSWD = 0.64), $^{206}Pb/^{238}U$ = 518.3 ± 1.4 (n = 34, MSWD = 0.71), $^{207}Pb/^{235}U$ = 512.3 ± 2.0 (n = 34, MSWD = 0.49); 222: $^{207}Pb/^{206}Pb$ = 433 ± 11 (n = 26, MSWD = 0.50), $^{206}Pb/^{238}U$ = 450 ± 1.3 (n = 26, MSWD = 0.96), $^{207}Pb/^{235}U$ = 449 ± 1.8 (n = 26, MSWD = 0.85); Ambat: $^{207}Pb/^{206}Pb$ = 484 ± 11 (n = 25, MSWD = 0.97), $^{206}Pb/^{238}U$ = 521.7 ± 1.4 (n = 25, MSWD = 0.82), $^{207}Pb/^{235}U$ = 515.1 ± 2.4 (n = 25, MSWD = 1.6).

Errors are all at the 2σ level (95% confidence), unless otherwise stated. Concordance for zircon was calculated using the ratio of ($^{206}Pb/^{238}U$)/($^{207}Pb/^{206}Pb$) with a concordance threshold of ≤ 95 and ≥105 %. Monazite analyses are deemed concordant if their 2σ error ellipse overlaps with the concordia curve (e.g. Spencer, Kirkland, & Taylor, 2016).

APPENDIX G: ZIRCON U–PB RESULTS

Analysis	Spot Size (µm)	$^{207}Pb/^{206}Pb$	2σ	$^{206}Pb/^{238}U$	2σ	$^{207}Pb/^{235}U$	2σ	rho	$^{207}Pb/^{206}Pb$ Age	2σ	$^{206}Pb/^{238}U$ Age	2σ	$^{207}Pb/^{235}U$ Age	2σ	Conc. (%)
53810															
FT1_10 - 1	29	0.0861	0.0021	0.2178	0.0025	2.583	0.056	0.03416	1324	47	1270	13	1293	16	95.92
FT1_10 - 2	29	0.084	0.0022	0.2292	0.0028	2.658	0.062	0.1837	1280	49	1330	15	1314	17	103.91
FT1_10 - 3	29	0.0942	0.0015	0.2721	0.0026	3.527	0.046	0.37093	1509	29	1551.1	13	1532.8	10	102.79
FT1_10 - 4	29	0.08453	0.0014	0.2207	0.0021	2.573	0.038	0.29291	1300	33	1285.6	11	1292.2	11	98.89
FT1_10 - 5	29	0.09503	0.0014	0.2646	0.0022	3.471	0.041	0.37212	1527	28	1513.2	11	1520.3	9.2	99.10
FT1_10 - 6	29	0.08488	0.0014	0.2243	0.0021	2.626	0.037	0.14984	1308	33	1304.7	11	1307.2	10	99.75
FT1_10 - 7	29	0.07959	0.0013	0.1695	0.0028	1.85	0.037	0.8466	1185	32	1009	15	1063	13	85.15
FT1_10 - 8	29	0.13101	0.0019	0.3853	0.0033	6.965	0.084	0.66036	2110.2	25	2100.6	15	2106.4	11	99.55
FT1_10 - 9	29	0.132	0.0022	0.311	0.01	5.62	0.19	0.96111	2122	29	1741	50	1914	29	82.05
FT1_10 - 10	29	0.1445	0.0023	0.4379	0.0047	8.717	0.13	0.55312	2279	28	2340	21	2307.5	13	102.68
FT1_10 - 11	29	0.1325	0.0019	0.3054	0.0059	5.585	0.11	0.94889	2129.7	25	1717	29	1910	18	80.62
FT1_10 - 12	29	0.08939	0.0014	0.1527	0.0018	1.883	0.028	0.70689	1410	30	916.2	9.9	1074.5	9.9	64.98
FT1_10 - 13	29	0.09562	0.0016	0.2621	0.0024	3.457	0.049	0.56873	1537	31	1500.5	12	1516.6	11	97.63
FT1_10 - 14	29	0.09429	0.0015	0.2651	0.0025	3.464	0.047	0.27025	1511	30	1515.9	13	1518.3	11	100.32
FT1_10 - 15	29	0.0849	0.0022	0.2327	0.0054	2.728	0.079	0.65837	1307	49	1348	28	1334	21	103.14
FT1_10 - 16	29	0.08502	0.0015	0.2216	0.0024	2.597	0.039	0.32254	1314	33	1290.3	13	1298.9	11	98.20

FT1_10 - 17	29	0.086	0.0026	0.1901	0.0032	2.257	0.066	0.26787	1316	64	1122	17	1194	21	85.26
FT1_10 - 18	29	0.0866	0.0014	0.2291	0.0022	2.745	0.038	0.44687	1350	31	1330.7	12	1340	10	98.57
FT1_10 - 19	29	0.0863	0.0013	0.2285	0.0021	2.719	0.033	0.56956	1343	29	1327.4	11	1334.1	9.3	98.84
FT1_10 - 20	29	0.0862	0.0027	0.2229	0.0034	2.604	0.073	0.27808	1325	62	1297	18	1299	21	97.89
FT1_10 - 21	29	0.0848	0.0029	0.2242	0.0033	2.612	0.08	0.071336	1274	67	1304	17	1297	23	102.35
FT1_10 - 22	29	0.0848	0.0017	0.2193	0.0022	2.558	0.042	0.082996	1302	39	1278.2	12	1288.9	12	98.17
FT1_10 - 23	29	0.1318	0.0021	0.382	0.0034	6.937	0.093	0.25332	2119	29	2085.6	16	2102.6	12	98.42
FT1_10 - 24	29	0.08889	0.0013	0.2203	0.0022	2.703	0.041	0.87404	1400	28	1283	12	1328.3	11	91.64
FT1_10 - 25	29	0.1295	0.0021	0.3928	0.0038	7.012	0.096	0.3157	2090	30	2135	18	2113.2	13	102.15
FT1_10 - 26	29	0.09608	0.0015	0.2668	0.0024	3.534	0.042	0.33984	1547	29	1524.2	12	1534.4	9.3	98.53
FT1_10 - 27	29	0.12269	0.0019	0.339	0.0054	5.685	0.091	0.81268	1994	28	1881	26	1931	13	94.33
FT1_10 - 28	29	0.09522	0.0014	0.2599	0.0024	3.393	0.042	0.67343	1530.9	27	1489.1	12	1502.5	9.6	97.27
FT1_10 - 29	29	0.08698	0.0013	0.229	0.002	2.754	0.032	0.25288	1357	30	1329.2	11	1342.9	8.8	97.95
FT1_10 - 30	29	0.0855	0.0024	0.2219	0.003	2.612	0.064	0.010361	1304	56	1291	16	1300	18	99.00
FT1_10 - 31	29	0.0866	0.0028	0.2259	0.0032	2.692	0.078	0.024908	1327	63	1313	17	1324	21	98.94
FT1_10 - 32	29	0.12651	0.0019	0.368	0.0037	6.422	0.091	0.62331	2048	27	2020	17	2034.1	12	98.63
FT1_10 - 33	29	0.0949	0.0017	0.2652	0.0029	3.495	0.048	0.17868	1524	33	1516	15	1525.7	11	99.48
FT1_10 - 34	29	0.09195	0.0015	0.2454	0.0026	3.089	0.042	0.44353	1464	31	1415	14	1429.6	11	96.65
FT1_10 - 35	29	0.0859	0.0017	0.2282	0.0029	2.684	0.041	0.17148	1332	38	1325	15	1323.6	11	99.47
FT1_10 - 36	29	0.08679	0.0014	0.2058	0.0021	2.45	0.033	0.44036	1354	31	1206.1	11	1257	9.7	89.08

FT1_10 - 37	29	0.08726	0.0014	0.2091	0.0028	2.504	0.038	0.65364	1364	32	1224	15	1272.8	11	89.74
FT1_10 - 38	29	0.08836	0.0013	0.21069	0.0018	2.568	0.031	0.46828	1388	28	1232.4	9.3	1291.1	8.8	88.79
FT1_10 - 39	29	0.1283	0.0023	0.3534	0.005	6.232	0.11	0.55517	2073	32	1950	24	2008	16	94.07
FT1_10 - 40	29	0.12707	0.0019	0.3811	0.0076	6.7	0.17	0.96743	2056	26	2079	36	2066	23	101.12
FT1_10 - 41	29	0.08233	0.0012	0.1571	0.0034	1.781	0.044	0.97197	1252	28	940	19	1036	16	75.08
FT1_10 - 42	29	0.1326	0.002	0.3884	0.0036	7.099	0.088	0.29923	2130	27	2115	17	2123.3	11	99.30
FT1_10 - 43	29	0.08115	0.0012	0.1388	0.0027	1.551	0.033	0.96514	1223.4	28	838	15	949	13	68.50
FT1_10 - 44	29	0.08642	0.0012	0.2163	0.0018	2.581	0.031	0.50993	1346	28	1262.5	9.7	1294.8	8.6	93.80
FT1_10 - 45	29	0.0956	0.0017	0.2542	0.0024	3.35	0.052	0.12621	1534	34	1460	12	1491.5	12	95.18
FT1_10 - 46	29	0.12976	0.002	0.3902	0.0042	6.937	0.09	0.59861	2093	27	2123	20	2102.8	11	101.43
FT1_10 - 47	29	0.12727	0.0019	0.3728	0.0032	6.547	0.078	0.2919	2058	27	2042.2	15	2051.8	11	99.23
FT1_10 - 48	29	0.0855	0.002	0.2318	0.0027	2.726	0.054	-0.013724	1319	44	1343	14	1333	15	101.82
FT1_10 - 49	29	0.09192	0.0015	0.2485	0.0022	3.149	0.043	0.35507	1462	31	1430.5	11	1444	11	97.85
FT1_10 - 50	29	0.12991	0.0019	0.3572	0.0034	6.398	0.08	0.73247	2095.1	25	1968	16	2031.3	11	93.93
FT1_10 - 51	29	0.10623	0.0016	0.306	0.0027	4.483	0.056	0.52143	1735	26	1721	13	1727.2	10	99.19
FT2_10 - 1	29	0.0864	0.0017	0.2318	0.0022	2.761	0.045	0.11926	1340	37	1344	12	1345.1	12	100.30
FT2_10 - 2	29	0.11878	0.0017	0.3634	0.0032	5.952	0.074	0.62041	1936	26	1998.1	15	1968.3	11	103.21
FT2_10 - 3	29	0.0852	0.0016	0.2262	0.0022	2.657	0.044	0.37633	1318	36	1314.5	12	1315.3	12	99.73
FT2_10 - 4	29	0.1165	0.002	0.3453	0.0035	5.545	0.09	0.38267	1898	32	1912	17	1906	14	100.74
FT2_10 - 5	29	0.0853	0.0018	0.2223	0.0023	2.613	0.05	0.11774	1316	44	1293.9	12	1304	15	98.32

FT2_10 - 6	29	0.1303	0.002	0.3712	0.0032	6.667	0.082	0.22227	2099	27	2035	15	2067.7	11	96.95
FT2_10 - 7	29	0.1447	0.0023	0.4134	0.0038	8.245	0.11	0.44524	2281	27	2232	17	2257.3	12	97.85
FT1_10 - 52	19	0.0955	0.0014	0.2609	0.0035	3.429	0.048	0.32668	1534	27	1494	18	1510.8	11	97.39
FT1_10 - 53	19	0.1324	0.0017	0.3837	0.0046	7.029	0.099	0.44862	2127	23	2095	21	2114.3	12	98.50
FT1_10 - 54	19	0.1341	0.0022	0.3455	0.0053	6.358	0.11	0.43405	2148	29	1913	25	2026	15	89.06
FT1_10 - 55	19	0.0856	0.0018	0.1792	0.0026	2.122	0.045	0.25325	1321	40	1062	14	1154	15	80.39
FT1_10 - 56	19	0.0847	0.0017	0.2192	0.0029	2.563	0.054	0.25218	1306	38	1278	16	1288	15	97.86
FT1_10 - 57	19	0.0859	0.0019	0.2117	0.0052	2.506	0.072	0.70178	1321	43	1236	28	1268	21	93.57
FT1_10 - 58	19	0.08548	0.001	0.2249	0.0034	2.656	0.043	0.84087	1324	22	1307	18	1315.2	12	98.72
FT1_10 - 59	19	0.0876	0.0023	0.2142	0.003	2.578	0.066	0.037042	1353	50	1251	16	1293	18	92.46
FT1_10 - 60	19	0.1262	0.002	0.314	0.0085	5.46	0.19	0.92263	2039	29	1757	42	1887	29	86.17
FT1_10 - 61	19	0.0891	0.0015	0.1435	0.0065	1.759	0.074	0.94419	1404	33	864	36	1028	27	61.54
FT1_10 - 62	19	0.08504	0.0013	0.1835	0.003	2.149	0.038	0.63844	1318	30	1086	16	1164	12	82.40
FT1_10 - 63	19	0.0776	0.0013	0.135	0.016	1.44	0.16	0.99426	1133	32	811	91	881	64	71.58
FT1_10 - 64	19	0.09631	0.0012	0.2634	0.0031	3.5	0.049	0.42228	1551	24	1507.3	16	1526.7	11	97.18
FT1_10 - 65	19	0.09406	0.0012	0.2443	0.003	3.179	0.048	0.63233	1506	24	1409	16	1451.2	12	93.56
FT1_10 - 66	19	0.09	0.0021	0.2104	0.0039	2.597	0.07	0.53585	1417	42	1230	21	1295	20	86.80
FT1_10 - 67	19	0.0841	0.0015	0.1995	0.0034	2.321	0.048	0.74402	1296	35	1172	18	1217	14	90.43
FT1_10 - 68	19	0.0849	0.0027	0.213	0.0044	2.487	0.079	0.25292	1305	63	1244	23	1267	23	95.33
FT1_10 - 69	19	0.0887	0.004	0.2324	0.0047	2.83	0.12	0.022714	1379	86	1347	24	1361	31	97.68

FT1_10 - 70	19	0.0872	0.0043	0.2295	0.0062	2.76	0.16	0.55651	1346	100	1331	32	1339	45	98.89
FT1_10 - 71	19	0.0817	0.0048	0.2249	0.0059	2.52	0.14	0.054883	1210	110	1307	31	1272	39	108.02
FT1_10 - 72	19	0.0851	0.0021	0.2104	0.0031	2.486	0.066	0.26586	1304	50	1231	17	1264	19	94.40
FT1_10 - 73	19	0.0863	0.0014	0.2087	0.0035	2.486	0.05	0.67494	1339	31	1222	19	1266	15	91.26
FT1_10 - 74	19	0.08832	0.0012	0.2288	0.0028	2.789	0.039	0.42393	1385	26	1328.2	15	1351.9	10	95.90
FT1_10 - 75	19	0.0873	0.0025	0.2055	0.0043	2.454	0.067	0.27365	1339	55	1204	23	1257	20	89.92
FT1_10 - 76	19	0.1352	0.0034	0.249	0.0072	4.63	0.16	0.69775	2162	43	1433	37	1752	28	66.28
FT1_10 - 77	19	0.0854	0.0017	0.2191	0.0032	2.57	0.053	0.38392	1318	38	1279	16	1292	16	97.04
FT1_10 - 78	19	0.0861	0.0024	0.2272	0.0045	2.688	0.07	0.16933	1330	55	1319	24	1324	19	99.17
FT1_10 - 79	19	0.0951	0.0034	0.2527	0.0049	3.32	0.12	0.099301	1494	72	1451	25	1476	28	97.12
FT1_10 - 80	19	0.0929	0.0017	0.2552	0.0039	3.272	0.061	0.38896	1478	34	1464	20	1472	14	99.05
FT1_10 - 81	19	0.0967	0.002	0.2589	0.0037	3.452	0.068	0.051803	1548	40	1484	19	1514	16	95.87
FT1_10 - 82	19	0.0954	0.0019	0.2627	0.0035	3.458	0.067	0.067643	1529	39	1503	18	1517	16	98.30
FT1_10 - 83	19	0.1045	0.0021	0.2223	0.0063	3.238	0.095	0.82653	1700	36	1292	34	1463	24	76.00
FT1_10 - 84	19	0.1324	0.0023	0.3529	0.0062	6.45	0.13	0.60105	2122	30	1947	29	2038	17	91.75
FT1_10 - 85	19	0.0815	0.0032	0.2086	0.0041	2.331	0.086	0.011738	1173	85	1221	22	1216	26	104.09
FT1_10 - 86	19	0.0859	0.0031	0.2165	0.0039	2.578	0.087	-0.012525	1304	71	1265	21	1287	25	97.01
FT1_10 - 87	19	0.0912	0.0015	0.2305	0.0028	2.903	0.051	0.31425	1443	32	1337.1	15	1381	13	92.66
FT1_10 - 88	19	0.0862	0.0021	0.2162	0.0036	2.566	0.062	0.23134	1323	48	1261	19	1288	18	95.31
FT1_10 - 90	19	0.097	0.0026	0.1087	0.0036	1.449	0.05	0.61355	1561	52	665	21	908	21	42.60

FT1_10 - 91	19	0.1155	0.0017	0.3274	0.0041	5.219	0.08	0.25105	1883	27	1827	19	1854.8	13	97.03
FT1_10 - 92	19	0.116	0.0016	0.3197	0.0045	5.124	0.078	0.58445	1892	24	1788	22	1838.9	13	94.50
FT1_10 - 93	19	0.08778	0.0011	0.1929	0.0041	2.338	0.055	0.9137	1374	25	1136	22	1221	17	82.68
FT1_10 - 94	19	0.0957	0.0017	0.2611	0.0039	3.465	0.069	0.53789	1546	31	1495	20	1517	16	96.70
FT1_10 - 95	19	0.1307	0.0023	0.3679	0.0048	6.665	0.12	0.29992	2104	31	2019	23	2066	16	95.96
FT1_10 - 96	19	0.1285	0.0031	0.4084	0.0065	7.23	0.18	0.3604	2073	43	2207	30	2138	23	106.46
FT1_10 - 97	19	0.136	0.011	0.2072	0.0068	3.85	0.29	0.11869	2120	130	1213	36	1593	56	57.22
FT1_10 - 98	19	0.0893	0.0027	0.1919	0.0051	2.357	0.079	0.53037	1401	59	1132	27	1228	24	80.80
FT1_10 - 99	19	0.084	0.0035	0.224	0.005	2.59	0.11	0.33037	1254	82	1302	27	1289	32	103.83
FT1_10 - 100	19	0.1187	0.0019	0.3357	0.0053	5.485	0.094	0.44215	1940	26	1866	25	1898	15	96.19
FT1_10 - 101	19	0.1046	0.0016	0.2669	0.0045	3.843	0.071	0.64606	1705	28	1525	23	1601	15	89.44
FT1_10 - 102	19	0.09567	0.0012	0.2607	0.0033	3.447	0.051	0.56772	1538	24	1493	17	1514.4	12	97.07
FT1_10 - 103	19	0.0846	0.0016	0.2136	0.0027	2.497	0.047	0.13891	1296	36	1247.9	14	1271	14	96.29
FT1_10 - 104	19	0.0832	0.004	0.2206	0.0048	2.54	0.11	0.096392	1240	91	1284	25	1276	31	103.55
FT1_10 - 105	19	0.09149	0.0012	0.2232	0.0032	2.822	0.048	0.68213	1453	25	1298	17	1361.5	13	89.33
FT1_10 - 106	19	0.0925	0.0023	0.2007	0.0035	2.555	0.062	0.22844	1469	49	1179	19	1287	18	80.26
FT1_10 - 107	19	0.08499	0.0012	0.2217	0.0026	2.606	0.043	0.39519	1310	29	1290.5	14	1302.3	13	98.51
FT1_10 - 108	19	0.08459	0.0011	0.2106	0.003	2.457	0.04	0.64755	1302	26	1232	16	1259.8	11	94.62
FT1_10 - 109	19	0.1311	0.0025	0.3792	0.0065	6.84	0.14	0.42532	2109	34	2072	30	2090	18	98.25
FT1_10 - 110	19	0.1342	0.0028	0.409	0.0075	7.56	0.17	0.481	2150	36	2210	34	2179	20	102.79

FT1_10 - 111	19	0.0875	0.0023	0.175	0.0044	2.088	0.072	0.66991	1355	51	1039	24	1141	23	76.68
FT1_10 - 112	19	0.1307	0.0018	0.3763	0.0046	6.8	0.1	0.38172	2104	25	2059	21	2085.9	13	97.86
FT1_10 - 113	19	0.1306	0.0021	0.3889	0.0056	7	0.13	0.50433	2099	29	2117	26	2111	16	100.86
FT1_10 - 114	19	0.0845	0.0013	0.1653	0.0026	1.924	0.034	0.55675	1299	31	986	14	1088.8	12	75.90
FT1_10 - 115	19	0.0844	0.003	0.2155	0.0051	2.483	0.084	0.24231	1307	77	1257	27	1272	28	96.17
FT1_10 - 116	19	0.08482	0.0012	0.2176	0.0027	2.551	0.04	0.45999	1307	27	1269	14	1285.8	11	97.09
FT1_10 - 117	19	0.1177	0.002	0.3155	0.0043	5.133	0.085	0.15948	1914	31	1767	21	1842	14	92.32
FT1_10 - 118	19	0.1239	0.0021	0.3616	0.0049	6.176	0.12	0.40724	2008	30	1989	23	2000	17	99.05
FT1_10 - 119	19	0.1072	0.0031	0.2384	0.0057	3.55	0.17	0.94493	1739	55	1377	30	1529	38	79.18
FT1_10 - 120	19	0.0977	0.0029	0.2832	0.0093	3.79	0.13	0.64946	1568	59	1603	47	1592	28	102.23
FT1_10 - 121	19	0.1416	0.0019	0.3687	0.0071	7.22	0.14	0.83021	2244	23	2022	33	2136	18	90.11
FT1_10 - 122	19	0.1455	0.002	0.3828	0.0091	7.71	0.21	0.93516	2293	23	2086	43	2194	25	90.97
FT1_10 - 123	19	0.1451	0.0017	0.3788	0.0072	7.62	0.17	0.94283	2287	21	2069	33	2183	21	90.47
FT1_10 - 124	19	0.0856	0.002	0.2194	0.0034	2.581	0.057	0.085085	1326	49	1279	18	1294	16	96.46
FT1_10 - 125	19	0.0826	0.0036	0.2009	0.0069	2.29	0.13	0.63225	1209	84	1178	37	1193	39	97.44
FT1_10 - 126	19	0.1418	0.0019	0.4129	0.0053	8.094	0.12	0.48465	2249	23	2227	24	2241.7	13	99.02
FT1_10 - 127	19	0.1304	0.002	0.34	0.012	6.15	0.24	0.93514	2100	28	1884	57	1988	38	89.71
FT1_10 - 128	19	0.0983	0.0024	0.2593	0.0041	3.524	0.088	0.28048	1574	45	1486	21	1528	20	94.41
FT1_10 - 129	19	0.0947	0.0018	0.2367	0.0036	3.097	0.062	0.43001	1512	36	1369	19	1432	15	90.54
FT1_10 - 130	19	0.1425	0.0027	0.4061	0.0054	7.99	0.15	0.21083	2249	33	2197	25	2227	17	97.69

FT1_10 - 131	19	0.1426	0.0023	0.4177	0.0064	8.23	0.15	0.54792	2254	28	2249	29	2254	17	99.78
FT1_10 - 132	19	0.1291	0.0025	0.321	0.0064	5.72	0.14	0.64806	2077	33	1793	31	1930	21	86.33
FT1_10 - 133	19	0.1582	0.0019	0.4348	0.0052	9.52	0.13	0.48586	2434	21	2327	24	2388.8	13	95.60
FT1_10 - 134	19	0.1566	0.0021	0.4309	0.0057	9.34	0.16	0.68229	2416	23	2309	26	2369	16	95.57
FT1_10 - 135	19	0.10568	0.0013	0.3018	0.0038	4.409	0.06	0.56541	1725	21	1700	19	1714.3	11	98.55
FT1_10 - 136	19	0.0848	0.0016	0.1956	0.0031	2.294	0.051	0.56478	1302	36	1151	17	1208	16	88.40
FT1_10 - 137	19	0.118	0.0021	0.2566	0.0078	4.18	0.14	0.87161	1918	33	1469	40	1661	27	76.59
FT1_10 - 138	19	0.1187	0.002	0.2746	0.0066	4.52	0.13	0.84702	1938	30	1562	34	1731	24	80.60
FT1_10 - 139	19	0.0938	0.0054	0.182	0.01	2.37	0.21	0.72557	1450	120	1077	57	1212	63	74.28
FT1_10 - 140	19	0.0958	0.0017	0.2143	0.0069	2.845	0.095	0.8889	1543	35	1249	37	1360	25	80.95
FT1_10 - 141	19	0.1278	0.0018	0.1965	0.0067	3.49	0.13	0.96644	2063	26	1154	37	1515	33	55.94
FT1_10 - 142	19	0.0948	0.0014	0.2092	0.005	2.741	0.069	0.88422	1522	26	1223	26	1336	19	80.35
FT1_10 - 143	19	0.096	0.0016	0.2756	0.0035	3.663	0.065	0.20462	1544	33	1569	18	1562	14	101.62
FT1_10 - 144	19	0.085	0.0015	0.2207	0.0031	2.592	0.049	0.36549	1312	34	1285	16	1298	13	97.94
FT1_10 - 145	19	0.085	0.0016	0.2229	0.0031	2.622	0.052	0.21173	1309	38	1297	17	1305	14	99.08
FT1_10 - 146	19	0.0875	0.0014	0.202	0.0035	2.447	0.052	0.69231	1367	32	1185	19	1254	15	86.69
FT1_10 - 147	19	0.0889	0.0018	0.1963	0.004	2.412	0.051	0.58834	1393	38	1155	22	1244	15	82.91
FT2_10 - 8	19	0.08607	0.0011	0.2053	0.0031	2.45	0.043	0.72628	1336	26	1203	16	1256.2	13	90.04
FT2_10 - 9	19	0.1069	0.0026	0.2408	0.0059	3.56	0.12	0.73155	1737	45	1390	31	1534	28	80.02
FT2_10 - 10	19	0.0944	0.0015	0.2536	0.0039	3.304	0.059	0.49314	1511	30	1457	20	1481	14	96.43

FT2_10 - 11	19	0.1186	0.002	0.2471	0.0036	4.04	0.075	0.52634	1928	29	1423	19	1640	15	73.81
FT2_10 - 12	19	0.1353	0.0022	0.4035	0.0056	7.545	0.12	0.30437	2163	28	2185	26	2177	14	101.02
FT2_10 - 13	19	0.1317	0.002	0.3896	0.0057	7.081	0.11	0.48254	2117	27	2120	26	2121	14	100.14
FT2_10 - 14	19	0.1552	0.0023	0.4539	0.0059	9.72	0.15	0.39411	2400	25	2412	26	2409	15	100.50
FT2_10 - 15	19	0.1548	0.0022	0.455	0.0058	9.75	0.15	0.45757	2395	25	2417	26	2410	14	100.92
FT2_10 - 16	19	0.084	0.0015	0.1977	0.0042	2.295	0.063	0.79085	1285	35	1162	23	1209	19	90.43
FT2_10 - 17	19	0.0905	0.0033	0.2193	0.0083	2.72	0.14	0.61283	1399	74	1274	44	1322	36	91.07
FT2_10 - 18	19	0.1322	0.0042	0.309	0.013	5.62	0.25	0.76358	2116	56	1734	66	1911	39	81.95
FT2_10 - 19	19	0.1244	0.0029	0.3069	0.0056	5.26	0.13	0.43701	2014	42	1725	28	1861	22	85.65
FT2_10 - 20	19	0.0724	0.0023	0.0477	0.0014	0.48	0.025	0.84883	980	66	300.1	8.7	396	17	30.62
FT2_10 - 21	19	0.096	0.0028	0.2237	0.0052	2.981	0.1	0.5414	1536	54	1301	27	1399	25	84.70
FT2_10 - 22	19	0.1316	0.0024	0.3804	0.0054	6.91	0.14	0.40219	2114	32	2078	26	2098	18	98.30
FT2_10 - 23	19	0.0827	0.0078	0.1489	0.0066	1.68	0.15	0.13548	1160	200	894	37	986	58	77.07
FT2_10 - 24	19	0.0855	0.0031	0.2108	0.004	2.479	0.084	0.025484	1304	72	1233	21	1262	24	94.56
FT2_10 - 25	19	0.0828	0.0024	0.1734	0.0036	1.978	0.059	0.39028	1242	57	1030	20	1105	20	82.93
FT2_10 - 26	19	0.0925	0.0017	0.2562	0.0039	3.28	0.064	0.3981	1469	35	1470	20	1474	15	100.07
FT2_10 - 27	19	0.0861	0.002	0.1952	0.0033	2.317	0.058	0.35636	1339	44	1149	18	1216	18	85.81
FT2_10 - 28	19	0.0916	0.0022	0.1991	0.0032	2.507	0.065	0.3897	1449	45	1170	17	1272	19	80.75
FT2_10 - 29	19	0.0902	0.0034	0.2444	0.0093	3.06	0.18	0.80868	1404	76	1407	49	1408	46	100.21
FT2_10 - 30	19	0.0945	0.0016	0.2705	0.0039	3.537	0.065	0.38352	1515	31	1543	20	1535	14	101.85

FT2_10 - 31	19	0.0932	0.0045	0.12	0.0027	1.551	0.072	0.039094	1467	90	731	16	945	28	49.83
FT2_10 - 32	19	0.1576	0.002	0.3953	0.0097	8.6	0.21	0.92837	2427	22	2143	46	2294	22	88.30
FT2_10 - 34	19	0.094	0.0014	0.2542	0.0037	3.3	0.059	0.59701	1504	28	1460	19	1480	14	97.07
FT2_10 - 35	19	0.1475	0.0028	0.25	0.016	5.07	0.31	0.9618	2313	33	1433	82	1815	56	61.95
FT2_10 - 36	19	0.0831	0.0016	0.1419	0.006	1.635	0.075	0.92703	1270	35	854	34	976	28	67.24
FT2_10 - 39	19	0.085	0.0026	0.2096	0.0037	2.462	0.075	0.17639	1292	62	1226	20	1258	21	94.89
FT2_10 - 40	19	0.1095	0.0037	0.219	0.015	3.36	0.31	0.96745	1790	59	1269	79	1464	73	70.89
FT2_10 - 41	19	0.126	0.004	0.3441	0.0065	5.98	0.2	0.74232	2032	57	1906	31	1969	30	93.80
FT2_10 - 42	19	0.133	0.0028	0.3775	0.0061	6.92	0.15	0.32099	2130	37	2064	29	2099	19	96.90
FT2_10 - 44	19	0.0868	0.0014	0.1898	0.0032	2.278	0.046	0.62757	1350	31	1120	18	1205	14	82.96
FT2_10 - 45	19	0.0855	0.0034	0.2085	0.0061	2.4	0.14	0.76772	1316	77	1220	33	1237	42	92.71
FT2_10 - 46	19	0.0857	0.0015	0.1968	0.0028	2.336	0.046	0.49454	1323	35	1158	15	1221	14	87.53
FT2_10 - 47	19	0.0869	0.0024	0.1977	0.0042	2.365	0.06	0.01213	1340	38	1162	23	1229	18	86.72
FT2_10 - 48	19	0.0898	0.0015	0.2153	0.0031	2.678	0.05	0.50044	1414	32	1257	16	1321	14	88.90
FT2_10 - 49	19	0.0849	0.0018	0.2309	0.0036	2.713	0.056	0.13162	1314	43	1339	19	1331	15	101.90
FT2_10 - 50	19	0.0869	0.0016	0.2119	0.0043	2.54	0.056	0.64236	1349	36	1238	23	1281	16	91.77
FT2_10 - 51	19	0.0925	0.0015	0.2281	0.0033	2.916	0.053	0.5338	1471	30	1326	17	1384	14	90.14
53806															
FT2_06 - 1	29	0.13044	0.002	0.3925	0.0036	7.068	0.084	0.2274	2101	27	2134	17	2119.5	11	101.57
FT1_06 - 1	29	0.12802	0.0019	0.381	0.0034	6.723	0.084	0.43662	2069	27	2080.5	16	2075.1	11	100.56

FT2_06 - 2	29	0.0863	0.0016	0.2254	0.0021	2.678	0.043	0.21726	1339	36	1310	11	1321.2	12	97.83
FT1_06 - 2	19	0.12732	0.0015	0.325	0.0048	5.718	0.085	0.75746	2061	20	1813	23	1934.2	13	87.97
FT1_06 - 3	19	0.1273	0.0016	0.33	0.0063	5.8	0.12	0.8971	2059	22	1837	31	1944	19	89.22
FT1_06 - 4	19	0.1047	0.002	0.2361	0.0059	3.44	0.12	0.86398	1719	33	1365	31	1505	28	79.41
FT1_06 - 5	19	0.1057	0.0048	0.1643	0.0043	2.42	0.11	0.20028	1703	85	980	24	1235	31	57.55
FT1_06 - 6	19	0.0924	0.0016	0.2363	0.003	3.02	0.056	0.37551	1469	32	1367	16	1411	14	93.06
FT1_06 - 7	19	0.0935	0.0017	0.2467	0.0034	3.183	0.055	0.16594	1488	34	1421	18	1452	13	95.50
FT1_06 - 8	19	0.0859	0.0016	0.2229	0.0029	2.651	0.052	0.34601	1332	34	1297	16	1313	14	97.37
FT1_06 - 9	19	0.132	0.0019	0.3753	0.0049	6.832	0.11	0.52217	2121	25	2056	22	2088	15	96.94
FT1_06 - 10	19	0.0938	0.0017	0.2478	0.0047	3.205	0.085	0.77205	1499	35	1427	24	1457	20	95.20
FT2_06 - 7	19	0.0814	0.0038	0.2059	0.0038	2.28	0.1	0.24199	1149	97	1206	20	1199	34	104.96
FT2_06 - 9	19	0.13074	0.0016	0.3747	0.0049	6.778	0.1	0.67723	2106	21	2051	23	2081.9	13	97.39
FT2_06 - 10	19	0.13074	0.0015	0.3757	0.0048	6.797	0.1	0.72007	2106	21	2056	23	2085.5	13	97.63
FT2_06 - 11	19	0.0853	0.0026	0.2154	0.0033	2.535	0.076	0.13628	1290	60	1257	18	1276	22	97.44
FT2_06 - 12	19	0.0847	0.0017	0.2324	0.0033	2.728	0.057	0.25669	1301	41	1347	17	1334	16	103.54
FT2_06 - 13	19	0.0871	0.0031	0.2071	0.0042	2.482	0.083	0.087052	1340	70	1213	22	1259	25	90.52
FT2_06 - 14	19	0.083	0.0023	0.2218	0.004	2.55	0.072	0.12514	1266	61	1291	21	1284	21	101.97
FT2_06 - 15	19	0.129	0.0041	0.2123	0.0066	3.81	0.21	0.75618	2071	60	1239	35	1582	45	59.83
FT2_06 - 16	19	0.093	0.0016	0.1138	0.0047	1.454	0.054	0.92953	1483	34	694	28	908	22	46.80
FT2_06 - 17	19	0.077	0.0049	0.0313	0.0017	0.321	0.014	0.32699	1050	120	199	11	282	11	18.95

FT2_06 - 18	19	0.1487	0.0021	0.4222	0.0054	8.685	0.14	0.49176	2330	23	2270	24	2304	14	97.42
FT2_06 - 19	19	0.1313	0.0016	0.3803	0.0046	6.907	0.1	0.59526	2114	22	2077	22	2099.7	12	98.25
FT2_06 - 20	19	0.0946	0.0014	0.2187	0.005	2.862	0.071	0.86428	1515	29	1273	27	1368	19	84.03
FT2_06 - 21	19	0.1297	0.0016	0.3203	0.0077	5.75	0.16	0.94544	2094	21	1789	38	1932	24	85.43
FT2_06 - 22	19	0.104	0.0017	0.2905	0.0037	4.163	0.071	0.36883	1693	29	1644	19	1667	14	97.11
FT2_06 - 23	19	0.1035	0.0015	0.2801	0.0039	4.009	0.064	0.47443	1683	27	1591	20	1636.1	13	94.53
GJ															
GJ - 1	29	0.0605	0.0016	0.09713	0.001	0.81	0.019	-0.023812	598	57	597.5	6	600.9	11	99.92
GJ - 2	29	0.0598	0.0016	0.09802	0.001	0.807	0.019	-0.14406	573	58	602.8	5.6	599.6	10	105.20
GJ - 3	29	0.0597	0.0015	0.09798	0.001	0.809	0.018	0.13622	589	52	602.5	6	600.9	10	102.29
GJ - 4	29	0.0605	0.0014	0.09749	0.001	0.814	0.017	0.057227	612	50	599.6	5.9	603.8	9.5	97.97
GJ - 5	29	0.0589	0.0014	0.09742	0.001	0.792	0.016	-0.031407	548	51	599.2	6	591.3	8.9	109.34
GJ - 6	29	0.0612	0.0015	0.09788	0.0011	0.826	0.019	0.074881	625	55	601.9	6.4	611.4	10	96.30
GJ - 7	29	0.0604	0.0015	0.09781	0.001	0.814	0.02	0.26118	595	56	601.5	5.8	603	11	101.09
GJ - 8	29	0.0598	0.0014	0.09734	0.001	0.802	0.017	0.095145	577	52	598.7	5.7	596.7	9.7	103.76
GJ - 9	29	0.0601	0.0015	0.09739	0.0011	0.806	0.018	0.0057552	587	56	599.1	6.2	599.3	10	102.06
GJ - 10	29	0.0599	0.0014	0.09746	0.001	0.807	0.018	0.16975	588	53	599.5	6	599.5	9.8	101.96
GJ - 11	29	0.0615	0.0015	0.09761	0.0011	0.827	0.017	0.06345	640	53	600.3	6.4	611	9.7	93.80
GJ - 12	29	0.0607	0.0015	0.0976	0.001	0.814	0.018	0.048177	608	54	600.3	6	603.8	9.9	98.73
GJ - 13	29	0.0608	0.0014	0.09745	0.001	0.816	0.017	0.16838	615	52	599.4	5.8	605	9.8	97.46
GJ - 14	29	0.0601	0.0015	0.09749	0.001	0.808	0.018	0.029566	596	52	600.3	6.3	600.4	10	100.72
GJ - 15	29	0.0591	0.0014	0.09861	0.001	0.804	0.018	0.17163	558	51	606.2	6	597.8	10	108.64
GJ - 16	29	0.0598	0.0014	0.09777	0.001	0.806	0.017	0.11774	586	51	601.3	5.7	600.3	9.6	102.61
GJ - 17	29	0.0601	0.0013	0.09807	0.001	0.812	0.017	0.19732	591	50	603.1	6	602.7	9.4	102.05
GJ - 18	29	0.0597	0.0015	0.09788	0.0011	0.805	0.018	0.14518	580	55	601.9	6.2	600	10	103.78
GJ - 19	29	0.0608	0.0015	0.09588	0.001	0.804	0.018	0.022826	613	56	590.2	5.9	598.1	10	96.28

GJ - 20	29	0.0595	0.0015	0.09748	0.001	0.799	0.018	0.13388	580	50	599.6	5.8	595.1	10	103.38
GJ - 21	29	0.0606	0.0015	0.09756	0.001	0.814	0.017	-0.026704	607	53	600	5.8	603.6	9.5	98.85
GJ - 22	29	0.0604	0.0015	0.0974	0.0011	0.81	0.017	0.033733	612	49	599.1	6.2	601.2	9.6	97.89
GJ - 23	29	0.0595	0.0014	0.09797	0.001	0.803	0.017	0.029392	568	54	602.5	6.1	597.4	9.6	106.07
GJ - 24	29	0.0612	0.0015	0.09738	0.001	0.82	0.018	0.0955	633	50	599	5.6	607.2	10	94.63
GJ - 25	29	0.0603	0.0015	0.09817	0.0011	0.815	0.018	-0.01544	594	55	603.6	6.4	604	10	101.62
GJ - 26	29	0.0589	0.0014	0.09817	0.0011	0.799	0.018	0.0081873	553	54	603.6	6.4	595.4	9.8	109.15
GJ - 27	29	0.0602	0.0015	0.09761	0.0011	0.809	0.017	0.035098	592	54	600.3	6.3	600.7	9.8	101.40
GJ - 28	29	0.0607	0.0015	0.0974	0.001	0.815	0.018	0.076529	617	54	599.1	5.9	603.9	9.9	97.10
GJ - 29	19	0.0617	0.0021	0.0964	0.0017	0.82	0.028	0.1773	619	75	593.4	9.7	605	16	95.86
GJ - 30	19	0.0616	0.002	0.0973	0.0016	0.821	0.026	0.10332	621	72	598.2	9.5	608	15	96.33
GJ - 31	19	0.0618	0.0021	0.0978	0.0015	0.832	0.028	0.13541	622	73	601.2	9	611	15	96.66
GJ - 32	19	0.0594	0.002	0.0982	0.0016	0.809	0.027	0.021516	560	74	603.8	9.1	599	15	107.82
GJ - 33	19	0.0606	0.0019	0.097	0.0015	0.812	0.025	0.072764	599	68	596.6	8.7	601	14	99.60
GJ - 34	19	0.0614	0.0022	0.0977	0.0018	0.829	0.028	0.091801	628	75	600.7	10	612	15	95.65
GJ - 35	19	0.0604	0.0022	0.0977	0.0016	0.81	0.03	0.18461	566	83	600.7	9.1	599	17	106.13
GJ - 36	19	0.0596	0.002	0.0995	0.0015	0.818	0.028	0.25897	548	73	611.5	9	604	16	111.59
GJ - 37	19	0.0596	0.0022	0.0982	0.0015	0.801	0.028	-0.045576	539	82	603.8	8.7	596	16	112.02
GJ - 38	19	0.0619	0.0022	0.0978	0.0016	0.834	0.029	0.0727	630	78	601.4	9.3	614	16	95.46
GJ - 39	19	0.058	0.0019	0.098	0.0015	0.788	0.027	0.036107	499	74	602.8	8.7	587	15	120.80
GJ - 40	19	0.0612	0.0022	0.098	0.0016	0.83	0.03	0.0054131	619	78	602.5	9.2	612	16	97.33
GJ - 41	19	0.0599	0.0022	0.0968	0.0016	0.806	0.028	0.033945	573	75	595.3	9.4	597	15	103.89
GJ - 42	19	0.0585	0.0022	0.0983	0.0016	0.792	0.028	0.063203	501	80	604.1	9.4	589	16	120.58
GJ - 43	19	0.0595	0.0021	0.0974	0.0016	0.799	0.028	0.17765	550	79	599.1	9.1	593	16	108.93
GJ - 44	19	0.0589	0.002	0.099	0.0016	0.8	0.027	0.18618	520	75	608.2	9.4	596	16	116.96
GJ - 45	19	0.0615	0.0023	0.0965	0.0016	0.805	0.03	0.12855	606	80	594	9.1	603	17	98.02
GJ - 46	19	0.0607	0.0021	0.0961	0.0015	0.802	0.025	0.042637	586	73	591.5	8.8	597	15	100.94
GJ - 47	19	0.0605	0.002	0.0961	0.0016	0.807	0.028	0.11364	588	74	591.3	9.3	598	15	100.56

GJ - 48	19	0.0585	0.0019	0.0986	0.0017	0.794	0.025	0.1551	518	73	606	9.8	591	14	116.99
GJ - 49	19	0.0594	0.002	0.0975	0.0016	0.8	0.027	0.078381	540	74	599.5	9.3	594	15	111.02
GJ - 50	19	0.0593	0.0022	0.0965	0.0015	0.787	0.029	0.25503	529	80	594	9.1	586	17	112.29
GJ - 51	19	0.0607	0.0022	0.0968	0.0015	0.808	0.027	0.082554	581	79	595.4	8.9	601	16	102.48
GJ - 52	19	0.0592	0.0019	0.0982	0.0016	0.804	0.025	-0.024986	544	74	603.7	9.5	597	14	110.97
GJ - 53	19	0.0605	0.002	0.0981	0.0017	0.817	0.026	0.15745	579	72	603.1	9.9	604	15	104.16
GJ - 54	19	0.0606	0.0024	0.0986	0.0016	0.827	0.03	0.060184	583	81	606.2	9.3	609	17	103.98
GJ - 55	19	0.0582	0.0021	0.0977	0.0016	0.787	0.028	0.0059232	498	81	600.6	9.2	586	16	120.60
GJ - 56	19	0.0612	0.0022	0.0976	0.0015	0.824	0.028	-0.051662	608	78	600.3	8.7	609	16	98.73
GJ - 57	19	0.059	0.002	0.0972	0.0017	0.79	0.027	0.19998	522	75	597.7	9.9	588	15	114.50
GJ - 58	19	0.0608	0.0023	0.0978	0.0017	0.823	0.029	0.0015223	591	83	601.6	10	606	16	101.79
GJ - 59	19	0.0606	0.0021	0.0976	0.0014	0.817	0.027	-0.11319	589	79	600.3	8.4	605	15	101.92
GJ - 60	19	0.0596	0.0018	0.0975	0.0016	0.801	0.025	0.23047	563	68	599.8	9.6	595	14	106.54
GJ - 61	19	0.061	0.0022	0.0987	0.0016	0.825	0.027	0.059135	605	73	606.4	9.6	610	16	100.23
GJ - 62	19	0.0604	0.0022	0.0973	0.0016	0.813	0.029	-0.084516	580	80	598.2	9.3	603	15	103.14
GJ - 63	19	0.0579	0.0021	0.0992	0.0017	0.793	0.026	-0.060087	489	79	609.6	9.7	590	15	124.66
GJ - 64	19	0.061	0.0022	0.0979	0.0016	0.818	0.029	0.01287	590	77	602.1	9.5	606	16	102.05
GJ - 65	19	0.0599	0.0021	0.0975	0.0017	0.803	0.026	0.025812	554	76	599.6	10	596	15	108.23
GJ - 66	19	0.0601	0.0021	0.0981	0.0017	0.811	0.027	0.059631	560	77	602.9	9.8	600	15	107.66
GJ - 67	19	0.06	0.0021	0.0971	0.0016	0.801	0.026	0.042749	556	76	597.4	9.6	595	15	107.45
GJ - 68	19	0.0601	0.0023	0.0975	0.0016	0.804	0.029	-0.011975	553	82	599.3	9.5	596	16	108.37
GJ - 69	19	0.0612	0.0019	0.0974	0.0016	0.825	0.027	0.22122	618	70	600.1	9.7	610	16	97.10
GJ - 70	19	0.0598	0.0019	0.097	0.0015	0.8	0.025	0.062416	558	69	596.9	9	596	15	106.97
GJ - 71	19	0.0623	0.0022	0.0972	0.0017	0.836	0.029	0.089833	644	80	597.8	9.7	614	16	92.83
GJ - 72	19	0.0608	0.0025	0.0968	0.0017	0.804	0.03	-0.1038	586	85	595.2	9.8	598	17	101.57
GJ - 73	19	0.0607	0.0022	0.0976	0.0016	0.821	0.03	0.0657	589	82	600.2	9.6	605	17	101.90
GJ - 74	19	0.0584	0.0024	0.0986	0.0017	0.798	0.033	0.055219	499	90	605.9	9.8	594	18	121.42
GJ - 75	19	0.0603	0.002	0.0977	0.0015	0.815	0.029	0.23958	591	76	602.1	9.3	604	16	101.88

GJ - 76	19	0.0612	0.0021	0.0981	0.0017	0.829	0.029	0.22496	600	76	603.3	9.7	610	16	100.55
GJ - 77	19	0.0609	0.0022	0.0966	0.0016	0.81	0.028	-0.01337	586	80	594.2	9.1	599	16	101.40
GJ - 78	19	0.0588	0.0024	0.0982	0.0018	0.799	0.032	0.12377	512	90	603.6	10	592	18	117.89
GJ - 79	19	0.0614	0.0021	0.0953	0.0016	0.809	0.027	0.16889	611	74	586.4	9.2	599	15	95.97
GJ - 80	19	0.0598	0.0022	0.0975	0.0017	0.802	0.029	0.013379	558	80	599.4	9.8	595	16	107.42
GJ - 81	19	0.0594	0.002	0.0972	0.0016	0.799	0.026	0.019165	546	75	598	9.6	593	15	109.52
GJ - 82	19	0.0593	0.002	0.098	0.0018	0.801	0.026	0.13789	533	74	602.3	10	595	15	113.00
GJ - 83	19	0.0598	0.0019	0.097	0.0016	0.797	0.026	0.27937	556	70	596.6	9.6	595	15	107.30
GJ - 84	19	0.0589	0.0021	0.0982	0.0015	0.801	0.029	0.12514	525	83	604	8.6	596	17	115.05
GJ - 85	19	0.0609	0.0022	0.0979	0.0018	0.828	0.031	0.11322	598	82	602.2	10	608	17	100.70
GJ - 86	19	0.0602	0.0022	0.0976	0.0017	0.812	0.03	0.12219	568	80	600.1	10	600	17	105.65
GJ - 87	19	0.0609	0.0022	0.0981	0.0016	0.825	0.029	0.054791	588	79	603.2	9.4	608	16	102.59
GJ - 88	19	0.0595	0.002	0.0962	0.0015	0.79	0.027	0.17669	544	75	591.9	8.7	588	15	108.81
GJ - 89	19	0.0596	0.0022	0.0976	0.0016	0.804	0.03	0.17805	547	82	599.9	9.5	595	17	109.67
GJ - 90	19	0.06	0.0024	0.0985	0.0017	0.81	0.031	0.16842	560	82	605.2	10	598	17	108.07
GJ - 91	19	0.0606	0.0021	0.0977	0.0019	0.815	0.028	0.19176	580	76	600.6	11	602	16	103.55
GJ - 92	19	0.0597	0.0023	0.0968	0.0018	0.791	0.028	0.012413	539	84	595.6	10	590	16	110.50
GJ - 93	19	0.0605	0.002	0.0983	0.0017	0.822	0.026	0.13733	581	74	604.5	10	606	15	104.04
GJ - 94	19	0.0605	0.0023	0.0972	0.0016	0.815	0.032	0.116	574	85	597.8	9.1	601	18	104.15
GJ - 95	19	0.0589	0.0022	0.0971	0.0017	0.784	0.028	0.075566	511	83	597.2	10	586	16	116.87
GJ - 96	19	0.0586	0.0023	0.0984	0.0017	0.796	0.029	0.05116	510	86	604.7	9.9	593	17	118.57
GJ - 97	19	0.0608	0.0021	0.099	0.0017	0.835	0.031	0.26528	595	77	608.3	9.7	613	17	102.24
GJ - 98	19	0.0625	0.0021	0.0972	0.0017	0.839	0.029	0.26956	646	76	597.7	9.7	615	17	92.52
GJ - 99	19	0.06	0.0023	0.0979	0.0016	0.806	0.029	0.095232	553	81	601.8	9.6	599	17	108.82
GJ - 100	19	0.0613	0.0024	0.0989	0.0017	0.834	0.032	0.030179	591	86	607.6	9.7	612	17	102.81
Plesovice															
Ples - 1	29	0.0536	0.0013	0.05365	0.0006	0.396	0.008	-0.031257	337	55	336.9	3.4	338.3	6.1	99.97
Ples - 2	29	0.0525	0.0013	0.05381	0.0006	0.3894	0.008	0.0030967	297	55	337.9	3.3	333.5	6	113.77

Ples - 3	29	0.0528	0.0012	0.05387	0.0006	0.3924	0.008	0.18332	306	52	338.2	3.4	335.7	6.1	110.52
Ples - 4	29	0.05295	0.0012	0.05367	0.0005	0.3917	0.008	0.013438	311	51	337	3	335.2	5.7	108.36
Ples - 5	29	0.0548	0.0014	0.05297	0.0006	0.3998	0.009	0.049477	383	58	332.7	3.4	341	6.8	86.87
Ples - 6	29	0.054	0.0014	0.05355	0.0005	0.3984	0.009	-0.064858	351	58	336.3	3.3	340	6.6	95.81
Ples - 7	29	0.0534	0.0013	0.05344	0.0005	0.3932	0.008	0.0074264	330	53	335.6	3.3	336.3	6	101.70
Ples - 8	29	0.05288	0.0011	0.05405	0.0006	0.3938	0.007	0.14674	312	47	339.4	3.4	336.9	5.2	108.78
Ples - 9	29	0.0536	0.0013	0.05363	0.0005	0.3963	0.008	0.17489	352	53	336.8	3.3	338.6	6.1	95.68
Ples - 10	29	0.0539	0.0013	0.05347	0.0006	0.3954	0.009	0.12284	349	55	335.8	3.4	338.7	6.5	96.22
Ples - 11	29	0.0526	0.0013	0.05373	0.0005	0.3893	0.008	-0.059211	297	53	337.3	3.2	333.5	5.8	113.57
Ples - 12	29	0.05261	0.0012	0.05373	0.0005	0.3914	0.008	0.25474	304	53	337.4	3.2	334.9	6.2	110.99
Ples - 13	29	0.0534	0.0014	0.05406	0.0005	0.3974	0.01	0.074445	326	59	339.4	3.2	339.1	7	104.11
Ples - 14	29	0.05276	0.0012	0.05386	0.0005	0.392	0.008	0.22866	303	52	338.1	3.3	335.4	6.1	111.58
Ples - 15	19	0.0521	0.0019	0.05407	0.001	0.387	0.013	0.012378	265	78	339.4	5.8	332.3	9.7	128.08
Ples - 16	19	0.0541	0.002	0.05356	0.001	0.402	0.015	0.032874	347	80	336.3	5.8	341.6	10	96.92
Ples - 17	19	0.0531	0.0018	0.05379	0.0009	0.395	0.014	0.16303	307	76	337.7	5.6	337	10	110.00
Ples - 18	19	0.0558	0.002	0.05275	0.0009	0.407	0.015	0.093965	408	81	331.3	5.4	346	11	81.20
Ples - 19	19	0.062	0.0024	0.05189	0.0009	0.439	0.016	0.051264	616	83	326.1	5.4	368	11	52.94
Ples - 20	19	0.0525	0.0023	0.05346	0.0008	0.388	0.017	0.077248	260	92	335.7	5.2	331	12	129.12
Ples - 21	19	0.0525	0.002	0.0536	0.0009	0.386	0.014	0.15129	272	81	336.6	5.5	332	11	123.75
Ples - 22	19	0.0552	0.0021	0.05321	0.0008	0.408	0.016	0.11621	380	84	334.2	4.7	346	11	87.95
Ples - 23	19	0.0536	0.002	0.05335	0.0009	0.394	0.014	0.17141	316	80	335	5.6	336	11	106.01
Ples - 24	19	0.0543	0.0022	0.05424	0.0009	0.406	0.016	0.042026	333	87	340.5	5.6	344	12	102.25
Ples - 25	19	0.0543	0.0021	0.05338	0.0008	0.401	0.015	0.055623	339	81	335.2	5	341	11	98.88
Ples - 26	19	0.0528	0.0021	0.05409	0.0009	0.394	0.016	0.10174	276	85	339.6	5.3	336	11	123.04
Ples - 27	19	0.0546	0.0023	0.05362	0.0009	0.401	0.016	0.04059	343	88	336.7	5.6	342	12	98.16
Ples - 28	19	0.0528	0.0019	0.05421	0.0009	0.394	0.015	0.17969	296	76	340.2	5.4	336	11	114.93
Ples - 29	19	0.0509	0.0019	0.05376	0.001	0.379	0.014	0.08212	215	81	337.5	6	324.7	10	156.98
Ples - 30	19	0.0523	0.0022	0.05387	0.0009	0.39	0.017	0.22265	257	91	338.2	5.2	333	12	131.60

Ples - 31	19	0.0517	0.002	0.05401	0.0009	0.385	0.014	0.1127	234	83	339.1	5.2	329.7	10	144.91
Ples - 32	19	0.0551	0.0022	0.05412	0.001	0.409	0.015	-0.080546	376	90	339.7	6.3	347	11	90.35
Ples - 33	19	0.0532	0.002	0.05355	0.0009	0.393	0.015	0.11703	305	85	336.2	5.7	336	11	110.23
Ples - 34	19	0.053	0.0021	0.05352	0.0009	0.391	0.015	0.12964	288	85	336	5.4	333	11	116.67
Ples - 35	19	0.0554	0.0023	0.05365	0.0009	0.407	0.016	0.17591	372	87	336.8	5.8	345	12	90.54
Ples - 36	19	0.0547	0.0023	0.05397	0.001	0.404	0.016	0.057692	346	89	338.8	6.1	343	11	97.92
Ples - 37	19	0.053	0.002	0.05407	0.0009	0.395	0.014	-0.057194	300	84	339.4	5.4	338	11	113.13
Ples - 38	19	0.0521	0.0023	0.0535	0.0008	0.385	0.016	0.047561	247	93	336	5.2	328	12	136.03
Ples - 39	19	0.0529	0.0022	0.05406	0.0009	0.395	0.016	0.14883	286	88	339.4	5.6	336	12	118.67
Ples - 40	19	0.0523	0.002	0.05338	0.0008	0.384	0.014	0.076933	258	85	335.2	5.2	330	11	129.92
Ples - 41	19	0.0539	0.002	0.0535	0.001	0.398	0.015	0.12292	335	78	336.6	6.2	339	11	100.48
Ples - 42	19	0.0547	0.0023	0.05338	0.0009	0.405	0.017	0.050491	360	94	335.2	5.3	343	12	93.11
Ples - 43	19	0.0524	0.002	0.05363	0.001	0.389	0.016	0.29797	264	84	336.7	5.9	332	12	127.54
Ples - 44	19	0.0541	0.0022	0.05303	0.0009	0.397	0.015	-0.024441	328	86	333	5.8	339	11	101.52
Ples - 45	19	0.0539	0.0021	0.0539	0.001	0.403	0.016	0.17704	325	83	338.4	5.8	342	11	104.12
Ples - 46	19	0.0553	0.0024	0.05262	0.0009	0.402	0.017	-0.001447	365	91	330.5	5.2	341	12	90.55
Ples - 47	19	0.053	0.002	0.05325	0.0009	0.389	0.014	0.17386	289	80	334.4	5.8	332	11	115.71
Ples - 48	19	0.055	0.0024	0.05364	0.0009	0.403	0.017	-0.031811	354	93	336.8	5.5	342	12	95.14
Ples - 49	19	0.0563	0.0021	0.05329	0.0009	0.414	0.015	0.11495	419	81	334.6	5.5	350	11	79.86
Ples - 50	19	0.0523	0.0019	0.05254	0.0009	0.379	0.014	0.22397	260	78	330.1	5.4	325.1	10	126.96
91500															
91500 - 1	29	0.0746	0.0023	0.1768	0.0024	1.814	0.051	0.050695	1024	68	1051	13	1048	18	102.64
91500 - 2	29	0.0753	0.0023	0.1778	0.0022	1.843	0.053	0.10272	1062	61	1055	12	1059	19	99.34
91500 - 3	29	0.0755	0.0021	0.1788	0.0024	1.858	0.048	0.15352	1065	56	1060	13	1063	17	99.53
91500 - 4	29	0.0757	0.0022	0.1761	0.0024	1.835	0.049	0.11515	1075	61	1046	13	1054	18	97.30
91500 - 5	29	0.0769	0.0022	0.176	0.0022	1.862	0.048	0.035501	1094	58	1045	12	1064	17	95.52
91500 - 6	29	0.0747	0.0024	0.1784	0.0025	1.825	0.054	0.1317	1026	65	1058	14	1052	20	103.12
91500 - 7	29	0.0766	0.0023	0.1762	0.0023	1.865	0.052	-7.00E-05	1088	64	1046	12	1064	19	96.14

91500 - 8	29	0.0755	0.0023	0.1776	0.0023	1.838	0.049	0.058403	1054	62	1053	13	1058	18	99.91
91500 - 9	29	0.0755	0.0021	0.1784	0.0023	1.857	0.048	0.11873	1073	55	1058	12	1062	17	98.60
91500 - 10	29	0.0752	0.0023	0.1806	0.0025	1.868	0.05	0.039564	1068	65	1070	14	1068	19	100.19
91500 - 11	29	0.0756	0.0024	0.1769	0.0024	1.84	0.053	0.074552	1052	64	1049	13	1055	19	99.71
91500 - 12	29	0.0775	0.0023	0.1771	0.0026	1.886	0.05	0.09622	1107	58	1051	14	1072	17	94.94
91500 - 13	29	0.075	0.0022	0.1755	0.0024	1.825	0.051	0.051983	1065	61	1042	13	1050	18	97.84
91500 - 14	29	0.0738	0.0023	0.179	0.0026	1.83	0.056	0.19371	1013	64	1061	14	1051	20	104.74
91500 - 15	19	0.0736	0.0031	0.176	0.0038	1.777	0.071	0.1468	992	81	1045	21	1028	26	105.34
91500 - 16	19	0.0745	0.0036	0.1782	0.0037	1.811	0.081	0.074972	970	100	1056	20	1042	30	108.87
91500 - 17	19	0.0733	0.0031	0.1787	0.0036	1.785	0.068	0.0074105	968	86	1059	20	1035	26	109.40
91500 - 18	19	0.0762	0.0034	0.1761	0.0038	1.834	0.076	0.18378	1041	89	1045	21	1048	28	100.38
91500 - 19	19	0.077	0.0035	0.1749	0.0038	1.85	0.076	0.030932	1044	95	1041	22	1054	27	99.71
91500 - 20	19	0.0768	0.0033	0.1782	0.0039	1.904	0.086	0.24316	1060	91	1057	21	1070	30	99.72
91500 - 21	19	0.0779	0.0036	0.174	0.0037	1.862	0.084	0.17359	1096	88	1034	20	1060	29	94.34
91500 - 22	19	0.0739	0.0038	0.1786	0.0039	1.787	0.087	0.20988	940	110	1059	21	1036	33	112.66
91500 - 23	19	0.0743	0.0038	0.1768	0.0036	1.786	0.085	0.12304	950	110	1049	20	1028	31	110.42
91500 - 24	19	0.0788	0.0038	0.1814	0.0037	1.965	0.094	0.1509	1080	100	1074	20	1089	33	99.44
91500 - 25	19	0.0746	0.0032	0.1781	0.0035	1.835	0.078	0.022064	1009	90	1056	19	1048	28	104.66
91500 - 26	19	0.077	0.0037	0.1766	0.0037	1.867	0.083	0.013765	1050	100	1048	20	1058	30	99.81
91500 - 27	19	0.0761	0.0036	0.1752	0.0035	1.842	0.077	0.052272	1051	92	1040	19	1059	26	98.95
91500 - 28	19	0.0763	0.003	0.1784	0.004	1.866	0.07	0.21301	1055	82	1057	22	1061	25	100.19

91500 - 29	19	0.0752	0.0035	0.1793	0.0039	1.861	0.083	0.17099	1020	92	1065	22	1055	30	104.41
91500 - 30	19	0.0757	0.0037	0.1781	0.0037	1.831	0.085	0.063604	1010	100	1056	20	1048	32	104.55
91500 - 31	19	0.071	0.0037	0.1758	0.0034	1.721	0.087	0.11156	860	110	1044	18	1002	33	121.40
91500 - 32	19	0.0771	0.0039	0.1785	0.0035	1.891	0.089	0.012231	1030	100	1058	19	1065	31	102.72
91500 - 33	19	0.0701	0.003	0.1749	0.004	1.704	0.077	0.22772	912	91	1038	22	1006	29	113.82
91500 - 34	19	0.0732	0.0037	0.1786	0.0036	1.799	0.085	-0.058251	940	110	1059	20	1032	32	112.66
91500 - 35	19	0.076	0.0038	0.1767	0.004	1.845	0.092	0.1914	1000	100	1048	22	1047	32	104.80
91500 - 36	19	0.0735	0.0038	0.1753	0.0038	1.786	0.091	0.045926	950	110	1043	22	1029	33	109.79
91500 - 37	19	0.0729	0.0026	0.1763	0.0042	1.774	0.07	0.43251	988	74	1046	23	1035	26	105.87
91500 - 38	19	0.073	0.0036	0.1764	0.0038	1.756	0.078	-0.14085	940	100	1046	21	1018	29	111.28
91500 - 39	19	0.0734	0.0035	0.1742	0.004	1.754	0.079	0.12563	950	100	1034	22	1020	31	108.84
91500 - 40	19	0.0739	0.0039	0.1789	0.0042	1.821	0.096	0.20379	940	110	1063	24	1037	35	113.09
91500 - 41	19	0.0734	0.0035	0.1763	0.0037	1.763	0.079	0.11502	940	100	1046	20	1020	30	111.28
91500 - 42	19	0.0742	0.004	0.1796	0.0045	1.813	0.091	0.050483	940	120	1064	24	1039	34	113.19
91500 - 43	19	0.0764	0.0037	0.1738	0.004	1.843	0.09	0.2393	1040	110	1032	22	1047	33	99.23
91500 - 44	19	0.0765	0.0038	0.1737	0.0038	1.822	0.086	0.10345	1047	99	1031	21	1050	31	98.47
91500 - 45	19	0.0735	0.0035	0.1773	0.0041	1.794	0.078	-0.099955	992	94	1051	22	1042	26	105.95
91500 - 46	19	0.0767	0.0038	0.1779	0.0042	1.874	0.087	0.092109	1050	100	1054	23	1068	31	100.38
91500 - 47	19	0.0786	0.0036	0.1749	0.0038	1.898	0.087	0.22711	1084	95	1041	22	1068	31	96.03
91500 - 48	19	0.0761	0.0035	0.1782	0.0039	1.879	0.086	0.16741	1030	100	1056	21	1065	32	102.52

91500 - 49	19	0.0754	0.0032	0.1788	0.0038	1.846	0.076	0.14751	1023	88	1060	21	1052	27	103.62	
91500 - 50	19	0.0711	0.0037	0.1791	0.0044	1.766	0.091	0.19061	870	110	1064	25	1018	33	122.30	

APPENDIX H: MONAZITE U–PB RESULTS

Analysis	Spot Size (µm)	$^{207}Pb/^{206}Pb$	2σ	$^{206}Pb/^{238}U$	2σ	$^{207}Pb/^{235}U$	2σ	rho	$^{207}Pb/^{206}Pb$ Age	2σ	$^{206}Pb/^{238}U$ Age	2σ	$^{207}Pb/^{235}U$ Age	2σ
MAdel														
MAdel - 1a	13	0.0572	0.002	0.0839	0.001	0.656	0.023	0.26701	483	76	519.2	6.2	511	14
MAdel - 2a	13	0.0573	0.0018	0.08358	0.00091	0.659	0.022	0.33086	501	73	517.4	5.4	513.2	13
MAdel - 3a	13	0.0571	0.0018	0.08345	0.00091	0.664	0.021	0.080312	480	72	516.7	5.4	516.6	13
MAdel - 4a	13	0.0553	0.0019	0.08366	0.00089	0.647	0.023	0.15859	408	76	517.9	5.3	505	14
MAdel - 5a	13	0.0569	0.0019	0.0844	0.00095	0.656	0.023	0.33268	471	75	522.3	5.6	511	14
MAdel - 6a	13	0.0576	0.0018	0.08381	0.00096	0.66	0.022	0.31413	511	72	518.8	5.7	514	13
MAdel - 7a	13	0.0568	0.0018	0.08398	0.00084	0.656	0.022	0.21465	479	76	519.8	5	511.5	14
MAdel - 8a	13	0.0573	0.0021	0.08309	0.00093	0.659	0.023	0.34994	496	75	514.5	5.6	513.1	14

MAdel - 1	13	0.0567	0.0012	0.0839	0.0019	0.655	0.015	0.44162	475	49	519.4	11	510.8	9.2
MAdel - 2	13	0.057	0.0013	0.0838	0.0019	0.656	0.016	0.49383	476	52	518.9	11	511	10
MAdel - 4	13	0.0561	0.0022	0.0831	0.0025	0.645	0.028	0.54468	443	90	514	15	504	18
MAdel - 6	13	0.0579	0.0015	0.08298	0.0018	0.658	0.017	0.27238	509	57	513.8	11	513	10
MAdel - 7	13	0.0591	0.002	0.0827	0.002	0.671	0.023	0.21926	546	77	511.9	12	520	14
MAdel - 8	13	0.0564	0.0014	0.0843	0.0019	0.656	0.015	0.17822	463	58	521.8	11	511.5	9.3
MAdel - 9	13	0.057	0.0016	0.0838	0.0019	0.663	0.016	0.24984	487	58	518.7	11	515.8	9.8
MAdel - 10	13	0.0574	0.0014	0.0841	0.0019	0.664	0.015	0.26412	502	52	520.3	11	516	9.5
MAdel - 11	13	0.056	0.0014	0.086	0.0019	0.662	0.016	0.19553	435	58	531.8	11	515.1	9.9
MAdel - 12	13	0.0569	0.0015	0.0826	0.0019	0.648	0.017	0.33123	468	58	511.3	11	506	11
MAdel - 13	13	0.0568	0.0014	0.08395	0.0018	0.657	0.014	0.11957	468	54	520.6	11	512.1	8.7
MAdel - 14	13	0.0573	0.0015	0.0842	0.0019	0.665	0.016	0.23168	487	56	520.9	11	517	9.5

MAdel - 15	13	0.0569	0.0015	0.0832	0.0019	0.651	0.016	0.18289	482	60	515.1	11	508.3	9.5
MAdel - 16	13	0.0577	0.0014	0.0834	0.0019	0.663	0.016	0.36271	502	52	516.5	11	515.8	9.5
MAdel - 17	13	0.0569	0.0016	0.0835	0.0019	0.655	0.019	0.33862	477	64	516.7	12	512	12
MAdel - 18	13	0.0563	0.0015	0.0835	0.002	0.648	0.017	0.4049	446	59	516.6	12	506	11
MAdel - 19	9	0.0558	0.0019	0.0832	0.0016	0.645	0.02	0.10172	430	88	514.9	9.6	504	13
MAdel - 20	9	0.0582	0.0021	0.0833	0.0017	0.674	0.027	0.43098	503	87	516	10	521	16
MAdel - 21	9	0.0575	0.0026	0.0839	0.0017	0.664	0.033	0.33065	470	110	520	10	514	20
MAdel - 22	9	0.0567	0.0022	0.0843	0.0017	0.654	0.027	0.24512	453	95	522	10	509	16
MAdel - 23	9	0.0561	0.0021	0.0843	0.0017	0.652	0.027	0.35335	424	92	521.3	9.9	508	17
MAdel - 24	9	0.0567	0.0023	0.0845	0.0017	0.661	0.029	0.15755	465	100	523	10	516	17
MAdel - 25	9	0.059	0.0024	0.0829	0.0016	0.671	0.025	0.25982	525	96	513.2	9.7	522	16
MAdel - 26	9	0.056	0.0023	0.0838	0.0017	0.65	0.028	0.35492	428	96	519	10	506	17

MAdel - 27	9	0.0571	0.0022	0.085	0.0019	0.663	0.03	0.41161	464	90	526	11	514	18
MAdel - 28	9	0.0575	0.0023	0.0828	0.0015	0.652	0.029	0.37224	474	100	512.5	9	507	18
Ambat														
Ambat - 1a	13	0.057	0.0017	0.08503	0.00084	0.664	0.021	0.44599	480	65	526	5	516.4	13
Ambat - 2a	13	0.0573	0.0017	0.08381	0.00092	0.66	0.021	0.37705	495	66	518.8	5.5	513.8	13
Ambat - 3a	13	0.05661	0.0016	0.08444	0.00099	0.67	0.021	0.49111	468	63	522.5	5.9	520.2	13
Ambat - 4a	13	0.0569	0.0018	0.08369	0.00089	0.666	0.021	0.13489	475	67	518.1	5.3	517.9	13
Ambat - 5a	13	0.05698	0.0016	0.08455	0.00085	0.655	0.02	0.31281	483	64	523.2	5	511.3	12
Ambat - 6a	13	0.05608	0.0016	0.08397	0.00094	0.639	0.02	0.39721	455	60	519.7	5.6	502.5	12
Ambat - 7a	13	0.05689	0.0016	0.08493	0.00084	0.665	0.021	0.41203	486	66	525.4	5	517	13
Ambat - 8a	13	0.056	0.0017	0.08414	0.00086	0.646	0.02	0.11561	442	68	520.8	5.1	505.7	12
Ambat - 1	13	0.0584	0.0012	0.0838	0.0019	0.67	0.012	0.17985	532	46	519	11	520.3	7.2

Ambat - 2	13	0.05768	0.00099	0.08426	0.0018	0.667	0.012	0.53647	510	38	521.5	11	518.3	7.2
Ambat - 3	13	0.0573	0.0012	0.0829	0.0019	0.651	0.013	0.32143	492	46	513.2	11	508.8	7.7
Ambat - 4	13	0.05714	0.001	0.08393	0.0018	0.659	0.012	0.54334	489	38	519.5	11	513.3	7.4
Ambat - 5	13	0.05659	0.001	0.08408	0.0018	0.656	0.012	0.3558	467	40	520.4	11	511.5	7.3
Ambat - 6	13	0.057	0.0011	0.0848	0.0019	0.664	0.011	0.21892	480	46	524.6	11	517.6	6.6
Ambat - 7	13	0.0567	0.0011	0.08306	0.0018	0.648	0.012	0.37301	487	44	514.3	11	506.9	7.6
Ambat - 9	13	0.0565	0.0011	0.08482	0.0019	0.66	0.011	0.14283	463	44	524.8	11	515.5	6.9
Ambat - 10	13	0.0564	0.0013	0.08442	0.0019	0.655	0.013	0.25254	455	50	522.4	11	511.2	8.2
Ambat - 11	13	0.0583	0.0012	0.084	0.0019	0.678	0.015	0.44927	538	47	519.9	12	524.9	9
Ambat - 12	13	0.0572	0.0013	0.0841	0.0019	0.662	0.014	0.2066	485	51	520.3	11	515.5	8.4
Ambat - 13	9	0.056	0.0016	0.0855	0.0013	0.672	0.021	0.37702	429	72	529	7.8	521	12
Ambat - 14	9	0.0572	0.0017	0.0845	0.0014	0.674	0.019	-0.006458	486	78	523	8.3	524	12

Ambat - 15	9	0.0583	0.0019	0.0846	0.0016	0.686	0.023	0.28313	514	77	523.3	9.7	528	14
Ambat - 16	9	0.0576	0.0017	0.0842	0.0014	0.674	0.021	0.060764	490	73	520.9	8.6	522	13
Ambat - 17	9	0.0574	0.0017	0.0841	0.0013	0.667	0.021	0.40545	483	75	520.6	7.5	518	13
Ambat - 18	9	0.0558	0.0019	0.0835	0.0015	0.638	0.021	0.20464	414	85	516.8	8.8	502	14
222														
223 - 1a	13	0.0555	0.0017	0.0724	0.00081	0.55	0.019	0.52533	421	69	450.5	4.9	444.6	12
223 - 2a	13	0.056	0.0017	0.07269	0.00088	0.558	0.018	0.35154	449	65	452.3	5.3	449.4	12
223 - 3a	13	0.0544	0.0017	0.07228	0.00083	0.551	0.019	0.27297	376	71	449.8	5	444.9	12
223 - 4a	13	0.0564	0.0018	0.07226	0.00083	0.57	0.019	0.40488	453	70	449.7	5	457.3	12
223 - 5a	13	0.0562	0.0017	0.07194	0.00082	0.549	0.018	0.33527	448	69	447.8	4.9	443.5	12
223 - 6a	13	0.05515	0.0016	0.07236	0.00069	0.5427	0.017	0.39752	410	64	450.4	4.1	439.9	11
223 - 7a	13	0.0555	0.0016	0.0716	0.00085	0.545	0.017	0.30835	431	68	445.8	5.1	442.8	10
223 - 8a	13	0.0562	0.0017	0.0722	0.00077	0.555	0.017	0.19496	449	67	449.3	4.7	448.1	11
223 - 1	13	0.05622	0.0011	0.07242	0.0017	0.559	0.012	0.55288	451	43	450.7	10	450	8.1
223 - 2	13	0.0557	0.0011	0.07263	0.0016	0.555	0.011	0.43372	432	44	452	9.8	448	7.1
223 - 3	13	0.0555	0.0012	0.07169	0.0017	0.548	0.013	0.57285	421	47	446.3	9.9	443.2	8.7
223 - 4	13	0.0558	0.0013	0.07217	0.0016	0.552	0.012	0.26119	428	52	449.2	9.4	446	8

223 - 5	13	0.0559	0.0012	0.07331	0.0017	0.561	0.011	0.40083	437	48	456	10	453.3	7.4
223 - 6	13	0.0555	0.0013	0.07262	0.0016	0.555	0.012	0.2637	420	52	452.7	9.8	447.9	8
223 - 7	13	0.0553	0.0012	0.0724	0.0017	0.55	0.012	0.47887	411	49	450.4	10	446	7.7
223 - 8	13	0.0558	0.0011	0.07221	0.0016	0.5521	0.0098	0.26147	441	43	449.4	9.5	447.2	6.8
223 - 9	13	0.0555	0.0012	0.0737	0.0017	0.562	0.01	0.27662	420	47	458.1	10	452.5	6.6
223 - 10	13	0.0557	0.0012	0.07366	0.0015	0.565	0.012	0.32657	436	44	458.2	9.1	454.4	7.6
223 - 11	13	0.0567	0.0013	0.07224	0.0016	0.565	0.013	0.36593	465	51	449.6	9.7	454.1	8.2
223 - 12	13	0.056	0.0012	0.07302	0.0016	0.565	0.011	0.24203	442	47	454.3	9.5	454.1	7.3
222 - 13	9	0.0551	0.0021	0.0735	0.0013	0.565	0.021	0.098445	381	90	457.4	7.8	453	13
222 - 14	9	0.0553	0.0018	0.0727	0.0014	0.554	0.017	0.2266	397	78	452.1	8.5	448	12
222 - 15	9	0.0573	0.0018	0.0707	0.0016	0.558	0.02	0.14988	481	81	440.1	9.5	449	13
222 - 16	9	0.0565	0.0018	0.0722	0.001	0.564	0.02	0.26926	457	83	449.5	6.2	453	13
222 - 17	9	0.0558	0.0018	0.072	0.0014	0.554	0.019	0.16912	417	80	447.8	8.4	446	12
222 - 18	9	0.056	0.0021	0.0714	0.0014	0.55	0.019	0.039112	429	91	444.6	8.2	444	13
53811														
11 - 1	13	0.0787	0.0041	0.1845	0.0041	2.025	0.1	0.32589	1180	120	1091	22	1122	33
11 - 2	13	0.0762	0.0022	0.1797	0.002	1.882	0.054	0.23233	1094	57	1065	11	1074	19
11 - 3	13	0.07503	0.002	0.1828	0.0018	1.884	0.055	0.62807	1065	52	1082	10	1074	20
11 - 4	13	0.077	0.0023	0.187	0.0023	1.98	0.063	0.44235	1118	62	1105	12	1107	22

11 - 5	13	0.07504	0.0019	0.1774	0.002	1.838	0.052	0.53723	1066	51	1052	11	1058.7	19
11 - 6	13	0.0756	0.0025	0.1783	0.0027	1.875	0.067	0.36975	1086	72	1058	15	1075	25
11 - 7	13	0.1094	0.0097	0.1778	0.0038	2.71	0.22	-0.18095	1710	180	1055	21	1316	63
11 - 9	13	0.0739	0.0035	0.1706	0.0043	1.784	0.095	0.45227	1055	81	1015	24	1037	35
11 - 10	13	0.0746	0.0022	0.1842	0.0022	1.916	0.062	0.28653	1065	61	1089	12	1085	22
11 - 11	13	0.0755	0.0024	0.1882	0.0029	1.986	0.07	0.49167	1080	66	1111	16	1108	24
11 - 12	13	0.0751	0.0026	0.1858	0.0027	1.951	0.072	0.29612	1064	75	1098	15	1096	25
11 - 13	13	0.0756	0.0023	0.1834	0.0019	1.951	0.068	0.56642	1075	62	1085	10	1096	24
11 - 14	13	0.0778	0.0025	0.182	0.0026	1.976	0.066	0.32667	1129	66	1077	14	1105	22
11 - 15	13	0.0766	0.0024	0.1866	0.003	1.993	0.068	0.56921	1100	61	1102	16	1111	23
11 - 16	13	0.0746	0.0023	0.1867	0.0028	1.939	0.063	0.36705	1048	62	1103	15	1093	22
11 - 17	13	0.0775	0.0024	0.1838	0.002	1.983	0.061	0.147	1124	62	1088	11	1108	21
11 - 18	13	0.0774	0.0025	0.1813	0.003	1.934	0.068	0.25784	1118	66	1074	16	1091	24
11 - 19	13	0.0745	0.0026	0.1891	0.0028	1.96	0.073	0.31883	1038	73	1116	15	1099	25
11 - 20	13	0.07645	0.002	0.1832	0.0018	1.937	0.058	0.57719	1102	53	1084.4	9.9	1093	20
11 - 21	13	0.0744	0.0022	0.1912	0.0026	1.973	0.062	0.6929	1054	63	1128	14	1105	21
11 - 22	13	0.07503	0.002	0.1836	0.0019	1.893	0.054	0.50613	1065	53	1087	11	1077.8	19
11 - 23	13	0.0753	0.0022	0.1808	0.0018	1.872	0.059	0.48807	1070	57	1071	10	1070	21
11 - 24	13	0.0766	0.0025	0.1868	0.0022	1.968	0.064	0.14284	1100	66	1104	12	1103	22

11 - 25	13	0.0752	0.0023	0.1844	0.0023	1.873	0.065	0.37374	1063	65	1091	12	1069	24
11 - 26	13	0.0751	0.0024	0.1838	0.0025	1.869	0.06	0.19514	1068	67	1087	14	1071	22
11 - 27	13	0.0771	0.003	0.1873	0.0038	1.983	0.084	0.48423	1113	74	1106	21	1107	28
11 - 28	13	0.0766	0.0021	0.1956	0.0043	2.045	0.071	0.8216	1106	55	1151	23	1128	23
11 - 29	13	0.205	0.035	0.318	0.054	11.6	3.6	0.93009	2590	280	1720	250	2160	280
11 - 30	13	0.07447	0.002	0.1799	0.0023	1.818	0.055	0.60524	1049	54	1066	13	1051	20
53815														
15 - 1	13	0.0573	0.0014	0.0828	0.0018	0.655	0.015	0.3193	492	54	512.8	11	511.2	9.2
15 - 2	13	0.0574	0.0014	0.0828	0.0022	0.657	0.02	0.67115	497	53	512.6	13	512	12
15 - 3	13	0.0573	0.0016	0.083	0.0022	0.66	0.021	0.52379	493	63	514.2	13	514	13
15 - 4	13	0.0591	0.0019	0.0837	0.0024	0.69	0.029	0.65303	560	66	518	14	532	17
15 - 5	13	0.0584	0.0021	0.0826	0.0026	0.67	0.03	0.57816	527	86	512	15	519	18
15 - 6	13	0.0575	0.0012	0.0821	0.0019	0.65	0.013	0.41866	500	47	508.8	12	507.6	8.2
15 - 7	13	0.0569	0.0016	0.0809	0.002	0.638	0.016	0.1209	475	64	501.7	12	500.5	9.7
15 - 9	13	0.0583	0.0019	0.0811	0.002	0.657	0.021	0.15459	525	72	502.8	12	512	13
15 - 10	13	0.0576	0.0024	0.0802	0.0023	0.638	0.029	0.36802	474	94	497	14	498	18
15 - 11	13	0.0558	0.0027	0.0828	0.0024	0.641	0.034	0.35081	420	110	513	14	501	21
15 - 13	13	0.0608	0.0031	0.0838	0.0042	0.697	0.035	0.42821	620	110	518	25	536	21
15 - 14	9	0.0582	0.0025	0.0814	0.0021	0.629	0.02	0.14157	508	97	504	12	495	13

15 - 15	9	0.055	0.0037	0.084	0.003	0.6	0.029	-0.1591	380	150	520	18	477	19
15 - 17	9	0.0581	0.0053	0.0847	0.0035	0.689	0.053	-0.010695	520	180	523	21	524	32
15 - 18	9	0.0619	0.0042	0.0808	0.0023	0.703	0.043	0.13333	610	150	501	14	537	26
15 - 21	9	0.0552	0.002	0.0826	0.0014	0.634	0.022	0.11098	401	90	511.3	8.3	497	14
15 - 22	9	0.059	0.0037	0.0799	0.002	0.634	0.037	0.069059	500	140	495	12	495	23
15 - 23	9	0.0597	0.0028	0.0825	0.0025	0.639	0.035	0.1555	570	110	511	15	506	19
15 - 26	9	0.1049	0.0083	0.0965	0.0031	1.33	0.12	0.68901	1630	160	594	18	857	57
53816														
16 - 1	13	0.0597	0.0022	0.0841	0.003	0.698	0.032	0.42316	596	89	520	18	536	19
16 - 2	13	0.0571	0.0022	0.0836	0.0022	0.657	0.024	0.23442	475	86	517.4	13	512	15
16 - 3	13	0.0599	0.0015	0.0831	0.0019	0.686	0.019	0.50069	586	55	514.8	11	529	11
16 - 4	13	0.0584	0.0014	0.08137	0.0018	0.653	0.015	0.17485	551	54	505.3	10	509.7	9.2
16 - 5	13	0.0582	0.0017	0.0811	0.0022	0.653	0.022	0.54751	526	63	502.7	13	510	13
16 - 6	13	0.0593	0.0022	0.0822	0.0021	0.673	0.024	0.15311	558	79	509	12	522	14
16 - 7	13	0.0583	0.0015	0.08199	0.0018	0.659	0.017	0.4072	526	55	508	11	513	10
16 - 8	13	0.0578	0.0012	0.0832	0.0019	0.658	0.013	0.43158	509	47	514.9	11	512.9	8.1
16 - 9	13	0.0602	0.0027	0.0816	0.002	0.682	0.028	0.034394	581	96	505.9	12	526	17
16 - 10	13	0.0585	0.0013	0.0816	0.0021	0.66	0.016	0.54639	541	50	505.6	13	514	10
16 - 11	13	0.0597	0.0019	0.0828	0.0024	0.683	0.021	0.2643	579	69	513	14	528	13

16 - 12	13	0.0588	0.0032	0.0856	0.0028	0.692	0.035	0.12569	540	120	529	17	533	21
16 - 13	13	0.0588	0.0016	0.0808	0.0019	0.654	0.017	0.31085	544	59	500.9	11	510	11
16 - 14	13	0.06	0.0021	0.0813	0.002	0.674	0.024	0.22041	588	74	503.7	12	522	14
16 - 15	13	0.0561	0.0013	0.0847	0.0019	0.657	0.013	0.22224	448	51	524.1	12	512.5	8
16 - 16	13	0.0573	0.0012	0.0813	0.0019	0.643	0.015	0.51294	495	48	503.6	12	503.3	9.3
16 - 17	13	0.05728	0.0011	0.0825	0.0018	0.649	0.014	0.54232	508	40	510.8	11	507.1	8.2
16 - 18	13	0.0573	0.0013	0.0844	0.002	0.664	0.015	0.37393	489	51	522.3	12	516.3	9.3
16 - 19	13	0.07	0.0028	0.0829	0.0028	0.802	0.036	0.46047	912	83	513	17	597	20
16 - 20	13	0.0592	0.0018	0.0837	0.0021	0.685	0.021	0.29497	561	69	518.3	12	529	13
16 - 21	13	0.0566	0.0014	0.08266	0.0018	0.646	0.015	0.20736	466	54	511.9	11	505.5	9.1
16 - 22	13	0.0571	0.0014	0.0833	0.0021	0.657	0.016	0.45222	484	54	515.8	12	512.5	9.6
16 - 23	13	0.0588	0.0016	0.0817	0.0019	0.664	0.018	0.33841	548	57	506.1	11	516	11
16 - 24	13	0.0644	0.0028	0.0854	0.0021	0.761	0.032	0.1946	721	89	527.9	12	572	18
16 - 25	13	0.0568	0.0013	0.0815	0.0019	0.638	0.015	0.34409	479	49	505.2	11	500.6	9.3
16 - 26	13	0.058	0.0033	0.0853	0.0024	0.684	0.038	0.15212	490	120	528	14	527	23
16 - 27	13	0.0585	0.0021	0.0806	0.0021	0.659	0.024	0.13541	551	86	499.5	12	513	14
16 - 28	13	0.0603	0.0016	0.0852	0.0019	0.71	0.019	0.2952	612	63	527.1	12	544	11
16 - 29	13	0.0609	0.0027	0.0818	0.0022	0.69	0.031	0.22396	616	100	506.5	13	531	19
16 - 30	13	0.0568	0.0017	0.0833	0.0021	0.655	0.021	0.4133	470	67	515.5	13	511	13

16 - 31	13	0.0578	0.0025	0.0829	0.0021	0.663	0.027	0.060683	498	96	513.4	13	516	16
16 - 32	13	0.0576	0.0019	0.0818	0.0011	0.641	0.021	0.24063	500	74	507.1	6.8	502.3	13
16 - 33	13	0.0576	0.0018	0.0836	0.0015	0.665	0.023	0.56564	509	67	517.8	9.1	517	14
16 - 34	13	0.0579	0.0018	0.0834	0.0012	0.657	0.022	0.27186	523	66	516.4	6.9	512.4	13
16 - 35	13	0.0559	0.0019	0.0822	0.0012	0.631	0.023	0.29979	437	76	509.3	7.1	496	14
16 - 36	13	0.0565	0.0019	0.08394	0.00097	0.645	0.022	0.13215	456	74	519.5	5.8	504.7	14
16 - 37	13	0.0577	0.0018	0.08406	0.00096	0.661	0.022	0.15778	506	70	520.3	5.7	514.3	13
16 - 38	13	0.0576	0.0017	0.0815	0.0011	0.643	0.02	0.35973	507	65	504.9	6.3	503.5	12
16 - 39	13	0.0595	0.0026	0.0824	0.0018	0.686	0.034	0.52101	575	93	511	11	529	20
16 - 40	13	0.0623	0.0022	0.0864	0.0014	0.745	0.026	0.17612	673	78	534.1	8.5	565	15
53817														
17 - 1	13	0.0582	0.0052	0.09	0.0036	0.736	0.065	-0.003113	490	200	555	21	553	38
17 - 2	13	0.0564	0.0026	0.0885	0.0024	0.684	0.03	0.11133	440	95	546	14	526	18
17 - 3	13	0.0564	0.0018	0.085	0.002	0.66	0.02	0.16638	443	71	526	12	513	12
17 - 5	13	0.0596	0.0023	0.0826	0.0024	0.684	0.028	0.43827	569	80	512	14	528	17
17 - 6	13	0.0563	0.004	0.0885	0.0035	0.673	0.046	0.28336	400	150	546	21	518	28
17 - 8	13	0.0771	0.0084	0.146	0.011	1.55	0.19	0.44788	1010	210	877	60	932	70
17 - 9	13	0.064	0.0045	0.0877	0.0033	0.81	0.072	0.44592	700	160	542	20	594	39
17 - 12	13	0.0737	0.0013	0.1746	0.0041	1.773	0.032	0.51363	1033	35	1037	22	1037	11

17 - 13	13	0.0653	0.0038	0.0861	0.0034	0.782	0.051	0.51669	750	120	532	20	587	30
17 - 14	13	0.0586	0.0031	0.0874	0.0031	0.707	0.042	0.57447	500	100	540	18	544	26
17 - 16	13	0.0559	0.0017	0.0836	0.002	0.644	0.019	0.31537	426	68	517.3	12	503	12
17 - 17	13	0.0694	0.0018	0.1435	0.0047	1.386	0.051	0.74569	903	55	864	26	881	22
17 - 18	9	0.0566	0.0025	0.0846	0.0015	0.666	0.029	0.05654	440	110	523.2	9.2	515	18
17 - 23	9	0.0567	0.0035	0.0861	0.0016	0.65	0.039	0.048743	430	140	532.3	9.7	505	24